Adventures in Holography

by

Razieh Pourhasan

A thesis
presented to the University of Waterloo
in fulfillment of the
thesis requirement for the degree of
Doctor of Philosophy
in
Physics

Waterloo, Ontario, Canada, 2014

Author's Declaration

I hereby declare that I am the sole author of this thesis. This is a true copy of the thesis, including any required final revisions, as accepted by my examiners.

I understand that my thesis may be made electronically available to the public.

Abstract

In this thesis, inspired by the holographic theories, we study a variety of interesting problems in gravity, condensed matter and cosmology.

First, we explore the entanglement entropy of a general region in a theory of quantum gravity using holographic calculations. In particular, we use holographic entanglement entropy prescription of Ryu-Takayanagi in the context of the Randall-Sundrum 2 model with considering three kind of gravity theory in the bulk: the Einstein gravity, the general $f(\mathcal{R})$ gravity and the Gauss-Bonnet gravity. Showing the leading term is given by the usual Bekenstein-Hawking formula, we confirm the conjecture by Bianchi and Myers for this theory. Further, we calculate the first subleading term to entanglement entropy and show that they agree with the Wald entropy up to the extrinsic curvature terms.

Then, we study the holographic dual of what is known as quantum Hall ferromagnetism in condensed matter theory. This phenomenon, which has been observed in graphene samples by applying strong magnetic field, is the emergence of energy gaps and Hall plateaus at integer filling fractions due to occurrence of spontaneous symmetry breaking. This effect is partially understood with certain perturbative calculations at weak coupling. The question is then whether this feature survives in a strongly coupled system as well. To address this question, we apply a well-established string theory dual, namely the D3-D5 system. In this framework, coincident D5 and D7-branes are embedded in the $AdS_5 \times S^5$ background of the D3-branes. Within this holographic set-up and through the numerical calculations, we investigate the possibility of spontaneous symmetry breaking and find interesting phase transitions at finite temperature.

Finally, we introduce a holographic description of our four-dimensional universe through a *"brane world"* scenario known as the Dvali-Gabadadze-Porrati (DGP) construction, where the brane refers to our universe embedded in a bulk space-time with five or more dimensions. In fact, we examine the DGP model as a theory of five-dimensional Einstein gravity coupled to four-dimensional branes while we assume five-dimensional spherical black hole metric in the bulk. Then, we study the phenomenological viability of the brane around this five-dimensional black hole. Further, we relate bulk, brane, and black hole parameters and the observational constraints on them. We find that viable solutions are indeed possible, hence we propose a holographic origin for the big bang. In particular, we suggest that our four-dimensional brane emerges from the gravitational collapse of matter in five dimensions which avoids the big bang singularity.

Acknowledgements

Foremost, I would like to express my sincere gratitude to Rob Myers for his constant support, endless patience, for encouraging my research and allowing me to grow as a researcher. I deeply appreciate his immense knowledge, enthusiasm, and his ultimate devotion to inspire and educate his students. His guidance kept me motivated throughout my research and also in writing this thesis.

I would also like to thank Robert Mann for the opportunity to work in his group and also for leading me through my PhD program at the University of Waterloo. Moreover, I thank Mohammadhossein Dehghani who supervised me as I primarily started my graduate studies at Shiraz University.

My sincere thanks also go to my collaborators Niayesh Afshordi, Sean Hartnoll, Charlotte Kristjansen, Gordon Semenoff, Misha Smolkin and Herman Verlinde. It was a great pleasure to learn from their excellent expertise in each project. I have been also enormously benefitted from discussion with Nima Doroud.

I acknowledge financial support through various scholarships and fellowships from the University of Waterloo specifically Ontario Graduate Scholarship and President's Graduate Scholarship. I also enjoyed a privilege to be a resident at the Perimeter Institute for Theoretical Physics which provides me with a rich scientific environment and financial support.

Finally, I deeply thank my family and all my friends for their continuous spiritual support and unconditional love. Without them this journey would have been very difficult, if possible at all. Besides, I would like to thank whoever I have learnt something from and all the people whose names even I may not know, but helped me go this far.

Dedication

To my Mother,

for her ultimate devotion to her family, particularly her children.

Table of Contents

List of Figures

Chapter 1

Introduction

In recent studies of theoretical physics, the holographic description of quantum gravity has attracted a great deal of attention. The most interesting outcome of the holographic principle is the AdS/CFT conjecture which posits a duality between quantum gravity theory with a negative cosmological constant described by an asymptotically anti-deSitter (AdS) metric in the bulk and a conformal field theory (CFT) defined on the boundary of this bulk space and hence in a spacetime with one less dimension relative to the bulk. According to this correspondence, strongly coupled systems of the boundary theory which are difficult to describe via usual field theoretical approaches have a dual description in terms of a weakly coupled gravity theory. In this chapter we give a brief introduction to the holographic principle, review some of the salient insights coming, *e.g.,* from the black hole thermodynamics and the entropy bounds in sections 1.1 and 1.2, respectively. In section 1.3 we pursue a heuristic approach to holography and will discuss the AdS/CFT correspondence in section 1.4. The outline for the rest of the thesis is given in section 1.5.

1.1 Black holes and entropy bounds

Two coincident theorems in general relativity sparked the discovery and development of black hole thermodynamics in early 70's. The first one was introduced by Hawking [112] as the *area theorem* which states that the area of a black hole event horizon never decreases with time, *i.e.,* $\delta A \geq 0$. Hence, for example, after the merging of two black holes, the area of the new black hole is larger than the sum of the areas of the original black holes.

The second known as the *no-hair theorem* indicates that only three parameters, *i.e.,* mass, angular momentum and electric charge are enough to characterize a stationary black

hole[1] [129, 130, 43, 115]. Indeed, the no-hair theorem implies when a *complex* matter system collapses to form a black hole, the phase space is drastically reduced. In other words, the collapsing matter with so many available states and consequently arbitrarily large entropy reduces to a particular black hole as a *unique* final state and so apparently with zero entropy. Hence, from the point of view of an outside observer, the formation of the black hole would naively violate the second law of thermodynamics [16].

A similar problem occurs when a matter system falls into an already existing black hole. However, according to the area theorem, the area of the black hole increases after absorbing the system. Thus as a resolution, Bekenstein [13, 14] suggested that a black hole should carry an entropy proportional to its horizon area measured in units of the Planck length; while later Hawking [116] showed that the proportionality constant is precisely 1/4. Therefore, the entropy of a black hole is given by a quarter of the area of its horizon, *i.e.,*

$$S_{BH} = \frac{A}{4G}. \tag{1.1}$$

Moreover, Bekenstein [13, 14] proposed the generalized second law of thermodynamics (GSL) stating that the total entropy of the black hole plus any matter never decreases:

$$\delta S_{total} \geq 0\,, \tag{1.2}$$

where

$$S_{total} = S_{matter} + S_{BH}\,. \tag{1.3}$$

Further, he argued that when the gravity is sufficiently weak, the GSL imposes a bound for the entropy of the matter as

$$S_{matter} \leq \lambda E R\,, \tag{1.4}$$

where E is the total energy of matter system, R is some scale characteristic of the size of the system and λ is a numerical constant of order one. In fact, the bound (1.4) was originally derived from the GSL through a thought experiment by purely classical analysis with R as the radius of the smallest sphere circumscribing the system and $\lambda = 2\pi$ [15]: consider a system much smaller than the black hole, which is dropped into a black hole from the vicinity of the horizon. It will be swallowed and disappear behind the horizon. According to the GSL, the lost entropy of the system has to be compensated by the growth

[1]This was proved for four-dimensional Einstein-Maxwell theory. In recent yeas, of course, people have studied black holes in higher dimensions and new parameters arise although it is still generally thought to be some finite number that characterize the black holes. For example, spin is characterized by $\lfloor d/2 \rfloor$ parameters in d dimensions [181] or the horizon may have distinct topologies in higher dimensions [73].

of the black hole area which is governed by the Einstein equation. Taking this into account and calculating the energy absorbed by the black hole yields equation (1.4). Although the derivation of the bound from the GSL has been challenged [233, 234, 173, 174] repeatedly, the bound, apart from its association to the GSL, is interesting by itself. Indeed recently in [45], Casini provided a more precise definition of the quantities in equation (1.4) and showed the validity of the Bekenstein bound based on some arguments involving the positivity of the relative entropy – see also [21].

On the other hand, instead of dropping a thermodynamic system into an existing black hole, Susskind [222] considered a process in which the system itself is *converted* to a black hole. He argued that the GSL then yields an upper bound, known as the *spherical entropy bound*, for the entropy of the matter enclosed in the spacelike region of finite volume

$$S_{matter} \leq \frac{A}{4G}\,, \tag{1.5}$$

where A is the area of the boundary of the region. Indeed, A is well-defined only if the metric near the system is at least approximately spherically symmetric which is the case for all spherically symmetric systems and all weakly gravitating systems, but not for strongly gravitating systems lacking spherical symmetry.

The spherical symmetry bound could be derived from the Bekenstien bound if the latter is assumed to hold for strongly gravitating systems. Indeed if one applies the Bekenestein bound for a system of mass M and radius R while requiring the gravitational stability, *i.e.,* $2MG \leq R$, one gets

$$S \leq 2\pi MR \leq \pi R^2/G = A/4G\,. \tag{1.6}$$

This shows that the spherical entropy bound is weaker than the Bekenestein bound where both can be applied. However, the spherical bound is more closely related to the holographic principle and it can be expressed in a covariant and general form as will be shown in the next section.

In fact, the spherical entropy bound suggests there is an underlying relationship between geometry and information. The foundation of this correspondence should show up in a theory of quantum gravity. If one tries to excite too many "degrees of freedom" in a spherical region of fixed boundary area A, then the region becomes very massive and undergoes a gravitational collapse to eventually form a black hole of area no larger than A with maximal entropy of $A/4G$. This hints that the maximum information which one can store inside any spacelike region retaining its gravitational stability, is proportional to the area of the region not its volume. This was probably the first motivation towards the "holographic principle" which will be discussed in the following.

1.2 The covariant entropy bound

The covariant entropy bound introduced by Bousso [28, 29] is a generalization of the spherical entropy bound to arbitrary spacelike regions in terms of the light-sheets. The precise definition becomes clear after the following steps [29]:

- In any d-dimensional Lorentzian spacetime M, choose any $(d-2)$-dimensional spatial surface B, and determine its area $A(B)$. There will be four families of light rays, see figure (1.1), projecting orthogonally away from B: $F_1, \cdots, F_4$.
- One can determine the expansion of the orthogonal light rays based on additional information such as knowing the macroscopic metric in a neighborhood of B. Out of the four families at least two will not expand, *i.e.,* F_1 and F_2 in figure (1.1).
- Select a portion of the non-expanding[2] F_i and follow each light ray no further than to a *caustic*, a focal point where it intersects with neighboring light rays. These light rays form a $(d-1)$-dimensional null hypersurface, *i.e.,* a light sheet $L(B)$.
- Determine the entropy on the light sheet, *i.e.,* $S[L(B)]$, which is simply given by the entropy of the matter system: indeed, the light sheet is just a different way of taking a snapshot of a matter system in light cone time: suppose B is a sphere around an isolated, weakly gravitating thermodynamic system. Therefore, given certain macroscopic constraints such as energy, pressure, volume, etcetera. the entropy of the system can be computed either thermodynamically or statistically.

This construction in the limit of classical gravity is well-defined and the quantities $S[L(B)]$ and $A(B)$ can then be compared. *The covariant entropy bound then states that the entropy on the light sheet $L(B)$ will not exceed a quarter of the area of the codimension-2 surface B:*

$$S[L(B)] \leq \frac{A(B)}{4G}. \tag{1.7}$$

This must hold for any surface B and it applies to each non-expanding null direction F_i separately. Indeed, the difference between the spherical bound (1.6) and the covariant bound (1.7) is how to define entropy content of the region surrounded by the surface B. Bousso [29] also pointed out some interesting features of the covariant bound which are worth mentioning:

[2]The families of light rays with non-positive expansion, *i.e.*, $\theta(\lambda) = \frac{dA/d\lambda}{A} \leq 0$ where λ is an affine parameter for the light rays generating F_i.

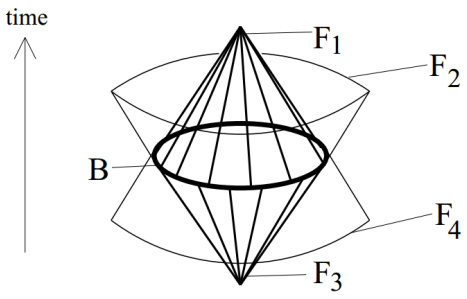

Figure 1.1: Four null hypersurfaces orthogonal to a spherical surface B. F_1 and F_2 have negative expansion corresponding to non-expanding light sheets [29].

- A codimension-2 surface B serves as the starting point for the construction of a codimension-1 region L. More precisely, L is a light-sheet constructed by the null geodesics that originate from the surface B, as long as their expansion is non-positive.
- Unlike Bekenstein bound and the spherical bound which are both inferred from the GSL, the covariant entropy bound cannot be derived from black hole thermodynamics. Rather, the GSL might be more appropriately regarded as a consequence of the covariant bound.
- There is no fundamental derivation of the covariant entropy bound. We present the bound because there is strong evidence that it holds universally in nature.[3] Therefore, we conclude that the bound is an imprint of a more "fundamental theory".
- The bound essentially involves the quantum states of matter. Thus we may conclude that the fundamental theory responsible for the bound unifies matter, gravity, and quantum mechanics. More precisely, the fundamental theory should be a theory of *quantum gravity*.
- The bound relates information to a single geometric quantity, *i.e.,* area. Then we conclude that the area A of any surface B measures the information content of an underlying theory describing all possible physics on the light-sheets of B.

[3] In [29], the bound has been applied to cosmology and verified explicitly that it is satisfied in a wide class of universes.

While the bound is conjectured to be valid for all physically realistic matter systems, it is regarded as evidence for the *holographic principle*. The interested reader is referred to the comprehensive review by Bousso [29] for further reading.

1.3 The rise of holography

As mentioned in the previous section the covariant entropy bound implies the existence of an underlying fundamental theory of quantum gravity. Then the question one may ask is: how much information would completely specify any physical configuration in a bounded region? In other words, how many degrees of freedom N are available in a given "fundamental system"?

Assume a local quantum field theory on a classical background satisfying the Einstein equations. That is, we have a particular collection of quantum mechanical systems where the Hilbert space is an infinite tensor product over all points in space with a finite number of degrees of freedom at each point. However, the infinite number of points on a spatial slice implies an infinite number of degrees of freedom, *i.e.,* $N = \infty$ with the number of degrees of freedom N being the logarithm of the dimension $\mathcal{N}$ of the Hilbert space. The infinite number of points on a spatial slice, which implies the infinite number of degrees of freedom, is the source of the well known UV (short-distance) and IR (long-distance) divergences of quantum field theory. The IR divergences can be regulated by working in finite volume, while the UV divergences can be controlled by instead considering a theory with degrees of freedom only on some fine spatial lattice of points, providing the UV cut-off. So if we include gravity in a minimal crude way in the theory, then the natural UV cut-off would be the Planck energy[4], $M_p \approx 1.3 \times 10^{19}$GeV. This is due to the fact that one might expect that distances smaller than the Planck length $\ell_p = 1.6 \times 10^{-33}$cm, cannot be resolved in quantum gravity and M_P is the largest amount of energy one can localize into a cube of the size of the Planck length without forming a black hole. Thus having a finite number of states n at each point in the Planck grid, the total number of degrees of freedom is

$$N \sim V \ln n \gtrsim V \,. \tag{1.8}$$

On the other hand, in statistical physics, entropy is a measure of the number of degrees of freedom of a theory. Indeed the number of degrees of freedom is $N = \log \mathcal{N} = S$ where

[4]This is the fundamental mass scale can be made out of the fundamental constants $\hbar$ (Plank constant), G (gravitational constant) and c (speed of light) in a theory of quantum gravity which in four dimensions is given as $M_p = \sqrt{\hbar c/G}$. Alternatively, one can make the fundamental length scale, *i.e.,* the so-called Plank length which in four dimensions is $\ell_p = \sqrt{\hbar G/c^3}$.

$\mathcal{N} = e^S$ is the number of states or the dimension of the Hilbert space. We already argued, in the previous section, that the entropy of any matter system in a finite region of spacetime is bounded from above by the covariant entropy bound, *i.e.,*

$$N \leq \frac{A}{4G}\,. \tag{1.9}$$

By comparing equations (1.8) and (1.9), one realizes that quantum field theory overcounts the number of degrees of freedom. Indeed because of gravity, not all degrees of freedom that field theory apparently supplies can be used for generating entropy, or storing information.

In summary, while the number of degrees of freedom in any local quantum field theory is extensive in volume, the holographic principle implies that the true number of degrees of freedom is proportional to the area of each region. Although physics appears to be local to a good approximation, the holographic principle seems to challenge the locality. Then we need to formulate the "fundamental theory" so as to resolve this tension. So far, there are two main approaches: one approach aims to retain locality through an enormous gauge invariance, leaving only as many physical degrees of freedom as needed by the covariant entropy bound. For example, 't Hooft [227, 226, 230, 228, 229] is pursuing a local approach in which quantum states arise as limit cycles of a classical dissipative system. The emergence of an area's worth of physical degrees of freedom has yet to be demonstrated in such models.

Another approach is to regard locality as an emergent phenomenon without fundamental significance. In this case, the holographic data are primary. Here, one major challenge is to understand their evolution. However, one must also explain how to translate this underlying data, in a suitable regime, into a classical spacetime inhabited by local quantum fields. In a successful construction, the geometry must be shaped and the matter distributed so as to satisfy the covariant entropy bound. Because the holographic data is most naturally associated with the area of surfaces, a serious difficulty arises in understanding how locality can emerge in this type of approach.

The AdS/CFT correspondence [171] belongs to the second type of approach. However, this correspondence only defines quantum gravity in a limited set of spacetimes. It contains a kind of holographic screen, a distant hypersurface on which holographic data is stored and is evolved forward using conformal field theory.

Which type of approach one prefers will depend, to a great extent, on which difficulties one would like to avoid: the elimination of most of the degrees of freedom, or the recovery of locality. One last thing to notice is that since light sheets are central to the formulation

of the holographic principle, one would expect null hypersurfaces to play a primary role in the classical limit of an underlying holographic theory.

1.4 Towards the AdS/CFT correspondence

The AdS/CFT correspondence, originally conjectured by Maldacena [171], is an intriguing equivalence (or duality) between theories with gravity and theories without gravity. In its original form, it is an equivalence between four dimensional $\mathcal{N} = 4$ super Yang-Mills theory and type IIB string theory compactified on $AdS_5 \times S^5$. The AdS_5 stands for the anti-de Sitter space in five dimensions while S^5 is a five-dimensional sphere. The AdS/CFT correspondence is a vast subject and has been extensively reviewed in literature, *e.g.,* see [7, 172, 178].

1.4.1 The AdS geometry

Anti-de Sitter space is a maximally symmetric solution of the vacuum Einstein equations with a negative cosmological constant. The geometry can be described as the $(d+1)$-dimensional hyperboloid

$$-y_0^2 + \sum_{i=1}^{d} y_i^2 - y_{d+1}^2 = -L^2\,, \tag{1.10}$$

embedded in a $(d+2)$-dimensional pseudo-Euclidean space with metric of signature $(-+\ldots+-)$

$$ds^2 = -dy_0^2 + \sum_{i=1}^{d} dy_i^2 - dy_{d+1}^2\,, \tag{1.11}$$

The pseudo-sphere (1.10) is both homogeneous and isotropic and has the isometry group $SO(2,d)$, *i.e.,* group of boosts in the embedding space. One can define the so-called global

coordinates $(\tau, \rho, \theta, \phi_1, \cdots, \phi_{d-2})$ on the AdS_{d+1} space with

$$\begin{aligned}
y_0 &= L \cosh\rho \cos\tau \,, \\
y_1 &= L \sinh\rho \cos\theta \,, \\
y_2 &= L \sinh\rho \sin\theta \cos\phi_1 \,, \\
&\vdots \\
y_{d-1} &= L \sinh\rho \sin\theta \sin\phi_1 \sin\phi_2 \cdots \cos\phi_{d-2} \,, \\
y_d &= L \sinh\rho \sin\theta \sin\phi_1 \sin\phi_2 \cdots \sin\phi_{d-2} \,, \\
y_{d+1} &= L \cosh\rho \sin\tau \,,
\end{aligned} \tag{1.12}$$

where $\rho \geq 0$, $\tau \in [0, 2\pi)$, and L is the radius of the pseudo-sphere. Therefore one can write the induced metric on the AdS_{d+1} hypersurface (1.10) in global coordinates as

$$ds^2 = L^2(-\cosh^2\rho\, d\tau^2 + d\rho^2 + \sinh^2\rho\, d\Omega_{d-1}^2) \,, \tag{1.13}$$

where $d\Omega_{d-1}^2$ represents the metric of the unit $(d-1)$-sphere.

From metric (1.13) it is evident that the isometry group $SO(2,d)$ of AdS has the maximal compact subgroup $SO(2) \times SO(d)$. The $SO(2)$ generate translation along the τ direction which has the topology of S^1 and $SO(d)$ represents the rotational symmetry along the angular directions on the S^{d-1}. As $\rho \to 0$ the radius of the S^1 approaches a constant as $\cosh\rho$ while the radius of the S^{d-1} shrinks to zero as $\sinh\rho$. As any space with more than one timelike coordinate, AdS contains closed timelike curves (CTC), *i.e.,* the S^1 along the time direction. However, CTC's are eliminated in the causal structure of the AdS by unrolling the S^1 by taking $\tau \in (-\infty, \infty)$, *i.e.,* extending the hyperboloid to an infinite-fold covering space. The latter geometry is what we are considering in the following.

It is also common to write the AdS metric in the so-called Poincaré coordinates $(z, t, \vec{x})$ which are defined as

$$\begin{aligned}
y_0 &= \frac{z}{2}\left(1 + \frac{1}{z^2}(L^2 + \vec{x}^2 - t^2)\right) \,, \\
y_i &= \frac{L}{z} x_i \qquad (i = 1, \cdots, d-1) \,, \\
y_d &= \frac{z}{2}\left(1 + \frac{1}{z^2}(L^2 - \vec{x}^2 + t^2)\right) \,, \qquad y_{d+1} = \frac{L}{z} t
\end{aligned} \tag{1.14}$$

with $z \geq 0$ and $\vec{x} \in \mathbb{R}^{d-1}$. Clearly distinguishing y_d among y_i's breaks the $SO(d)$ symmetry and the metric takes the form

$$ds^2 = \frac{L^2}{z^2}\left(dz^2 + \eta_{\mu\nu} dx^\mu dx^\nu\right) \,. \tag{1.15}$$

With $z \geq 0$, the metric (1.15) covers only half of the hyperboloid (1.10) and only a small wedge in the full covering space. This is called the Poincaré patch and is conformally equivalent to a half of the Minkowski spacetime in $(d+1)$ dimensions. The Penrose diagram of the AdS_{d+1} with the Poincaré patch highlighted is shown in figure 1.2.

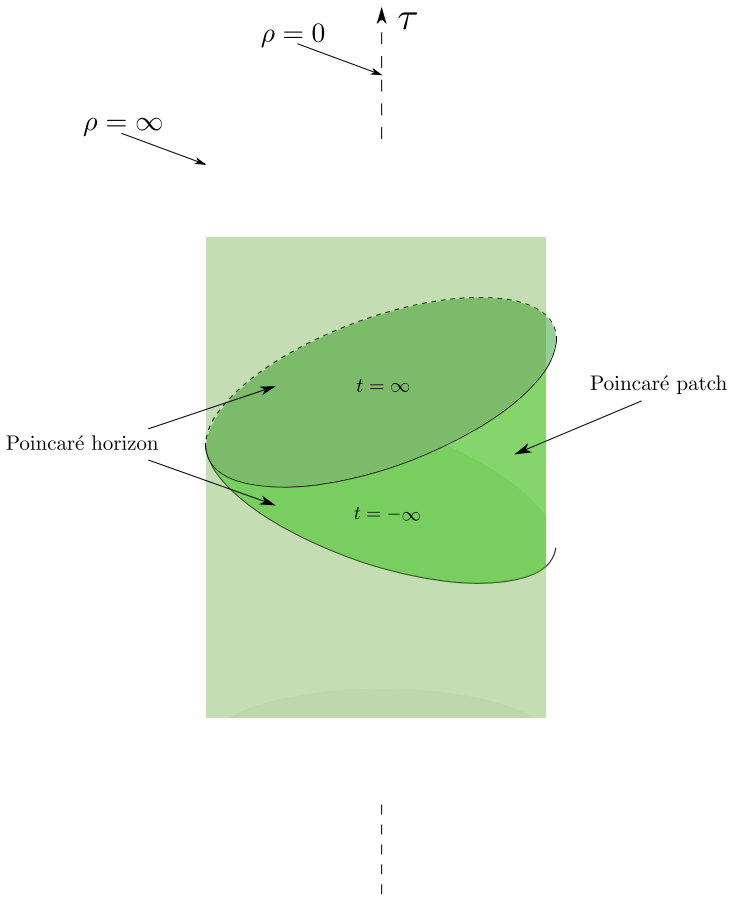

Figure 1.2: Penrose diagram of the AdS_{d+1} which can be conformally mapped on $R \times S^d$. The cross section of the cylinder is half of the sphere S^d. The highlighted region is the Poincarè patch which only covers part of the AdS_{d+1}
as it is bounded by the Poincarè horizon.

Clearly Poincaré transformations are part of the symmetry group of AdS spacetime. Moreover, it is easy to check that the metric (1.15) is invariant under the scaling symmetry of the form

$$(z, x_\mu) \to (\lambda z, \lambda x_\mu)\,, \qquad \lambda > 0\,. \tag{1.16}$$

Therefore, AdS spacetime enjoys a bigger symmetry which in fact matches the conformal symmetry group in d-dimensions. In particular, the above geometric scaling (1.16) is identified with the dilatation symmetry in the conformal symmetry group of $\mathbb{R}^{1,d-1}$ according to the AdS/CFT conjecture. Indeed one of the key motivations for the conjecture is the correspondence between the symmetries on both sides of the duality.

With one more redefinition of the coordinates, it is easy to see that the AdS spacetime can be described by a standard warped metric. Indeed, by defining $z = Le^{-r/L}$, the AdS metric (1.15) can be rewritten as

$$ds^2 = dr^2 + e^{2r/L}\eta_{\mu\nu}dx^\mu dx^\nu\,, \tag{1.17}$$

with $r \in (-\infty, \infty)$. Here the metric appears as the warped product of d-dimensional Minkowski space times an extra radial coordinate. That is, the Minkowski metric is multiplied by an exponential function of the radial coordinate. As the radial coordinate approaches the infinity, the exponential factor blows up. This is commonly called the AdS boundary, which is often interpreted as the place where the dual conformal field theory resides. It can be shown that the massless excitations in the bulk can propagate all the way to the AdS boundary in a finite proper time. Hence one must supplement the bulk theory with suitable boundary conditions at infinity. A standard choice is Dirichlet boundary conditions so that the massless fields are simply reflected back into the bulk.

Moreover, as we will be discussing below, the AdS/CFT correspondence is a strong/weak coupling duality. Indeed, weakly coupled string theory in the bulk, which is well described by supergravity, can be used to provide information about the strongly coupled gauge theory on the boundary, which is difficult to describe with standard field theoretical approaches. However, the AdS/CFT correspondence can also be applied in the opposite direction, *i.e.,* we can learn more about string theory in the bulk by understanding the properties of the gauge theory on the boundary. Therefore, the conjecture works in two directions. To clarify this point we briefly review some interesting features on both sides of the correspondence in the following.

1.4.2 Large N limit

One remarkable hint towards the AdS/CFT correspondence was the novel work by 't Hooft [225] indicating that large N gauge theory is equivalent to a string theory: considering a

gauge theory with $U(N)$ gauge group in the limit of $N \to \infty$ and fixed finite $g^2_{\rm YM}N$, where N is the rank of the gauge group and $g_{\rm YM}$ is the coupling constant of the gauge theory, one can show that the structure of observables as a perturbation series in $1/N$ is identical to the loop expansion in a dual string theory. This is true provided one identifies string coupling g_s with $1/N$ which is very small in the large N limit indicating weak coupling regime of the string theory in the bulk. One may be concerned that fixing $g^2_{\rm YM}N$ for large N could only be achieved if the coupling $g_{\rm YM}$ is very small and that is not consistent with what we expect in a strong/weak duality. However, this is not the case, since in the large N limit the true effective coupling of the gauge theory could be redefined as $\lambda_t \equiv g^2_{\rm YM}N$. Therefore in this set up λ_t, which is known as the 't Hooft coupling, is fixed but could be sufficiently large.

To see the point, let us consider ordinary $D = 4$ Yang-Mills theory with $U(N)$ gauge group and physical coupling $g_{\rm YM}$ and coupled to one flavor of quarks. The beta function for the coupling to lowest order in perturbation theory is given by [106]

$$\frac{\partial g_{YM}}{\partial \log \mu} = -\frac{1}{16\pi^2}\frac{11}{3}g^3_{YM}N + \cdots . \tag{1.18}$$

However, it is easy to see that the RG equation (1.18) is independent of N if it is rewritten in terms of the 't Hooft coupling $\lambda_t = g^2_{YM}N$

$$\frac{\partial \lambda_t}{\partial \log \mu} = -\frac{1}{8\pi^2}\frac{11}{3}\lambda^2_t + \cdots . \tag{1.19}$$

Then in the large N limit, we can have strongly coupled field theory with sufficiently large 't Hooft coupling.

Furthermore, the perturbative expansion for the partition function of a large N gauge theory in terms of $1/N$ and λ_t has the form

$$Z_{YM} = \sum_{g\geq 0} N^{2-2g} f_g(\lambda_t) . \tag{1.20}$$

where g is the genus for certain two-dimensional surfaces. In this setting, the Feynman diagrams are organized by the genus of the two-dimensional surfaces on which they can be drawn without any line crossings. This is similar to the loop expansion of the partition function of string theory with both closed and open strings (including quarks)

$$Z_{string} = \sum_{g\geq 0} g_s^{2g-2} Z_g \tag{1.21}$$

when we identify the string coupling g_s with $1/N$. Hence, of course, the surfaces are the two-dimensional world-sheets of the string.

1.4.3 Non-abelian gauge symmetry from string theory

A heuristic derivation of the AdS/CFT correspondence from string theory begins with Dp-branes. In fact, using Dp-branes, one can build a non-abelian gauge group. First discovered by Polchinski [197], Dp-branes are extended dynamical objects with p spatial dimensions. For example, a $D0$-brane describes a particle, a $D1$-brane is a string, a $D2$ is a membrane and so on.

In particular, there are two ways to describe a Dp-brane, both of which will arise in our heuristic derivation of the AdS/CFT correspondence. The first one arises from the open string theory on the D-branes where consistency require that the endpoints of an open string satisfy either the Neumann, or the Dirichlet boundary conditions independently in each spatial direction. The Neumann boundary condition along a direction corresponds to the free moving endpoints of the open strings in that direction whereas the Dirichlet boundary condition along a direction pins the string endpoint to a particular place along that direction. Out of 9 spatial directions, we can allow p Neumann and $9-p$ Dirichlet boundary conditions. Then the string endpoint confined to move within a p-dimensional spatial hypersurface (as well as time) in ten-dimensional spacetime. This hypersurface is the Dp-brane, generalizing a notion of the membrane.

The second description comes from the equations of motion in the low-energy limit of the closed string theory describing the coupling of the D-branes to (super)gravity. Consider an open string with both ends on the same brane. Since open strings can interact locally at their endpoints, the two ends might meet and form a closed string, thus leave the brane. Then we expect both open and closed strings coexist in the same theory. However, closed strings live in 10 dimensions and respect the full Lorentz invariance of this space. So a D-brane must be an excitation within the closed string theory. Indeed in this viewpoint, D-brane can be regarded a non-perturbative object in the full 'string' theory, or a solitonic excitation of the supergravity.

Quantization of the open strings with *NN boundary conditions* in all 10 dimensions will lead to massless states including a photon A_μ in 10 dimensions as well as a fermionic superpartner λ_α. On the other hand, quantizing open strings confined to a Dp-brane with *DD boundary conditions* in $9-p$ directions, gives us a photon A_μ in $p+1$ dimensions plus $9-p$ scalar fields ϕ_i, corresponding to the fluctuations of the D brane position. In particular, there is one scalar field for each direction transverse to the brane. The vacuum expectation values of these scalars indicate the location of the brane in the corresponding direction. Hence time-dependent scalars describe a brane in motion. As in 10 dimensions, these bosonic fields come with fermionic superpartners.

Now we are ready to build a nonabelian gauge symmetry in string theory. Consider

a stack of N parallel coincident Dp-branes: an open string can start on any one of these branes and end on any other. In particular, each endpoint of the string has N possible places to end, giving N^2 possibilities in total. We can label each endpoint with a number $a, b = 1, \ldots, N$ telling us which brane they lie on. These labels are often called Chan-Paton factors. Each of these strings has the mass spectrum of an open string, meaning that there are now N^2 different particles of each type. It is natural to arrange the associated fields to sit inside $N \times N$ Hermitian matrices. Therefore, we have massless scalars ϕ_i^{ab} and a gauge field A_μ^{ab}. Here the components of the matrix tell us from which class of strings the field came. Diagonal components arise from the strings which have both ends on the same brane, so for the $N \times N$ gauge field A_μ^{ab}, the diagonal elements represent the abelian gauge fields of the individual branes and together they provide a $U(1)^N$ gauge group.

On the other hand, it can be shown that in the presence of a background gauge field $U(1)$, the endpoint of a string on a D-brane will behave like a point charge on the brane world-volume. Therefore, in our story of N coincident Dp-branes, those strings having their endpoints on different branes are charged under the background gauge fields $U(1)^N$. Consequently, it turns out that they provide the extra gauge fields needed to enhance $U(1)^N \to U(N)$. Now if we separate some of the branes, the strings stretching between them become massive which implies the corresponding gauge fields must be massive and a smaller gauge group emerges. Hence separating the branes provides a stringy version of the Higgs mechanism. For more details on D-branes see, for example, [141].

To summarize, quantization of the N^2 strings on a stack of N coincident Dp-branes results in a low-energy effective Yang-Mills theory of a $U(N)$ gauge field $A_\mu^{ab}(a, b = 1, \ldots, N)$ coupled to scalars and fermions, also in the adjoint representation of $U(N)$.

1.4.4 The AdS/CFT conjecture

So far we have introduced the necessary material which we need to derive the conjecture. Hence we now try to give a brief heuristic "derivation" of the AdS/CFT correspondence without explicit mathematical calculations. To begin, let us consider the special case of a stack of N coincident D3-branes in addition to the closed strings in the ten-dimensional background. The only scale in this configuration is the string length ℓ_s which fixes the rest energy of typical excited string states as $E_0 \sim 1/\ell_s$. Another important parameter is the (dimensionless) string coupling g_s controlling the strength of interactions of the strings, both open and closed, among themselves. Now having two parameters in hand, we are interested in two separate limits: the low energy limit where the energies of any process satisfy $E\ell_s \ll 1$, and the strong coupling limit where $g_s N \gg 1$ and the open string sector

is strongly coupled. In particular, we are interested in these limits where they applied one after the other. That is, one can go to the low energy limit first by taking $E\ell_s \ll 1$ while the coupling g_s is fixed, and then in the low energy limit, increase the coupling g_s to produce $g_s N \gg 1$, or the two limits can be applied the other way around. It turns out depending in which order we take the limits, two completely different theories will emerge. However, Maldacena [171] made the bold conjecture that these two theories should describe the same physics. We try to clarify these ideas in the following, which has been also illustrated in figure (1.3).

Let us first consider the limit where $E\ell_s \ll 1$ while keeping g_s and N fixed (with $g_s N \ll 1$). In fact, this corresponds to the low-energy limit of the system, in which all the massive excitations of the strings can be ignored and only the massless modes will play a role. Further, in this low energy limit, the massless open strings on the four-dimensional D3-brane and the massless closed string modes in the full ten-dimensional spacetime decouple and so we can focus on the open string gauge theory alone. As we discussed in the previous section, the massless excitations for open strings at low energy limit will be described by a $U(N)$ gauge theory, specifically $\mathcal{N} = 4$ supersymmetric Yang-Mills on the D3-branes. Also, from the D-brane dynamics, it is realized that the string coupling g_s is related to the gauge coupling $g_{\rm YM}$ through $g_s = 2\pi g_{\rm YM}^2$. Now, we go to the strong coupling limit of gauge theory by increasing g_s. Therefore, we end up with the *strongly coupled gauge theory* where the effective coupling being the 't Hooft coupling $\lambda_t = g_s N/2\pi \gg 1$.

On the other hand, we can start by taking the strong coupling limit first, *i.e.,* $g_s N \to \infty$ (with N large and fixed). Note that with fixed large N, we can still arrange that $g_s N \gg 1$ while $g_s \ll 1$. This is important because in this case, the closed string interactions are still weak among themselves so that we can treat them perturbatively. For example, the leading terms in closed string scattering come from the tree level amplitudes and we can ignore loop corrections. However, the closed string interactions with the stack of D3-branes is controlled by $g_s N$ and hence these interactions are strong. Therefore in this limit, it is more efficient to think of the D3-branes as sourcing the background of closed string fields.[5] Hence, the D3-branes deform the spacetime geometry and the other background fields such that a closed string moving close to the stack of D3-branes propagate in a curved ten-dimensional spacetime. Effectively, replacing the perturbative D3-branes with this curved spacetime geometry is integrating out the strongly coupled open string sector. Now if we take the low energy limit, *i.e.,* $E\ell_s \ll 1$, we are left with two kinds of low energy modes: first, the massless closed string excitations propagating in the asymptotically flat

[5]For example, Newton constant is $G \propto g_s^2$ while the energy density of the stack of D3-branes, *i.e.,* the effective brane tension is $T_3 \propto N/g_s$. Hence the effective source for the gravitational field is $GT_3 \propto g_s N$.

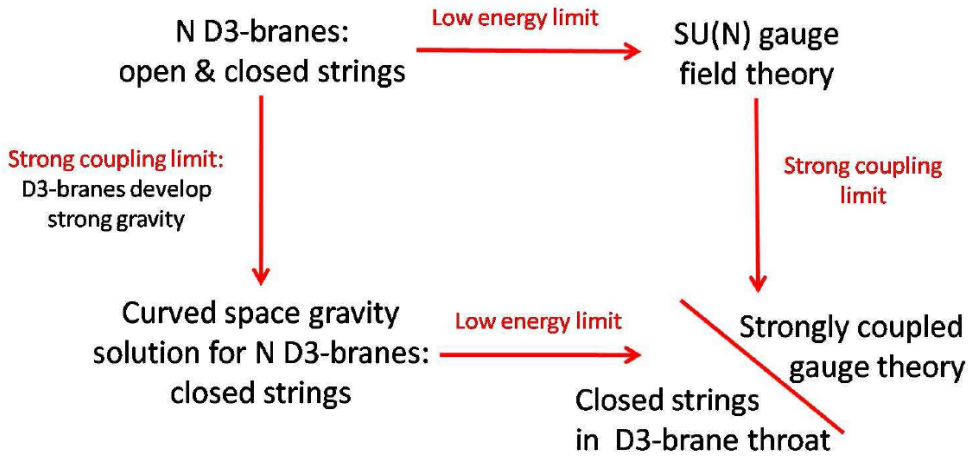

Figure 1.3: Derivation of the AdS/CFT correspondence [178].

region, *i.e.,* far from the branes. Second, all of the closed string modes propagating in the D3-brane throat (close to the stack of D3-branes) are indeed lowest energy modes. Since for an observer at infinity, the energy of these modes are highly red-shifted so that $E\ell_s \ll 1$ is valid for any mode deep in the D3-brane throat. At sufficiently low energies, these two kinds of massless modes are again decoupled. So one can ignore the first ones, *i.e.,* the supergravity modes in the asymptotically flat region, and focus on the second type in the throat. Examining the throat geometry, one realizes that the metric takes the form of $AdS_5 \times S^5$, where the radius of curvature L for both the AdS and sphere is the same and given by

$$\frac{L^4}{\ell_s^4} = g_s N = 2\pi\lambda_t \,. \tag{1.22}$$

Hence, in this second approach we recover the entire ten-dimensional closed string theory however restricted to the throat, *i.e.,* on the $AdS_5 \times S^5$ background. Again Maldacena's conjecture was that the physics of this system was the same as that for the strongly coupled $\mathcal{N} = 4$ super Yang-Mills theory.

1.5 Outline

Motivated by holographic conjecture and gauge/gravity duality, in the rest of this thesis we investigate holographic models describing physical phenomena in three interesting areas: gravity, condensed matter and cosmology.

In chapter 2, we study the entanglement entropy of a general region in a theory of induced gravity using holographic calculations. In particular, we use the holographic entanglement entropy prescription of Ryu-Takayanagi in the context of the Randall-Sundrum 2 model while considering three types of gravity theories in the bulk: the Einstein gravity, the general $f(\mathcal{R})$ gravity and the Gauss-Bonnet gravity. We show the leading term in the entanglement entropy for arbitrary regions on the UV brane is given by the usual Bekenstein-Hawking formula. This result confirms the spacetime entanglement conjecture by Bianchi and Myers for these theories. Moreover, we calculate the first subleading term to entanglement entropy and show they agree with the Wald entropy up to extrinsic curvature terms. Chapter 2 is based on the two following papers:

- Robert C. Myers, Razieh Pourhasan and Misha Smolkin,
  "On Spacetime Entanglement,"
  JHEP 06 (2013) 013 [arXiv:1304.2030]

- Razieh Pourhasan,
  "Spacetime Entanglement with $f(\mathcal{R})$ gravity,"
  Submitted to JHEP [arXiv:1403.0951]

which correspond to references [182, 199] in the bibliography. In the first one which was a collaborative work, I did the calculations and the initial draft of chapter 4 of the paper while supervised by my senior collaborators. The second one is a single authored paper by myself, although I also benefited from discussions with my collaborators on the previous paper. This paper is under review by the referee but has more or less been accepted subject to minor corrections.

In chapter 3, a detailed numerical study of a recent proposal [158] for exotic states of the D3-probe D5 brane system with charge density and an external magnetic field is presented. The state has a large number of coincident D5-branes blowing up to a D7-brane in the presence of the worldvolume electric and magnetic fields which are necessary to construct the holographic state. Numerical solutions have shown that these states can compete with the the previously known chiral symmetry breaking and maximally symmetric phases of the D3-D5 system. Moreover, at integer filling fractions, they are incompressible with integer quantized Hall conductivities. In the dual superconformal defect field theory, these

solutions correspond to states which break the chiral and global flavor symmetries spontaneously. The region of the temperature-density plane where the D7-brane has lower energy than the other known D5-brane solutions is identified. A hypothesis for the structure of states with filling fraction and Hall conductivity greater than one is made and tested by numerical computation. A parallel is drawn with the quantum Hall ferromagnetism or the magnetic catalysis phenomenon, which is observed in graphene. As well as demonstrating that the phenomenon can exist in a strongly coupled system, this work makes a number of predictions of symmetry breaking patterns and phase transitions for such systems. The contents of chapter 3 are from the paper:

- Charlotte Kristjansen, Razieh Pourhasan and Gordon Semenoff,
  "A Holographic Quantum Hall Ferromagnet,"
  JHEP 02 (2014) 097 [arXiv:1311.6999].

which corresponds to reference [157]. This project originated in a discussion with Semenoff about his previous paper with Kristjansen [158] when I suggested to extend that work and look for the solutions at finite temperature. I carried all the numerical calculations except for $\nu = 1$ which was done by Kristjansen.

In chapter 4, we studied an early universe cosmology in a holographic framework. While most of the singularities of General Relativity are expected to be safely hidden behind event horizons by the cosmic censorship conjecture, we happen to live in the causal future of the classical *big bang* singularity, whose resolution constitutes the active field of early universe cosmology. Could the big bang be also hidden behind a causal horizon, making us immune to the impacts of a naked singularity? We describe a braneworld description of cosmology with both four-dimensional induced and five-dimensional bulk gravity (otherwise known as the Dvali-Gabadadze-Porati or DGP model), which exhibits this feature: The universe emerges as a spherical three-brane out of the formation of a five-dimensional Schwarzschild black hole. In particular, we show that a pressure singularity of the holographic fluid, discovered earlier, happens inside the white hole horizon, and thus need not be real or imply any pathology. Furthermore, we outline a novel mechanism through which any thermal atmosphere for the brane, with comoving temperature of approximately 20% of the five-dimensional Planck mass can induce scale-invariant primordial curvature perturbations on the brane, circumventing the need for a separate process (such as cosmic inflation) to explain current cosmological observations. Finally, we note that five-dimensional space-time is asymptotically flat, and thus potentially allows an S-matrix or (after minor modifications) AdS/CFT description of the cosmological big bang. The material in this chapter comes from the following paper:

- Razieh Pourhasan, Niayesh Afshordi and Robert B. Mann,
  "Out of the white hole: a holographic origin for the Big Bang,"
  JCAP 04 (2014) 005 [arXiv:1309.1487]

corresponding to reference [200]. It was featured in *Nature News* and received a great deal of attention in the media. Further, we were invited to write an article, based on our results, for the *Scientific American* which will be published in August 2014. The idea was initiated through a series of discussions with Afshordi and Mann. I did the calculations while supervised by Afshordi and Mann. I also wrote the first draft of the paper except for chapter 4 of the paper which was added by Afshordi.

Finally we close the thesis with a summary of our results and a brief discussion of future direction in chapter 5.

Chapter 2

On Spacetime Entanglement

2.1 Introduction

Considerations of the second law of thermodynamics in the presence of black holes, led Bekenstein[16, 13, 14] to make the bold conjecture some forty years ago that black holes carry an intrinsic entropy given by the surface area of the horizon measured in Planck units multiplied by a dimensionless number of order one. This conjecture was also supported by Hawking's area theorem [115], which shows that, like entropy, the horizon area can never decrease (in classical general relativity). Bekenstein offered arguments for the proportionality of entropy and area, which relied on information theory, as well as the properties of charged rotating black holes in general relativity [16, 13, 14]. Of course, a crucial insight came with Hawking's discovery that external observers around a black hole would detect the emission of thermal radiation with a temperature proportional to its surface gravity [116, 117], *i.e.,* $T = \frac{\kappa}{2\pi}$. Combining this result with the four laws of black hole mechanics [10], the black hole entropy was recognized to be precisely

$$S_{BH} = \frac{\mathcal{A}}{4G}\,, \tag{2.1}$$

where $\mathcal{A}$ is the area of the event horizon. In fact, this expression applies equally well to any Killing horizon, including de Sitter [100] and Rindler [159] horizons. While originally derived with considerations of general relativity in four spacetime dimensions, equation (2.1) also describes the entropy for black hole solutions of Einstein's equations in higher dimensions.[1] Further, it has been shown that the Bekenstein-Hawking (BH) expression (2.1) can

[1] In d spacetime dimensions, the 'area' has units of $length^{d-2}$.

be extended to a general geometric formula, the 'Wald entropy', to describe the horizon entropy in gravitational theories with higher curvature interactions [239, 136, 132].

Of course, much of the interest in black hole entropy, and black hole thermodynamics, stems in the hope that it provides a window into the nature of quantum gravity. A recent conjecture [19] proposes the above area law (2.1) has much wider applicability and serves as a characteristic signature for the emergence of a semiclassical metric in a theory of quantum gravity.[2] The precise conjecture was that in a theory of quantum gravity, for any sufficiently large region in a smooth background spacetime, the entanglement entropy between the degrees of freedom describing a given region with those describing its complement is finite and to leading order, takes the form given in equation (2.1). Of course, an implicit assumption here is that the usual Einstein-Hilbert action (as well as, possibly, a cosmological constant term) emerges as the leading contribution to the low energy effective gravitational action. This conjecture was supported by various lines of evidence: First of all, in the context of gauge/gravity duality, equation (2.1) is applied to general surfaces in evaluating holographic entanglement entropy [204, 203]. Second, it can be shown that in perturbative quantum field theory, the leading area law divergence [26, 221] appearing in calculations of the entanglement entropy for a general region V can be absorbed by the renormalization of Newton's constant in the BH formula applied to the boundary of V, *i.e.,* with the area $\mathcal{A}(\partial V)$. These arguments are framed in terms of the entanglement Hamiltonian describing the reduced density matrix and require understanding certain general properties of the latter operator. However, this new understanding can also be combined with Jacobson's 'thermodynamic' arguments [134, 135] for the origin of gravity to provide further independent support of the above conjecture. A preliminary calculation in loop quantum gravity also provides support for this new idea. Finally, in models of induced gravity [205], certain results [70, 93, 94] were again in agreement with the idea that equation (2.1) describes the entanglement entropy of general regions, in particular even when the entangling surface does not coincide with an event horizon.

In this chapter, we study this conjecture in more detail in the context of induced gravity. In particular, following [70, 94], we will study entanglement entropy in the Randall-Sundrum II (RS2) braneworld [202] and our main result is as follows: The induced gravity action on the brane takes the form

$$I_{ind} = \int d^d x \sqrt{-\tilde{g}} \left[\frac{R}{16\pi G_d} + \frac{\kappa_1}{2\pi} \left(R_{ij} R^{ij} - \frac{d}{4(d-1)} R^2 \right) + \frac{\kappa_2}{2\pi} C_{ijkl} C^{ijkl} + \cdots \right] . \quad (2.2)$$

where the various curvatures are calculated for the brane metric $\tilde{g}_{ij}$ and the ellipsis indicates cubic and higher curvature interactions. The precise value of the d-dimensional Newton's

[2] See also discussion in [56].

constant and the induced couplings of the curvature-squared terms depend on the details of the dual bulk theory and we determine these for two different examples. In principle, these calculations can be extended to higher orders in the derivative expansion but as indicated above, we ignore any contributions beyond curvature-squared. Then with holographic calculations of entanglement entropy, we find for any sufficiently large region V on the brane, the corresponding entanglement entropy is given by

$$\begin{aligned} S_{\rm EE} &= \frac{\mathcal{A}(\tilde{\Sigma})}{4G_d} + \kappa_1 \int_{\tilde{\Sigma}} d^{d-2}y\sqrt{\tilde{h}}\left[2R^{ij}\,\tilde{g}^{\perp}_{ij} - \frac{d}{d-1}\,R - K^iK_i\right] \\ &\quad + 4\kappa_2 \int_{\tilde{\Sigma}} d^{d-2}y\sqrt{\tilde{h}}\left[\tilde{h}^{ac}\tilde{h}^{bd}C_{abcd} - K^i_{ab}K_i{}^{ab} + \frac{1}{d-2}K^iK_i\right] + \cdots\,, \end{aligned} \tag{2.3}$$

where $\tilde{h}_{ab}$ and K^i_{ab} are, respectively, the induced metric and the second fundamental form of the entangling surface $\tilde{\Sigma} = \partial V$. The leading contribution here is captured by the Bekenstein-Hawking formula (2.1), in precise agreement with the conjecture of [19]. We can also compare the above result with the Wald entropy [239, 136, 132] for the induced gravitational action (2.2). Then we find that $S_{\rm EE}$ and $S_{\rm Wald}$ also agree at this order in the derivative expansion, except that the extrinsic curvature terms in equation (2.3) do not appear in the Wald entropy. It is noteworthy that the coefficients of these additional terms are still determined by the higher curvature couplings in the effective gravity action (2.2). We emphasize that our calculations only capture the leading terms in an expansion for large central charge of the braneworld conformal field theory. We should also note that apart from [70, 94], discussions of horizon entropy as entanglement entropy in the RS2 braneworld also appear in [113, 131, 218, 66].

An overview of the remainder of this chapter is as follows: We begin a brief review of the RS2 model as a theory of induced gravity, in section 2.2. In section 2.3, we use holographic entanglement entropy to evaluate $S_{\rm EE}$ for general regions on the RS2 brane, with the result given in equation (2.3). In section 2.4, we consider our results in the context of various inequalities that the entanglement entropy must satisfy. This comparison points out certain limitations with the present approach. Then we conclude with a discussion of our results in section 2.5. Section (2.6) includes some supplementary material which describes various technical details. In section 2.6.1, we derive the induced gravity action on the brane for the case when the dual bulk theory is described by Gauss-Bonnet gravity. Of course, setting the curvature-squared coupling to zero in the previous result yields the induced action for Einstein gravity in the bulk. Section 2.6.2 considers in detail the geometry of the codimension-two surfaces in the bulk and derives various expressions for the curvatures that are useful in deriving the holographic entanglement entropy in section 2.3. In section 2.6.3, we compare the perturbative results for the entanglement entropy

given in section 2.3 with those for the simple case of a spherical entangling surface in flat space where the entire holographic result can be calculated analytically.

2.2 Randall-Sundrum II

In their seminal work [202], Randall and Sundrum showed that standard four-dimensional gravity will arise at long distances on a brane embedded in a noncompact but warped five-dimensional background. Their construction starts by taking two copies of five-dimensional anti-de Sitter (AdS) space and gluing them together along a cut-off surface at some large radius with the three-brane inserted at this junction. This construction readily extends to an arbitrary number of spacetime dimensions to produce gravity on a d-dimensional brane [71] and in fact, it is straightforward to see that the braneworld metric is governed by the full nonlinear Einstein equations in d dimensions, to leading order in a derivative expansion [71]. Our understanding of these Randall-Sundrum II (RS2) models is greatly extended by realizing the close connection with the AdS/CFT correspondence — see [238, 107] and references therein. Given the holographic description of AdS space, we have a dual description of the braneworld which is entirely in d dimensions, namely, gravity, as well as any brane matter, coupled to (two copies of) a strongly coupled CFT with a UV cut-off. Interestingly, in this context, we can think of the RS2 model as a theory of induced gravity [70, 94, 113, 98].

Of course, the key difference between the standard AdS/CFT correspondence and the RS2 model is that the bulk geometry is cut off at some finite $\rho = \rho_c$, which gives rise to a new normalizable zero-mode in the bulk gravity theory. This extra mode is localized at the brane position and becomes the propagating graviton of the d-dimensional gravity theory. One may make use of the calculations and techniques for regulating the bulk theory in AdS/CFT correspondence [72, 60, 217] to determine the action of the induced gravity theory on the brane. We sketch this approach here and relegate a detailed calculation of the boundary action to section 2.6.1.[3] As a theory of $(d+1)$-dimensional gravity, the RS2 model has the following action

$$I_{RS} = 2\, I_{bulk} + I_{brane}\,, \tag{2.4}$$

where I_{bulk} is the bulk gravitational action[4] and I_{brane} includes contributions of matter fields localized on the brane, as well as the brane tension. To determine the effective

[3] Although the context is somewhat different, our approach is similar in spirit to the discussion of boundary actions in [139, 213].

[4] We introduced a factor of two here as a reminder that there are two copies of the AdS geometry.

action for the d-dimensional gravity theory on the brane, one needs to integrate out the extra radial geometry in the AdS bulk. In the context of AdS/CFT correspondence, one must introduce a cut-off radius[5] $\rho = \rho_c$ to regulate this calculation. Of course, in the RS2 model, this cut-off acquires a physical meaning as the position of the brane and so the integral is naturally regulated. The general result takes the form:

$$I_{bulk} = I_{fin} + \sum_{n=0}^{\lfloor d/2 \rfloor} I^{(n)} \,, \tag{2.5}$$

where each of the terms in the sum, $I^{(n)}$, diverges as $\rho_c^{n-d/2}$ in the limit $\rho_c \to 0$,[6] while I_{fin} is a non-local contribution which remains finite in this limit. In fact, each $I^{(n)}$ is given by an integral over the brane of a (local) geometric term constructed from the boundary metric, its curvature and derivatives of the curvature. The label n designates the number of derivatives appearing in the geometric term, *i.e.,* $I^{(n)}$ contains $2n$ derivatives of the metric.

In the context of AdS/CFT correspondence, these expressions can be seen as local divergences that result from integrating out the CFT degrees of freedom with the regulator $\rho = \rho_c$. Boundary counterterms are added to precisely cancel the $I^{(n)}$, allowing one to take the limit $\rho_c \to 0$ with a finite result for the gravitational action [72]. In the context of the RS2 model, the cut-off is fixed, no additional counter-terms are added and the total action (2.4) becomes

$$I_{ind} = 2 \sum_{n=0}^{\lfloor d/2 \rfloor} I^{(n)} + 2I_{fin} + I_{brane} \,. \tag{2.6}$$

Hence, the effective gravitational action on the brane is given by the sum of the geometric terms $I^{(n)}$, which can be interpreted in terms of a standard derivative expansion, *e.g.,* the $n = 0$, 1 and 2 terms will correspond to the cosmological constant term, the Einstein term and a curvature-squared term, respectively. In section 2.6.1, we explicitly illustrate these ideas by deriving these three terms for both Einstein and Gauss-Bonnet gravity in the bulk. In this regard, the brane tension in I_{brane} may be said to play the role of a counter-term, in that we will tune the tension to precisely cancel the $I^{(0)}$ contribution so that the effective cosmological constant vanishes. Further let us note that we must be working in a regime where the brane geometry is weakly curved in order for the above derivative expansion to be effective and for the local gravitational terms to dominate the I_{fin} contribution — see further details in section 2.3.

[5] We will assume that $\rho = 0$ corresponds to the AdS boundary — see section 2.3 from more details.

[6] For even d, the divergence is logarithmic for $n = d/2$.

Above, the bulk cut-off $\rho = \rho_c$ plays an essential role in both the AdS/CFT calculations and the RS2 model. Holography indicates that there is a corresponding short-distance cut-off δ in the dual CFT. Again in the AdS/CFT context, this is simply a convenient regulator and one imagines taking the limit $\delta \to 0$ after the appropriate counterterms are added. In the RS2 model, the cut-off remains fixed and one finds that $\delta = \tilde{L}$, *i.e.,* the short-distance cut-off matches the AdS curvature scale in the bulk.[7] Therefore if δ is to be a small scale, then the bulk AdS geometry is highly curved.

In fact, we can think of the RS2 model as having a single independent scale, *i.e.,* the cut-off δ. To illustrate this point, we focus on the case of Einstein gravity in the bulk forthe following discussion.[8] First of all, we saw that $\tilde{L}$ is fixed by δ above. Another scale in the bulk gravitational theory would be the Planck scale, *i.e.,* $\ell_{P,bulk}^{d-1} \equiv 8\pi G_{d+1}$. The standard AdS/CFT dictionary relates the ratio of the AdS curvature scale to Planck scale in terms of a central charge C_T, which measures the number of degrees of freedom in the boundary CFT. Hence in the RS2 model with $\delta = \tilde{L}$, we define

$$C_T \equiv \pi^2 \, \delta^{d-1} / \ell_{P,bulk}^{d-1} \,. \tag{2.7}$$

Now the construction described above determines the induced couplings of the brane gravity action (2.6) in terms of the bulk Newton's constant (or equivalently $\ell_{P,bulk}$) and the short-distance cut-off. Hence these couplings can also be expressed in terms of δ and C_T. For example, the effective Newton's constant [71] (see also section 2.6.1) is given by

$$G_d = \frac{d-2}{2\,\delta}\, G_{d+1} = \frac{\pi(d-2)}{16}\, \frac{\delta^{d-2}}{C_T} \,. \tag{2.8}$$

Hence, in the RS2 model, both the bulk and boundary Planck scales are derived quantities given in terms of δ and C_T, which we can regard as the fundamental parameters defining the RS2 theory.

We must emphasize that throughout the following, we will assume that $C_T \gg 1$ and our calculations only capture the leading terms in an expansion with large C_T. First of all, this assumption is implicit in the fact that we will treat the bulk gravity theory classically. Quantum corrections in the bulk will be suppressed by inverse powers of C_T. Further,

[7] Note that this result is independent of the choice of ρ_c. Rather in the RS2 model, δ is defined in terms of the induced metric on the brane. This should be contrasted with the standard AdS/CFT approach where the CFT metric defining δ is the boundary metric rescaled by a factor of ρ_c.

[8] As we will see later, the situation for Gauss-Bonnet gravity is slightly more complicated. In particular, the boundary CFT is characterized by two independent central charges, both of which will be assumed to be large — see equations (2.86) and (2.87).

one must imagine that the simple description of the RS2 model, with a discrete cut-off in the AdS bulk, is an approximation to some construction within a UV complete theory, *e.g.,* a stringy construction as described in [238, 237, 152, 149, 6]. In such a scenario, the bulk cut-off will have a more elaborate realization, *e.g.,* where the AdS space would extend smoothly into some compact UV geometry. Hence one should expect that there will be additional contributions to the effective gravitational action (2.6). Effectively, these can be catalogued as additional counterterms (beyond the cosmological constant term) in I_{brane}. However, it is reasonable to expect that these corrections should be independent of the central charge defining the AdS contributions and so they are again suppressed in the limit of large C_T. We might note that in the limit $C_T \gg 1$, we have $\delta \gg \ell_P$ for both the Planck scale in the bulk and on the brane.

Finally, we observed above that the local terms in equation (2.5) can be seen as being generated by integrating out the CFT degrees of freedom in the context of the AdS/CFT correspondence. The same interpretation applies to the RS2 model and so in this sense, this model [70, 94, 113, 98] provides a theory of induced gravity [205]. Such models received particular attention in discussions of the idea that black hole entropy coincides with the entanglement entropy between degrees of freedom inside and outside of the event horizon [133, 91]. In fact, [70] used the RS2 model to illustrate this idea. The approach taken there was to use the usual holographic prescription to calculate entanglement entropy [204, 203]. That is, to calculate the entanglement entropy between a spatial region V and its complement $\bar{V}$ in the d-dimensional boundary theory, one extremizes the following expression

$$S(V) = \underset{v\sim A}{\text{ext}} \frac{\mathcal{A}(v)}{4G_{d+1}} \tag{2.9}$$

over (d–1)-dimensional surfaces v in the bulk spacetime, which are homologous to the boundary region V.[9] In particular then, the boundary of v matches the 'entangling surface' $\Sigma = \partial V$ in the boundary geometry. While a general derivation of equation (2.9) remains lacking, there is a good amount of evidence supporting this proposal in the context of the AdS/CFT correspondence, *e.g.,* see [204, 203, 124, 49, 118]. In [70, 94] and in the following, it is assumed that the same prescription could be applied to the RS2 model. In an expansion for large C_T, it seems reasonable to assume that $S(V)$ is dominated by correlations of the CFT degrees of freedom and equation (2.9) yields the leading contribution to the entanglement entropy. In section 2.4, we discuss further limitations in applying equation (2.9) in the RS2 model.

The essential argument in [70] was that in the RS2 model, extending the event horizon

[9] Hence the 'area' $\mathcal{A}(v)$ to denotes the (d–1)-dimensional volume of v.

of a black hole on the brane into the bulk naturally defines an extremal surface in the AdS geometry. Hence if the entangling surface $\tilde{\Sigma}$ on the brane coincides with the event horizon, equation (2.9) simply evaluates the expected black hole entropy. Similar, considerations were made for de Sitter horizons for the RS2 braneworld in [113]. In [70], calculations were presented for an explicit black hole solution in a $d = 3$ braneworld [71] and it was shown that the leading contribution takes the expected BH form (2.1) for large black holes. However, it was also noted that equation (2.9) yields a finite entanglement entropy for a circular entangling surface in empty (three-dimensional) Minkowski space and further, the leading contribution is again $\mathcal{A}(\tilde{\Sigma})/4G_3$, as long as its radius satisfies $R \gg \delta$. In fact, it is straightforward to see that the holographic prescription (2.9) will yield a finite entanglement entropy in any number of spacetime dimensions and for general entangling surfaces in the RS2 model. We confirm, in the next section, that the leading contribution takes precisely the form $\mathcal{A}(\tilde{\Sigma})/4G_d$ for sufficiently large regions, in agreement with the conjecture of [19]. Similar arguments appeared previously in [94]. Further, we will examine the first higher curvature corrections to the BH expression (2.1).

2.3 Entanglement entropy for general regions

In this section, we use the holographic prescription (2.9) [204, 203] and its generalization to Gauss-Bonnet gravity [124, 59] — see equation (2.49) — to evaluate the entanglement entropy associated with general entangling surfaces on the d-dimensional brane of the RS2 model. Our calculations will make use of the Fefferman-Graham (FG) expansion [83] as developed to describe the boundary theory in the AdS/CFT correspondence [60, 217]. To begin, we write the asymptotic geometry of AdS space in $d+1$ dimensions as[10]

$$ds^2 = G_{\mu\nu} dx^\mu dx^\nu = \frac{\delta^2}{4} \frac{d\rho^2}{\rho^2} + \frac{1}{\rho}\, g_{ij}(x,\rho)\, dx^i dx^j \,, \tag{2.10}$$

[10]Let us comment on our index conventions throughout this chapter. Directions in the full (AdS) geometry are labeled with letters from the second half of the Greek alphabet, *i.e.,* $\mu, \nu, \rho, \cdots$. Letters from the 'second' half of the Latin alphabet, *i.e.,* $i, j, k, \cdots$, correspond to directions in the background geometry on the brane or on the boundary of AdS. Meanwhile, directions along the entangling surface on the brane are denoted with letters from the beginning of the Latin alphabet, *i.e.,* $a, b, c, \cdots$, and directions along the corresponding bulk surface are denoted with letters from the beginning of the Greek alphabet, *i.e.,* $\alpha, \beta, \gamma, \cdots$. Finally, we use hatted letters from the later part of the Latin alphabet to denote frame indices in the transverse space to both of these surfaces, *i.e.,* $\hat{\imath}, \hat{\jmath}$.

where $\delta = \tilde{L}$ is the AdS curvature scale and $\rho = 0$ is the boundary of AdS. Now the metric $g_{ij}(x,\rho)$ admits a series expansion in the (dimensionless) radial coordinate ρ

$$g_{ij}(x,\rho) \;=\; \overset{(0)}{g}_{ij}(x^i) + \rho\, \overset{(1)}{g}_{ij}(x^i) + \rho^2\, \overset{(2)}{g}_{ij}(x^i) + \cdots . \tag{2.11}$$

The leading term $\overset{(0)}{g}_{ij}$ corresponds to the metric on the boundary of AdS space. The next set of contributions in this expansion, *i.e.,* with $n < d/2$ (for either odd or even d), are covariant tensors constructed from this boundary metric [60, 217]. At higher orders $n \geq d/2$, the coefficients $\overset{(n)}{g}_{ij}$ will also depend on the specific state of the boundary CFT that is being described, *e.g.,* $\langle T_{ij}\rangle$. However, in the context of AdS/CFT correspondence, it was shown [126] that only the coefficients with $n < d/2$ contribute to the divergences appearing in the entanglement entropy of the dual CFT. As we will see below, in the RS2 model, the analogous terms become the leading contributions to the entanglement entropy. Moreover, rather than being divergent, they can be expressed in terms of the couplings appearing in the induced gravity action (2.6). These terms will be the focus of our present calculations and so our results will be independent of the state of the CFT.

In fact, the metric coefficients in the range $1 \leq n < d/2$ are almost completely fixed by conformal symmetries at the boundary [127, 207]. For example, the first coefficient in the FG expansion in equation (2.11) is independent of the details of the bulk gravity action and is given by

$$\overset{(1)}{g}_{ij} = -\frac{\delta^2}{d-2}\left(R_{ij}[\overset{(0)}{g}] - \frac{\overset{(0)}{g}_{ij}}{2(d-1)} R[\overset{(0)}{g}] \right), \tag{2.12}$$

where R_{ij} is the Ricci tensor constructed with the boundary metric $\overset{(0)}{g}_{ij}$. At higher orders, certain constants (corresponding to coefficients of conformally covariant tensors) must be fixed by the bulk equations of motion and so depend on the specific bulk gravity theory. For example, for arbitrary $\overset{(0)}{g}_{ij}$, the coefficient $\overset{(2)}{g}_{ij}$ is given by [127, 207]

$$\begin{aligned}
\overset{(2)}{g}_{ij} \;=\; & \delta^4 \Bigg(k_1\, C_{mnkl} C^{mnkl}\, \overset{(0)}{g}_{ij} + k_2\, C_{iklm} C_j{}^{klm} \\
& + \frac{1}{d-4}\left[\frac{1}{8(d-1)} \nabla_i \nabla_j R - \frac{1}{4(d-2)} \Box R_{ij} + \frac{1}{8(d-1)(d-2)} \Box R\, \overset{(0)}{g}_{ij} \right. \\
& - \frac{1}{2(d-2)} R^{kl} R_{ikjl} + \frac{d-4}{2(d-2)^2} R_i{}^k R_{jk} + \frac{1}{(d-1)(d-2)^2} R R_{ij} \\
& \left. + \frac{1}{4(d-2)^2} R^{kl} R_{kl}\, \overset{(0)}{g}_{ij} - \frac{3d}{16(d-1)^2(d-2)^2} R^2\, \overset{(0)}{g}_{ij} \right] \Bigg),
\end{aligned} \tag{2.13}$$

where C_{mnkl} is Weyl tensor for the boundary metric. Above the two constants, k_1 and k_2, will depend on the bulk gravity theory. For example, they vanish with Einstein gravity in the bulk, while with Gauss-Bonnet gravity they are given by equation (2.88).

In the RS2 model, the standard choice which we adopt is to set the position of the brane at $\rho = \rho_c = 1$. A scaling symmetry of the AdS geometry allows us to make this choice without loss of generality. However, note that generally, one thinks of the FG expansion, described by equations (2.10) and (2.11), as being justified because it is applied in the vicinity of the AdS boundary, *i.e.,* for $\rho \ll 1$. Hence, some extra attention is required to justify the FG expansion when it is applied in the RS2 model with the brane at $\rho = 1$. By a simple scaling argument, $\overset{(n)}{g}_{ij}$ contains $2n$ derivatives with respect to the boundary coordinates, as can be seen explicitly in equations (2.12) and (2.13). Hence we can regard the expansion (2.11) as a derivative expansion and it will converge effectively as long as the boundary metric $\overset{(0)}{g}_{ij}$ is weakly curved on the scale of the AdS curvature $\tilde{L}$, which in the RS2 models matches the short-distance cut-off δ in the dual CFT. That is, we will require

$$\delta^2 \, R^{ij}{}_{kl}[\overset{(0)}{g}] \ll 1 \,, \tag{2.14}$$

and similarly for (covariant) derivatives of the curvatures.[11] Further, we must keep in mind that the boundary metric $\overset{(0)}{g}_{ij}$, which as we described above determines the leading coefficients in the FG expansion (2.11), does not match the brane metric. Rather using equations (2.10) and (2.11), the induced metric on the brane is given by

$$\tilde{g}_{ij} = G_{ij}|_{\rho=1} = g_{ij}(x, \rho = 1) = \overset{(0)}{g}_{ij}(x) + \overset{(1)}{g}_{ij}(x) + \cdots = \sum_{n=0}^{\infty} \overset{(n)}{g}_{ij}(x) \,. \tag{2.15}$$

However, note that given the constraint (2.14) on the boundary geometry (and using equation (2.12)), the differences between these two metrics must be small since

$$\tilde{g}_{ij} - \overset{(0)}{g}_{ij} \sim \overset{(1)}{g}_{ij} \ll 1 \,. \tag{2.16}$$

There is a similar (small) shift in the geometry of the entangling surface. Standard calculations, *e.g.,* [124, 126, 127, 207], define the entangling surface Σ on the AdS boundary at $\rho = 0$ — see figure 2.1. Following the holographic prescription (2.9), one determines the corresponding extremal surface σ in the bulk. Now the entangling surface $\tilde{\Sigma}$ on the brane is defined as the intersection of σ with the cut-off surface at $\rho = 1$. Hence the geometries of these two surfaces will not coincide but differences can be precisely determined using the FG expansion, as we show in the following.

[11] One should imagine that the curvature is expressed in an orthonormal frame in this inequality.

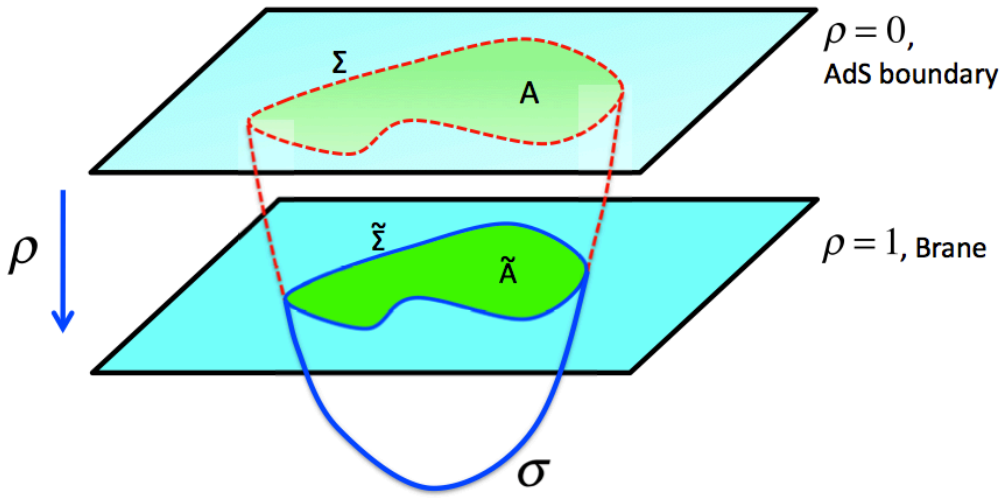

Figure 2.1: The entangling surfaces, Σ on the AdS boundary and $\tilde{\Sigma}$ on the brane, do not quite coincide because of the nontrivial radial profile of the extremal surface v in the bulk.

Given the framework described above and shown in figure 2.1, let y^a with $a = 1, \cdots, d-2$ be coordinates running along the entangling surface Σ in the AdS boundary and let $h_{\alpha\beta}$ be the induced metric on extremal v. Reparametrizations on this bulk surface are fixed by imposing $h_{a\rho} = 0$. In the same way that the FG expansion makes a Taylor series expansion of the bulk metric in the vicinity of the AdS boundary, we can represent the induced metric $h_{\alpha\beta}$ with a Taylor series about $\rho = 0$:[12]

$$h_{\rho\rho} = \frac{\delta^2}{4\rho^2}\left(1 + \overset{(1)}{h}_{\rho\rho}\,\rho + \cdots\right), \qquad h_{ab} = \frac{1}{\rho}\left(\overset{(0)}{h}_{ab} + \overset{(1)}{h}_{ab}\,\rho + \cdots\right), \tag{2.17}$$

where $\overset{(0)}{h}_{ab}$ is the induced metric on the entangling surface Σ. The first order coefficients in this expansion again independent of the specific form of the bulk gravity action and are

[12] For further details, see section 2.6.2.

given by [124, 126, 127, 207]

$$\overset{(1)}{h}_{ab} = \overset{(1)}{g}_{ab} - \frac{\delta^2}{d-2} K^i \, K^j_{ab} \, \overset{(0)}{g}_{ij} \,, \quad \overset{(1)}{h}_{\rho\rho} = \frac{\delta^2}{(d-2)^2} \, K^i \, K^j \, \overset{(0)}{g}_{ij} \,, \tag{2.18}$$

with K^i_{ab} being the second fundamental form of Σ (and $K^i = \overset{(0)}{h}{}^{ab} K^i_{ab}$).[13]

As above, we require that this expansion (2.17) is applicable in the vicinity of the brane at $\rho = 1$. The latter requires both that the background curvatures are small as in equation (2.14) but the characteristic scale of the extrinsic curvatures is also much less than δ, *i.e.,*

$$\delta \, K^i_{ab} \ll 1 \,. \tag{2.19}$$

Analogous inequalities would also have to apply for (covariant) derivatives of K^i_{ab}, as these would appear at higher orders. Further, recall that the entangling surface $\tilde{\Sigma}$ on the brane is defined by the intersection of the extremal surface with $\rho = 1$ and hence equation (2.17) yields

$$\tilde{h}_{ab} = h_{ab}\big|_{\rho=1} = \overset{(0)}{h}_{ab} + \overset{(1)}{h}_{ab} + \cdots \tag{2.20}$$

for the induced metric on the $\tilde{\Sigma}$. Again the curvature constraints, (2.14) and (2.19), ensure that the differences between these two metrics is small, *i.e.,* using equation (2.18), we have

$$\tilde{h}_{ij} - \overset{(0)}{h}_{ij} \sim \overset{(1)}{h}_{ij} \ll 1 \,. \tag{2.21}$$

The discussion up to this point was absolutely general, and there was no need to specify the details of the bulk gravity action in the bulk. However, the detailed expressions for the holographic entanglement entropy across $\tilde{\Sigma}$ are sensitive to the form of this action. Next, we illustrate this calculation using the usual prescription (2.9) for the case where the bulk theory is just Einstein gravity (coupled to a negative cosmological constant). Then we follow with a brief discussion describing results for Gauss-Bonnet gravity in the bulk. In this case, we use the generalized prescription of [124, 59] to calculate the holographic entanglement entropy.

[13] Here we adopt the notation of [127, 207]. Let $n^{\hat{\imath}}{}_j$ (with $\hat{\imath} = 0, 1$) be a pair of orthonormal vectors which span the transverse space to Σ. The extrinsic curvatures are then defined by $K^{\hat{\imath}}_{ab} = \nabla_a n^{\hat{\imath}}{}_b$ and contracting with a normal vector gives $K^i_{ab} = n_{\hat{\jmath}}{}^i \, K^{\hat{\jmath}}_{ab}$. Hence in the following formulae, the extrinsic curvatures carry a coordinate index i, rather than a frame index $\hat{\imath}$.

2.3.1 Einstein gravity

Our bulk gravity action consists of the Einstein-Hilbert action with a negative cosmological constant and we must also include the usual Gibbons-Hawking-York surface term[14]

$$I^{\rm E}_{bulk} = \frac{1}{16\pi G_{d+1}} \int d^{d+1}x\sqrt{-G}\Big[\frac{d(d-1)}{\delta^2} + \mathcal{R}\Big] + \frac{1}{8\pi G_{d+1}} \int d^d x\sqrt{-\tilde{g}}\,\mathcal{K}\ . \tag{2.22}$$

In section 2.6.1, we show that with this bulk theory, the induced gravity action on the brane is given by

$$I^{\rm E}_{ind} = \int d^d x\sqrt{-\tilde{g}}\left[\frac{R}{16\pi G_d} + \frac{\kappa_1}{2\pi}\left(R_{ij}R^{ij} - \frac{d}{4(d-1)}R^2\right) + \mathcal{O}(\partial^6)\right]\ , \tag{2.23}$$

where the expressions defining the effective Newton's constant and the curvature-squared coupling in terms of δ and G_{d+1} or the central charge are given in equations (2.107) and (2.108).

The holographic entanglement entropy for generic entangling surfaces in the boundary is evaluated using equation (2.9). We begin by evaluating the area $\mathcal{A}(\sigma)$ of the extremal surface to the first two leading orders in the expansion given in equation (2.17)[15]

$$\begin{aligned}\mathcal{A}(\sigma) &= 2\int d^{d-2}y\, d\rho\,\sqrt{h} \\ &= \int_{\tilde{\Sigma}} d^{d-2}y \int_1^\infty d\rho\,\frac{\delta}{\rho^{d/2}}\sqrt{\overset{(0)}{h}}\left[1 + \left(\overset{(1)}{h}_{\rho\rho} + \overset{(0)}{h}^{ab}\ \overset{(1)}{h}_{ab}\right)\frac{\rho}{2} + \mathcal{O}(\partial^4)\right]\ .\end{aligned} \tag{2.24}$$

Now we can use equation (2.20) to re-express this result in terms of induced metric on the brane $\tilde{h}_{ab}$ rather than the boundary metric $\overset{(0)}{h}_{ab}$. In particular, we have

$$\sqrt{\overset{(0)}{h}} = \sqrt{\tilde{h}}\left(1 - \frac{1}{2}\overset{(0)}{h}^{ab}\overset{(1)}{h}_{ab} + \mathcal{O}(\partial^4)\right)\ . \tag{2.25}$$

Recall that the difference between the two metrics is small, as shown in equation (2.21). Therefore explicitly applying the conversion to $\tilde{h}_{ab}$ in the first-order terms here and in equation (2.24) is not necessary. This would only generate terms of order $O(\partial^4)$, which

[14] Calligraphic $\mathcal{R}$ and $\mathcal{K}$ will be used to denote bulk curvature and the second fundamental form of the brane respectively. We implicitly assume that bulk integral runs over both copies of the AdS space whereas surface integral is carried over both sides of the brane.

[15] Factor two accounts for the two copies of AdS space in the construction.

we are not evaluating here. Now carrying out integration over ρ in equation (2.24) (and keeping only the lower limit at $\rho = 1$) yields

$$S_{\rm EE} = \frac{\delta}{2(d-2)G_{d+1}} \int_{\tilde{\Sigma}} d^{d-2}y \sqrt{\tilde{h}} \left[1 + \frac{d-2}{2(d-4)} \overset{(1)}{h}{}_{\rho\rho} + \frac{1}{d-4} \overset{(0)}{h}{}^{ab} \overset{(1)}{h}{}_{ab} + \mathcal{O}(\partial^4) \right] . \quad (2.26)$$

Finally we can substitute for $\overset{(1)}{h}{}_{\alpha\beta}$ using equation (2.18) and at the same time, we use equations (2.107) and (2.108) to express the result in terms of the gravitational couplings in the induced action (2.23). Our final expression for the entanglement entropy becomes

$$S_{\rm EE} = \frac{\mathcal{A}(\tilde{\Sigma})}{4G_d} + \kappa_1 \int_{\tilde{\Sigma}} d^{d-2}y \sqrt{\tilde{h}} \left(2R^{ij}\, \tilde{g}^{\perp}_{ij} - \frac{d}{d-1} R - K^i K_i \right) + \mathcal{O}(\partial^4) . \quad (2.27)$$

Here, all curvatures are evaluated on the entangling surface $\tilde{\Sigma}$ and $\tilde{g}^{\perp}_{ij} = \eta_{\hat{i}\hat{j}}\, n^{\hat{i}}_i\, n^{\hat{j}}_j$ is the metric in the transverse space to the entangling surface, *i.e.*, $\tilde{g}^{\perp}_{ij} = \tilde{g}_{ij} - \tilde{h}_{ij}$.

The first important feature to note about this result is that leading term precisely matches the BH formula (2.1) for the induced gravity theory (2.23). However, here it appears in $S_{\rm EE}$ for a general entangling surface rather than a horizon entropy. That is, subject to the constraints in equations (2.14) and (2.19) in this RS2 model, we find that the leading contribution to the entanglement entropy for any general (large) regions is given precisely by the Bekenstein-Hawking formula. Of course, this result precisely matches the conjecture of [19]!

The next-to-leading term in equation (2.27) reveals a non-trivial correction to the area law. The appearance of κ_1 here suggests that it is connected to the curvature-squared interaction appearing in the induced gravity action (2.23). Of course, this connection naturally brings to mind the Wald entropy [239, 136, 132], which describes the horizon entropy of (stationary) black hole solutions in theories with higher curvature interactions. In particular, let $\tilde{\Sigma}$ be (a cross-section of) a Killing horizon in a gravity theory with a general (covariant) Lagrangian $\mathcal{L}(g, R, \nabla R, \cdots)$. Then the Wald entropy is [239, 136, 132]

$$S_{\rm Wald} = -2\pi \int_{\tilde{\Sigma}} d^{d-2}y \sqrt{\tilde{h}}\, \frac{\partial \mathcal{L}}{\partial R^{ij}{}_{kl}}\, \hat{\varepsilon}^{ij}\, \hat{\varepsilon}_{kl} , \quad (2.28)$$

where as above, $\tilde{h}_{ab}$ is the induced metric on $\tilde{\Sigma}$ and $\hat{\varepsilon}_{ij}$ is the volume-form in the two-dimensional transverse space to $\tilde{\Sigma}$. Some useful identities for the latter include:[16]

$$\hat{\varepsilon}_{ij}\, \hat{\varepsilon}_{kl} = \tilde{g}^{\perp}_{il}\, \tilde{g}^{\perp}_{jk} - \tilde{g}^{\perp}_{ik}\, \tilde{g}^{\perp}_{jl} , \qquad \hat{\varepsilon}_{ik}\, \hat{\varepsilon}_j{}^k = -\tilde{g}^{\perp}_{ij} , \quad \hat{\varepsilon}_{ij}\, \hat{\varepsilon}^{ij} = -2 . \quad (2.29)$$

[16] Recall that the signature of the transverse space is $(-,+)$.

Applying equation (2.28) (as well as the above identities) to the induced gravity theory (2.23), we obtain

$$S_{\rm Wald} = \frac{\mathcal{A}(\tilde{\Sigma})}{4G_d} + \kappa_1 \int_{\tilde{\Sigma}} d^{d-2}y\sqrt{\tilde{h}}\left(2R^{ij}\,\tilde{g}^{\perp}_{ij} - \frac{d}{d-1}\,R\right) + \mathcal{O}(\partial^4)\,. \tag{2.30}$$

Comparing equations (2.27) and (2.30), we see that $S_{\rm EE}$ and $S_{\rm Wald}$ agree up to the absence of the extrinsic curvature terms in the Wald entropy. However, this discrepancy might have been expected since, as we emphasized above, the Wald formula (2.28) was constructed to be applied to Killing horizons, for which the extrinsic curvature vanishes.[17] Hence if equation (2.27) is evaluated on a Killing horizon, we will find $S_{\rm EE} = S_{\rm Wald}$. Note that this match for boundary black holes between the entanglement entropy (2.27) and the Wald entropy (2.30) was previously observed in [218].

2.3.2 $f(\mathcal{R})$ gravity

In the next two sections, we will consider extended theories of gravity in the bulk as a generalization of the usual Einstein-Hilbert action (2.22). In particular in this section, we study the RS2 model with $f(\mathcal{R})$ gravity where f is an arbitrary function of the Ricci scalar [220] as an interesting toy-model. Thus the action for the AdS_{d+1} bulk becomes

$$I_{bulk} = \frac{1}{16\pi G_{d+1}}\int d^dx\,d\rho\,\sqrt{-G}\left[\frac{d(d-1)}{L^2} + f(\mathcal{R}(G))\right] + I_{surf} \tag{2.31}$$

where G_{d+1} is the gravitational constant in the bulk metric $G_{\mu\nu}$, L is the scale of cosmological constant and $\mathcal{R}$ is the curvature scalar in the bulk. As before, the dimensionless coordinate ρ is the extra radial direction in the bulk and x^i are the coordinates along the brane located at $\rho = \rho_c$ whereas $\rho = 0$ would be the boundary of AdS_{d+1}. Note that the AdS_{d+1} geometry again has a radius of curvature δ which matches the short-distance cut-off in the boundary theory. However, we will see that the AdS_{d+1} scale no longer corresponds to the scale of the cosmological constant, *i.e.*, $\delta \neq L$. To have a well-defined variational principle, the proper surface term is added to the action (2.31) with the form [69]

$$I_{surf} = \frac{1}{8\pi G_{d+1}}\int d^dx\sqrt{-\tilde{g}}\,\mathcal{K}\,f'(\mathcal{R})|_{\rho=\rho_c}\,, \tag{2.32}$$

[17] On a Killing horizon, the extrinsic curvature will vanish precisely on the bifurcation surface. For a general cross-section of the Killing horizon, the extrinsic curvature is nonvanishing but only for a null normal vector. Hence one finds that any scalar invariants constructed with the extrinsic curvature still vanish, *e.g.*, in general, $K^i \neq 0$ however $K^iK_i = 0$.

where $\mathcal{K}$ is the trace of second fundamental form of the metric on the brane and prime denotes a derivative with respect to $\mathcal{R}$.

We use Fefferman-Graham gauge (2.10) for the metric in the bulk. However δ, the curvature radius of AdS_{d+1}, is related to the cosmological constant L and the gravitational couplings implicit in $f(\mathcal{R})$ through the equation of motion in the bulk, *i.e.,*

$$f'(\mathcal{R})\mathcal{R}_{\mu\nu} + \left(G_{\mu\nu}\nabla^{\sigma}\nabla_{\sigma} - \nabla_{\mu}\nabla_{\nu}\right)f'(\mathcal{R}) - \frac{G_{\mu\nu}}{2}\left(f(\mathcal{R}) + \frac{d(d-1)}{L^2}\right) = 0\,. \tag{2.33}$$

That is, if one inserts the metric (2.10) with $g_{ij} = \eta_{ij}$, *i.e.,* pure AdS space, into equation of motion (2.33) one obtains

$$\frac{1}{L^2} = -\frac{1}{d(d-1)\delta^2}\left[2df'(\mathcal{R}_0) + \delta^2 f(\mathcal{R}_0)\right], \tag{2.34}$$

where $\mathcal{R}_0$ is the curvature of AdS_{d+1} spacetime, *i.e.,*

$$\mathcal{R}_0 = -\frac{d(d+1)}{\delta^2}\,. \tag{2.35}$$

One can obtain the induced gravity action on the brane by integrating out the extra radial dimension of the bulk action (2.31). To do so, we use the derivative expansion (2.11) for the metric g_{ij} about the position of the brane. The two constants k_1 and k_2 in expression (2.13) depend on the type of gravity theory in the bulk. By solving the equation of motion (2.33) for $f(\mathcal{R})$ in the bulk, one explicitly finds k_1, $k_2 = 0$. The latter are most easily determined if one picks a fixed geometry on the boundary for $\overset{(0)}{g}_{ij}$ and then plugs the metric expansion (2.10) into equation of motion (2.33).

Also, using the expansion (2.97) one finds

$$\mathcal{R} = \mathcal{R}_0 + \cdots\,, \tag{2.36}$$

since we are just interested in the terms up to curvature squared, we don't really need to specify ellipsis which are of $\mathcal{O}(\partial^6)$ and higher. Indeed, as it is manifest in the expansion (2.97), the only curvature squared term has a coefficient depending on the constants k_1 and k_2. However, this term is absent in the present case with $f(\mathcal{R})$ gravity for which k_1 and k_2 are both zero.

In order to calculate the induced gravity action on the brane which is given by expression (2.4), we also need to find the derivative expansions for the extrinsic curvature. Using equation (2.92) one can easily derive (up to curvature squared terms)

$$\mathcal{K} = \frac{1}{\delta}\left[d + \frac{\delta^2}{2(d-1)}R + \frac{\delta^4}{2(d-1)(d-2)^2}\left(R_{ij}R^{ij} - \frac{d}{4(d-1)}R^2\right)\right] + \mathcal{O}(\delta^6)\,. \tag{2.37}$$

Note that curvatures in the above expression are constructed from the brane metric $\tilde{g}_{ij}$.

Finally putting together equations (2.4), (2.31) and (2.32) while using the derivative expansions for the bulk and brane metrics and curvatures as well as the constraint (2.34) and integrating over the radial direction ρ we get

$$I_{ind} = \int d^d x \sqrt{-\tilde{g}} \left[\frac{R}{16\pi G_d} + \frac{\kappa_1}{2\pi} \left(R_{ij} R^{ij} - \frac{d}{4(d-1)} R^2 \right) + \cdots \right] . \tag{2.38}$$

The ellipsis in the induced action (2.38) are of order $\mathcal{O}(\partial^6)$ and higher and

$$\frac{1}{G_d} = \frac{2\delta}{d-2} \frac{f'(\mathcal{R}_0)}{G_{d+1}} , \qquad \kappa_1 = \frac{\delta^3}{4(d-2)^2(d-4)} \frac{f'(\mathcal{R}_0)}{G_{d+1}} , \tag{2.39}$$

with $\mathcal{R}_0$ is given by equation (2.35) and we have tuned the brane tension to be

$$T_{brane} = \frac{d-1}{4\pi\delta G_{d+1}} f'(\mathcal{R}_0) . \tag{2.40}$$

Note that all the curvatures in the induced action (2.38) are constructed from the brane metric $\tilde{g}_{ij}$. Also, since the effective Newton constant and the brane tension are positive, then $f'(\mathcal{R}_0)$ and consequently the coupling κ_1 are positive. So far, we have found the effective Newton constant of the brane G_d in terms of the bulk gravitational constant G_{d+1}. Moreover, we have an additional parameter κ_1 on the brane which is expressed in terms of bulk gravity parameters. It is worth to mention that the expression (2.38) for the induced action has the same form as previously obtained for the induced action (2.23) in Einstein gravity. However, the effective Newton constant G_d and the coupling κ_1 have different definitions in terms of the bulk gravitational couplings.

Now, in order to calculate the leading term and the first subleading term of the entanglement entropy of a general surface on the brane with $f(\mathcal{R})$ gravity in the bulk, we need to find the appropriate entropy functional for the bulk surface σ and then extremise the functional to find holographic entanglement entropy [125]. A natural guess with a general covariant Lagrangian $\mathcal{L}(g, R, \nabla R, \cdots)$ would be the Wald entropy formula (2.28). However, this is known not to be correct in general [125]. In general, one must add terms involving the second fundamental forms of the boundary of σ. However there is evidence such terms do not occur for $f(\mathcal{R})$ gravity, *e.g.,* using a novel method called squashed cone, it has been shown in [97] that for the bulk action of the $\mathcal{R}^2$ form, which is specific form of $f(\mathcal{R})$, no extrinsic curvature appears in the entanglement entropy. Also performing a field redefinition, one can show that $f(\mathcal{R})$ gravity can be transformed into a pure Einstein gravity minimally coupled to matter [240]. For the latter, the entropy functional is simply

$A/4G$ and transforming back yields no $\mathcal{K}$ terms. Therefore, we assume in order to obtain the entropy functional associated with the bulk surface σ for $f(\mathcal{R})$ gravity in the bulk, it is enough to use the Wald entropy formula (2.28). This yields

$$S_\sigma = \frac{1}{2G_{d+1}} \int_{\widetilde{\Sigma}} d^{d-2}y \int_1^\infty d\rho \sqrt{h} f'(\mathcal{R}) \,, \tag{2.41}$$

where y^i are the coordinates along the entangling surface $\widetilde{\Sigma}$ and $h_{\alpha\beta}$ is the induced metric on the codimension-2 surface σ with its components are given by expression (2.17). Applying Taylor expansion for $f(\mathcal{R})$ and integrating over the radial direction ρ from the location of the brane to infinity we get

$$S_{EE} = \frac{\delta}{2(d-2)G_{d+1}} \int d^{d-2}y \sqrt{\tilde{h}} f'(\mathcal{R}_0) \left[1 + \frac{d-2}{2(d-4)} \overset{(1)}{h}_{\rho\rho} + \frac{1}{d-4} \overset{(0)}{h}^{ab} \overset{(1)}{h}_{ab} + \cdots \right] , \tag{2.42}$$

where we have used equation (2.25). Note that there is no f'' term in expression (2.42), since curvature squared term is absent in the derivative expansion (2.36).

Finally if we use equation (2.18) along with the expressions in (2.39) for the effective Newton constant G_d and parameter κ_1 we can rewrite the entanglement entropy (2.42) as following

$$S_{EE} = \frac{\mathcal{A}(\widetilde{\Sigma})}{4G_d} + \kappa_1 \int_{\widetilde{\Sigma}} d^{d-2}y \sqrt{\tilde{h}} \left(2R^{ij} \tilde{g}^\perp_{ij} - \frac{d}{d-1} R - K^i K_i \right) + \mathcal{O}(\partial^4) \,. \tag{2.43}$$

It is clear that the leading term is just the area law as it has been already conjectured in [19]. Again one should note that the expression (2.43) for entanglement entropy has the same form as previously obtained for the entanglement entropy (2.27) in Einstein gravity in the bulk. The only distinction is that the effective Newton constant G_d and the coupling κ_1 are defined differently in terms of bulk parameters.

Moreover, the first subleading term can also teach us an interesting lesson: Let's evaluate the Wald entropy associated to the entangling surface $\widetilde{\Sigma}$ by directly applying the Wald formula (2.28) for this surface which is a codimension-2 hypersurface on the brane with induced action (2.38). Doing so, one obtains

$$S_{\widetilde{\Sigma}} = \frac{\mathcal{A}(\widetilde{\Sigma})}{4G_d} + \kappa_1 \int_{\widetilde{\Sigma}} d^{d-2}y \sqrt{\tilde{h}} \left(2R^{ij} \tilde{g}^\perp_{ij} - \frac{d}{d-1} R \right) + \mathcal{O}(\partial^4) \,. \tag{2.44}$$

where we have used the following identities:

$$\hat{\varepsilon}_{ik} \hat{\varepsilon}_j{}^k = -\tilde{g}^\perp_{ij} \,, \qquad \hat{\varepsilon}_{ij} \hat{\varepsilon}^{ij} = -2 \,. \tag{2.45}$$

Now comparing equations (2.43) with (2.44), it is evident that the entanglement entropy for a general surface agrees to the Wald entropy up to the extrinsic curvature terms. In fact, if the entangling surface is a *Killing horizon*, for which extrinsic curvatures are vanishing, then both entropies coincide. However, for a general entangling surface, the Wald entropy does not give the whole entanglement entropy for the surface; there are some contributions to the entanglement entropy from non vanishing extrinsic curvature terms which they do not appear in the Wald entropy. Indeed, the fact that the entanglement entropy cannot be completely extracted from the Wald formula has been recently studied in [182, 97, 64].

2.3.3 Gauss-Bonnet gravity

In this section we analyze another higher curvature theory of gravity in the bulk. In particular, our discussion will focus on Gauss-Bonnet (GB) gravity, and as before, we regard the latter as simply a convenient toy-model which may provide some insights into more general bulk theories. The bulk action is given by

$$I^{\rm GB}_{bulk} = \frac{1}{16\pi G_{d+1}} \int d^{d+1}x \sqrt{-G} \left[\frac{d(d-1)}{L^2} + \mathcal{R} + \frac{L^2\,\lambda}{(d-2)(d-3)}\,\chi_4 \right] + I^{\rm GB}_{surf}\,. \tag{2.46}$$

where χ_4 is proportional to the four-dimensional Euler density,

$$\chi_4 = \mathcal{R}_{\mu\nu\rho\sigma}\mathcal{R}^{\mu\nu\rho\sigma} - 4\,\mathcal{R}_{\mu\nu}\mathcal{R}^{\rho\sigma} + \mathcal{R}^2\,. \tag{2.47}$$

The detailed form of the surface term $I^{\rm GB}_{surf}$ is given in equation (2.83). Now with the above bulk action, we showed in section 2.6.1 that the induced gravity action for the RS2 braneworld becomes

$$I^{\rm GB}_{ind} = \int d^dx\sqrt{-\tilde{g}} \left[\frac{R}{16\pi G_d} + \frac{\kappa_1}{2\pi}\left(R_{ij}R^{ij} - \frac{d}{4(d-1)}R^2 \right) + \frac{\kappa_2}{2\pi}\,C_{ijkl}C^{ijkl} + \mathcal{O}(\partial^6) \right]. \tag{2.48}$$

where C_{ijkl} is the Weyl tensor of the brane geometry. The d-dimensional Newton's constant and the couplings for the curvature-squared terms are defined in equations (2.103–2.105).

The prescription for the holographic entanglement entropy is modified for GB gravity [124, 59]. In particular, it still involves extremizing over bulk surfaces as in the original prescription (2.9) but the functional to be evaluated on these surfaces is no longer the BH formula. Rather the latter is replaced by the following expression:

$$S_{\rm JM} = \frac{1}{2G_{d+1}} \int_\sigma d^{d-2}y\, d\rho\sqrt{h} \left[1 + \frac{2\,L^2\,\lambda}{(d-2)(d-3)}\,\mathcal{R} \right] + \frac{2\,L^2\,\lambda}{(d-2)(d-3)G_{d+1}} \int_{\tilde{\Sigma}} \mathcal{K}\,, \tag{2.49}$$

where $\mathcal{R}$ is intrinsic curvature of the bulk surface σ, $\mathcal{K}$ is the trace of the second fundamental form on the boundary of σ, which coincides with the entangling surface $\tilde{\Sigma}$ on the brane. In equation (2.49), we already introduced a factor two to account for both copies of AdS space on either side of the brane. Apart from this factor of two, we note that $S_{\rm JM}$ was derived to describe black hole entropy in GB gravity [137] but it only coincides with $S_{\rm Wald}$ for surfaces with vanishing extrinsic curvature [124].

As before, we assume that the background geometry on the brane and the entangling surface $\tilde{\Sigma}$ are big enough such that equations (2.14) and (2.19) are satisfied. Then derivative expansion can be applied to make a Taylor series expansion of the intrinsic and extrinsic curvatures, $\mathcal{R}$ and $\mathcal{K}$, however, we relegate details to section 2.6.2. Substituting equations (2.115) and (2.117) into equation (2.49) and integrating out radial direction ρ, yields

$$\begin{aligned} S_{\rm EE} &= \frac{\mathcal{A}(\tilde{\Sigma})}{4G_d} + \kappa_1 \int_{\tilde{\Sigma}} d^{d-2}y\sqrt{\tilde{h}}\left[2R^{ij}\,\tilde{g}^{\perp}_{ij} - \frac{d}{d-1}\,R - K^iK_i\right] \\ &\quad + 4\kappa_2 \int_{\tilde{\Sigma}} d^{d-2}y\sqrt{\tilde{h}}\left[\tilde{h}^{ac}\tilde{h}^{bd}C_{abcd} - K^i_{ab}K_i{}^{ab} + \frac{1}{d-2}K^iK_i\right] + \mathcal{O}(\partial^4)\,. \end{aligned} \tag{2.50}$$

Again, we find that in this RS2 model, the leading contribution to the entanglement entropy evaluated for arbitrary large regions is given precisely by the Bekenstein-Hawking formula (2.1), in agreement with the conjecture of [19]. As in the previous section, we can also compare above result with the Wald entropy (2.28) for the induced gravitational action (2.48). Again $S_{\rm EE}$ and $S_{\rm Wald}$ match except that the extrinsic curvature terms above do not appear in the Wald entropy.

As a final note, it is amusing to observe that the geometric terms appearing in equation (2.50) are almost the same. Using the geometric identities provided in section 2.6.2, we can write

$$\begin{aligned} 2R^{ij}\,\tilde{g}^{\perp}_{ij} - \frac{d}{d-1}\,R - K^iK_i = \\ \frac{d-2}{d-3}\left[\tilde{h}^{ac}\tilde{h}^{bd}C_{abcd} - K^i_{ab}K_i{}^{ab} + \frac{1}{d-2}K^iK_i - R_{\tilde{\Sigma}}\right]\,, \end{aligned} \tag{2.51}$$

where $R_{\tilde{\Sigma}}$ denotes the intrinsic Ricci scalar of the entangling surface $\tilde{\Sigma}$. Given this expression, equation (2.50) can be rewritten as

$$\begin{aligned} S_{\rm EE} &= \frac{\mathcal{A}(\tilde{\Sigma})}{4G_d} - \frac{d-2}{d-3}\,\kappa_1 \int_{\tilde{\Sigma}} d^{d-2}y\sqrt{\tilde{h}}\;R_{\tilde{\Sigma}} \\ &\quad + \kappa_3 \int_{\tilde{\Sigma}} d^{d-2}y\sqrt{\tilde{h}}\left[\tilde{h}^{ac}\tilde{h}^{bd}C_{abcd} - K^i_{ab}K_i{}^{ab} + \frac{1}{d-2}K^iK_i\right] + \mathcal{O}(\partial^4)\,, \end{aligned} \tag{2.52}$$

where

$$\kappa_3 = 4\,\kappa_2 + \frac{d-2}{d-3}\,\kappa_1 = \frac{2}{\pi(d-2)(d-3)(d-4)}\,\frac{C_T}{\delta^{d-4}}\,. \tag{2.53}$$

The last expression for the new coupling κ_3 comes from combining equations (2.104) and (2.105). Now it is interesting to consider this result in the special case $d = 4$. In this case, the κ_n couplings are all dimensionless, but at the same time the expressions that we have provided above and in section 2.6.1 are not quite correct — they all appear to diverge because of a factor $1/(d-4)$. Re-visiting the derivation of these expressions, one finds that in fact these couplings contain a logarithmic dependence on the cut-off δ. In particular, we write for $d = 4$:

$$\kappa_1 = -\frac{a_d^*}{2\pi}\log(\mu\delta)\,, \qquad \kappa_3 = -\frac{C_T}{\pi}\log(\mu\delta)\,. \tag{2.54}$$

where μ is some renormalization scale. Further note that with the normalization chosen in equations (2.86) and (2.87), the central charges, C_T and a_d^* match precisely the standard central charges appearing in the trace anomaly, *i.e.*, $a_d^* = a$ and $C_T = c$ [185, 186, 34]. Hence, the entanglement entropy (2.52) becomes, for $d = 4$

$$\begin{aligned} S_{\text{EE}} \;&=\; \frac{\mathcal{A}(\tilde{\Sigma})}{4G_4} \\ &-\frac{\log(\mu\delta)}{\pi}\int_{\tilde{\Sigma}} d^{d-2}y\sqrt{\tilde{h}}\left(c\left[\tilde{h}^{ac}\tilde{h}^{bd}C_{abcd} - K^i_{ab}K_i{}^{ab} + \frac{1}{d-2}K^iK_i\right] - a\,R_{\tilde{\Sigma}}\right) + \cdots\,. \end{aligned} \tag{2.55}$$

We can recognize the second term above as the universal contribution to the entanglement entropy of a four-dimensional CFT [219]. Actually, the attentive reader may notice that there is an extra overall factor of two, which arises because there are actually two copies of the CFT corresponding to the two copies of AdS space.

2.4 Beyond the Area

Recent progress has revealed an interesting interplay between entanglement entropy and renormalization group flows, *e.g.*, [185, 186, 46, 47, 48, 165, 184]. One important result is an elegant proof for the c-theorem in two dimensions [245] formulated in terms of entanglement entropy [46, 47]. In particular, one begins by considering the entanglement entropy on an interval of length ℓ and then evaluates

$$C_2(\ell) \equiv \ell\,\partial_\ell S(\ell)\,. \tag{2.56}$$

If the underlying field theory is a two-dimensional CFT, then C_2 is a constant independent of ℓ and in fact, $3\,C_2 = c$, the central charge characterizing the CFT. Now in general, if one assumes only Lorentz invariance, unitarity and strong subadditivity [164], one can demonstrate [46, 47]

$$\partial_\ell C_2(\ell) \leq 0\,. \tag{2.57}$$

Therefore comparing C_2 found at short scales with that determined by probing the system at long distances, one has $[C_2]_{UV} \geq [C_2]_{IR}$ and of course, if the underlying field theory describes an RG flow connecting two fixed points, then the same inequality holds for the corresponding central charges. In an exciting recent development, [48] extended this construction to prove an analogous c-theorem which had been conjectured for three dimensions [185, 186, 138, 155]. In three dimensions, one considers the entanglement entropy of a disk of radius R and arrives at the following construction [48, 165]

$$C_3(R) \equiv R\,\partial_R S(R) - S(R)\,, \tag{2.58}$$

which yields an interesting (constant) central charge in the case where the underlying theory is a CFT. In general, again with the assumptions of Lorentz invariance, unitarity and strong subadditivity, one can establish the following inequality:

$$\partial_R C_3(R) = R\,\partial_R^2 S \leq 0\,, \tag{2.59}$$

which establishes the three-dimensional version of the c-theorem.

Now, turning to higher dimensions, one can observe [184, 121] the inequality (2.57) will still apply in any situation where the background geometry preserves Lorentz symmetry in a plane and the entangling surface is chosen as two points (spacelike) separated in this plane by a distance ℓ. The simplest example to consider is a 'strip' or 'slab' geometry in R^d, *i.e.,* the entangling surface is chosen to be two parallel $(d-2)$-dimensional planes separated by a distance ℓ along the x-axis — see figure 2.2a. As before, one can evaluate the entanglement entropy for the region between the two planes and then construct the function $C_2(\ell)$, as in equation (2.56). However, note that $C_2(\ell)$ will not be a constant even when the underlying theory is a CFT for $d \geq 3$ [184]. The geometric approach of [46, 47] only relies on making Lorentz transformations in the (t, x)-plane and then comparing entropies for different pairs of planes. Hence with the same assumptions of Lorentz invariance, unitarity and strong subadditivity, the inequality (2.57) again holds in this situation.

Similarly, the inequality (2.59) will apply in higher dimensions, as long as the background geometry preserves Lorentz symmetry in a three-dimensional Minkowski subspace and the entangling surface is chosen as a circle in a spacelike plane in this subspace (without any additional structure in the extra dimensions). Of course, the simplest example to

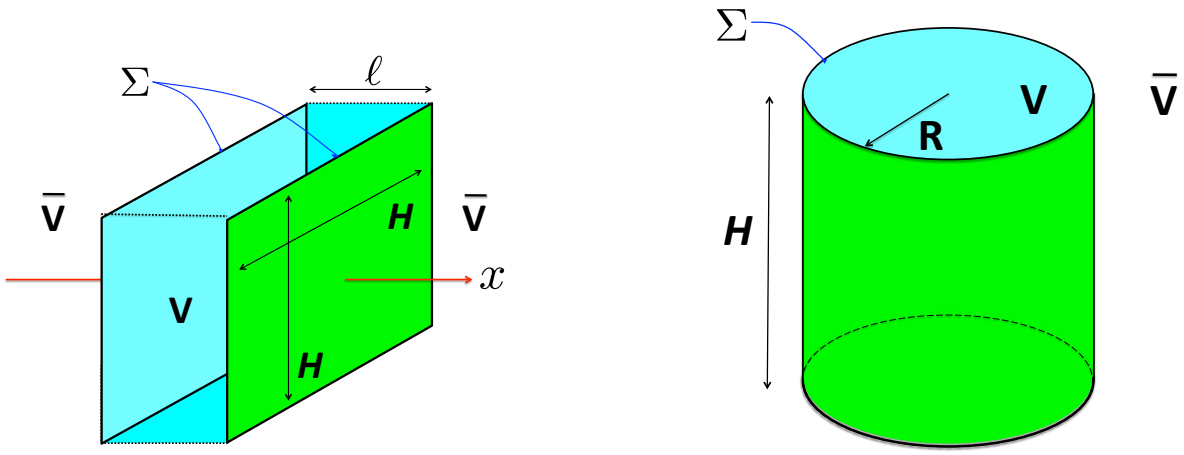

Figure 2.2: Panel (a) shows the slab geometry on a constant time slice. The entangling surface consists of two parallel (hyper)planes separated by a distance ℓ. The reduced density matrix is calculated for the region V between these two planes by integrating out the degrees of freedom in the exterior region $\bar{V}$. Panel (b) shows a cylindrical entangling geometry with radius R. In both cases, the distance H is introduced to regulate the area of the entangling surfaces.

consider is a cylindrical entangling surface in R^d, *i.e.,* the $(d-2)$-dimensional entangling surface has topology $S^1 \times R^{d-3}$, as shown in figure 2.2b. Here the approach of [48] can again be applied to establish the inequality (2.59) for $C_3(R)$, which is again constructed as in equation (2.58).

In the following, we will consider testing our holographic results for the RS2 model with the above inequalities, (2.57) and (2.59). In this case, the bulk geometry will still be empty AdS space and so we are not considering a nontrivial RG flow in the boundary CFT. However, in comparison to [46, 47, 48], there are unconventional aspects of the present calculations, including that the underlying degrees of freedom include gravity and that the boundary CFT has an explicit cut-off δ. On the other hand, it seems that the basic assumptions of [46, 47, 48] still seem to apply in the present context, *i.e.,* Lorentz invariance, unitarity and strong subadditivity. Hence we will find that demanding that our results for slab and cylindrical geometries satisfy equations (2.57) and (2.59), respectively, provide new insights into our model. For simplicity, we will only present our calculations for the case with Einstein gravity in the bulk.

2.4.1 Slab geometries

We begin by considering the slab geometry shown in figure 2.2a for $d \geq 3$. We will denote the separation of the two planes on the brane as $\tilde{\ell}$ and reserve ℓ to denote the corresponding distance on the AdS boundary in our holographic calculations. Note that from our previous calculations, we can expect that the BH term (2.1) will appear as the leading contribution in the entanglement entropy, *i.e.,*

$$S_{\rm EE} = \frac{H^{d-2}}{2G_d} + \cdots \,, \tag{2.60}$$

where H^{d-2} corresponds to the regulated area of one of the planes and hence the total area of the entangling surface is $\mathcal{A}(\tilde{\Sigma}) = 2H^{d-2}$. Note that this leading term is independent of the separation $\tilde{\ell}$ and so $C_2(\tilde{\ell})$ depends entirely on the higher order terms in equation (2.60). Further, since the background geometry is flat space and the entangling surface itself is flat, any higher order geometric contributions, like those explicitly shown in equation (2.52), will vanish. Hence the contributions that we are probing in our calculations here should be thought of as coming from long-range correlations in the CFT. From previous holographic calculations [184], we can expect that to leading order, $C_2(\tilde{\ell})$ takes the form

$$C_2(\tilde{\ell}) = \pi\, \gamma^{d-1}\, C_T\, \frac{H^{d-2}}{\tilde{\ell}^{d-2}} + \cdots \,, \quad \text{with} \quad \gamma = \frac{\Gamma(\frac{1}{2(d-1)})}{2\sqrt{\pi}\,\Gamma(\frac{d}{2(d-1)})} \,. \tag{2.61}$$

As the corresponding holographic calculations have been extensively described elsewhere, *e.g.,* [204, 203, 184], our description here is brief. To begin, we write the AdS metric in Poincaré coordindates

$$ds^2_{d+1} = \frac{\delta^2}{z^2}\left(-dt^2 + dx^2 + d\vec{y}^2 + dz^2\right) \,. \tag{2.62}$$

where y^i with $i = 1, 3, \cdots, d-2$ describe the directions parallel to the entangling surface. In the standard holographic calculation, one sets the planes defining the entangling surface at $x = \ell/2$ and $x = -\ell/2$ where ℓ denotes the separation at the AdS boundary $z = 0$. As above, we set the area of each of the two planes to be H^{d-2}, where H is an arbitrary IR regulator with $H \gg \ell$. As usual, the entanglement entropy is evaluated with equation (2.9) and area is extremized by a bulk surface with a profile $x(z)$ satisfying

$$x' = \frac{z^{d-1}}{\sqrt{(\gamma\ell)^{2(d-1)} - z^{2(d-1)}}} \,. \tag{2.63}$$

For $d \geq 3$, the final result can be written as

$$S_{\rm EE} = \frac{H^{d-2}}{2G_d}\left[{}_2F_1\left(\frac{2-d}{2(d-1)}, \frac{1}{2}, \frac{d}{2(d-1)}, \left(\frac{\delta}{\gamma\ell}\right)^{2(d-1)}\right) - \frac{1}{2\gamma}\left(\frac{\delta}{\gamma\ell}\right)^{d-2}\right], \tag{2.64}$$

where the effective d-dimensional Newton's constant is given by equation (2.8). If this expression is expanded for $\delta \ll \ell$, we recover the expected area law, as in equation (2.60). Now this result is written in terms of ℓ, the separation of the two planes on the AdS boundary, whereas we would like to express the results in terms of $\tilde{\ell}$, the separation on the brane. The relation between these two distances is readily found by integrating equation (2.63) between $z = 0$ and $z = \delta$, with the final result given by

$$\tilde{\ell} = \ell\left[1 - \frac{2}{d}\left(\frac{\delta}{\gamma\ell}\right)^{d} {}_2F_1\left(\frac{1}{2}, \frac{d}{2(d-1)}, \frac{3d-2}{2(d-1)}, \left(\frac{\delta}{\gamma\ell}\right)^{2(d-1)}\right)\right]. \tag{2.65}$$

Given equations (2.64) and (2.65), figure 2.3 plots the results for $S_{\rm EE}$, C_2 and $\partial_{\tilde{\ell}} C_2$ in terms of $\tilde{\ell}/\delta$, for $d \geq 3$. The plot of the entanglement entropy confirms that $S_{\rm EE} \to S_0 = H^{d-2}/(2G_d)$ asymptotically for $\tilde{\ell}/\delta \to \infty$ but note that $S_{\rm EE} - S_0 < 0$ for all values of $\tilde{\ell}$. Further $S_{\rm EE}$ goes to zero at $\tilde{\ell} = 0$, as would be expected since the region V has shrunk to zero size at this point. Now the plot of $C_2(\tilde{\ell})$ shows that it is increasing for relatively small separations, *i.e.*, $\tilde{\ell} \lesssim \delta$, and it decreases for large values of $\tilde{\ell}$. Hence in the next plot, we see $\partial_{\tilde{\ell}} C_2$ is negative as required when the separation is large. However, we also find $\partial_{\tilde{\ell}} C_2 > 0$ for $\tilde{\ell} \lesssim \delta$.

Presumably we have found an inconsistency in our model for small separations, *i.e.*, $\tilde{\ell} \sim \delta$. Of course, it should not be surprising to find unusual behaviour when the width of the slab is of the same order as the short-distance cut-off. In particular, with this intrinsic cut-off, the model has only a finite resolution of order δ and hence it is not actually meaningful to consider evaluating the entanglement entropy for the slab when $\tilde{\ell} \lesssim \delta$. Essentially the assumption of strong subadditivity is lost at this scale because we cannot effectively distinguish the degrees of freedom inside and outside of the slab. The fact that $\partial_{\tilde{\ell}} C_2$ becomes positive in this regime is simply pointing out this limitation of the model.

2.4.2 Cylindrical geometries

In this section, we examine the entanglement entropy for a cylindrical entangling surface with $d \geq 3$, *i.e.*, $\tilde{\Sigma} = S^1 \times R^{d-3}$ in a flat R^d background, as shown in figure 2.2b. We

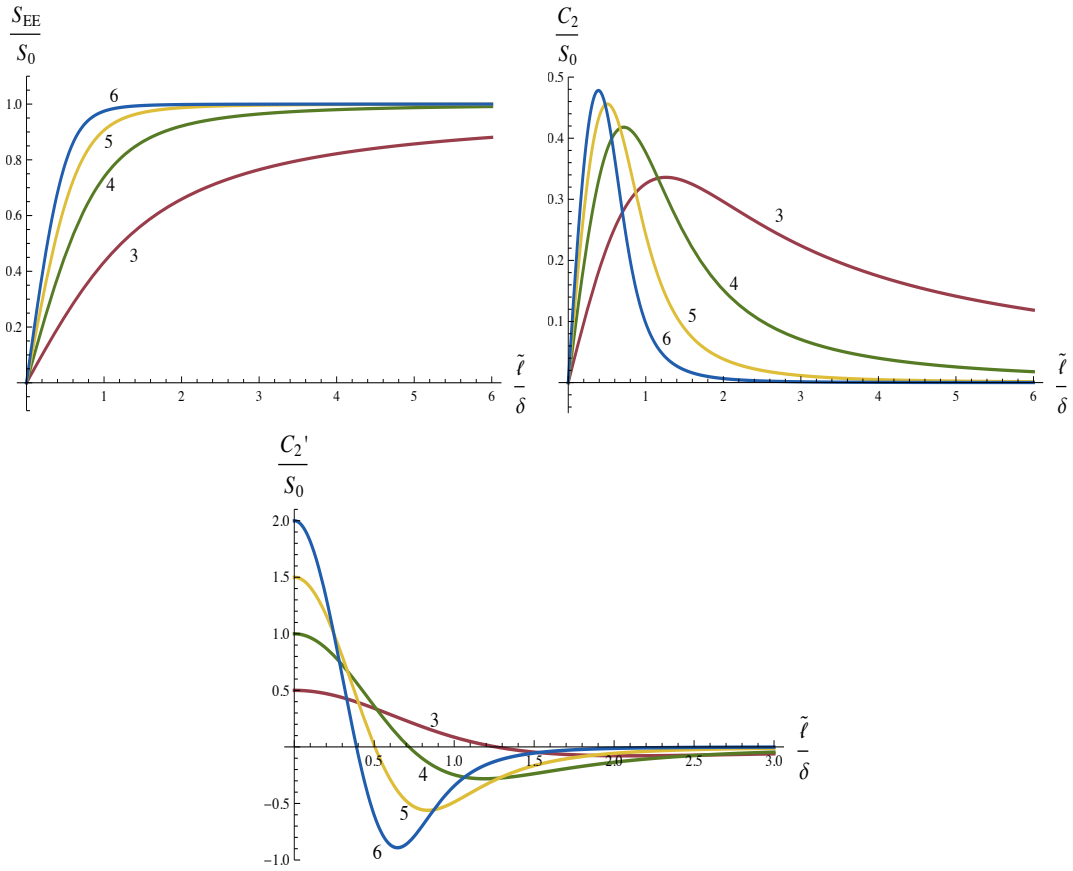

Figure 2.3: $S_{\rm EE}$, C_2 and $C_2' = \delta\partial_{\tilde{\ell}} C_2$ as a function of $\tilde{\ell}$ for $d = 3, 4, 5, 6$. The vertical axes are normalized with $S_0 = \frac{H^{d-2}}{2G_d}$. The first plot confirms that for $\tilde{\ell} \gg \delta$, the dominant contribution in entanglement entropy is the BH term, *i.e.,* S_0. Also the last plot reveals that C_2' becomes positive for $\tilde{\ell} \lesssim \delta$, indicating a limitation with this model.

will denote the radius of the circle on the brane as $\tilde{R}$ while R will be the corresponding radius on the AdS boundary. equation (2.52) indicates that the leading contributions to the entanglement entropy should take the form

$$S_{\rm EE} = \frac{\pi \tilde{R}\, H^{d-3}}{2G_d} - 2\pi\kappa_3 \frac{d-3}{d-2} \frac{H^{d-3}}{\tilde{R}} + \cdots , \tag{2.66}$$

where H is the scale which regulates the area of $\tilde{\Sigma}$, *i.e.,* $\mathcal{A}(\tilde{\Sigma}) = 2\pi \tilde{R}\, H^{d-3}$. Hence we expect that for large radius ($\tilde{R} \gg \delta$), the BH area term (2.1) will be the leading contribution to

$S_{\rm EE}$. However, note that the construction of C_3 in equation (2.58) is designed to precisely remove the area term for the cylindrical geometry [165] and so to leading order, we expect

$$C_3 = 4\pi\kappa_3 \frac{d-3}{d-2} \frac{H^{d-3}}{\tilde{R}} + \cdots \,. \tag{2.67}$$

Hence in this case, $C_3(\tilde{R})$ contains geometric terms arising from short-range correlations across the entangling surface, as well as nonlocal contributions coming from long-range correlations in the CFT.

To begin the holographic calculation, we write the AdS metric in Poincaré coordinates as,

$$ds^2_{d+1} = \frac{\delta^2}{z^2}\left(-dt^2 + dr^2 + r^2 d\phi^2 + d\vec{y}^2 + dz^2\right) \,. \tag{2.68}$$

where y^i with $i = 1, 3, \cdots, d-3$ describe the directions parallel to the entangling surface. In the standard holographic approach, one would define the entangling surface with $r = R$ at the AdS boundary $z = 0$. The entanglement entropy is then evaluated with equation (2.9) and we consider bulk surfaces with a profile $r(z)$. The induced metric on such a bulk surface then becomes

$$ds^2_{d-1} = \frac{\delta^2}{z^2}\left[\left(1 + r'^2(z)\right) dz^2 + r^2 d\phi^2 + d\vec{y}^2\right] \,. \tag{2.69}$$

Using equation (2.8), the entanglement entropy can then be written as

$$S = \frac{\mathcal{A}(\tilde{\Sigma})}{4G_d} \frac{(d-2)\delta^{d-2}}{\tilde{R}} \int_\delta^{z_*} \frac{r\sqrt{1+r'^2}}{z^{d-1}} dz \,, \tag{2.70}$$

where z_* is the maximum value of z where the surface reaches $r = 0$ and closes off in the bulk. The above functional can be used to derive an equation of motion in order for the profile $r(z)$ to extremize the area:

$$rr'' - \left(1 + \frac{d-1}{z} rr'\right)(1 + r'^2) = 0 \,. \tag{2.71}$$

The latter must be solved subject to the boundary conditions $r(z = 0) = R$ on the AdS boundary and $r' = 0$ at $r = 0$ to ensure that the surface closes of smoothly in the bulk. For $d = 3$, one can obtain an analytic solution, since the calculation is a special case of the analysis given in section 2.6.3 — also, see below. For $d > 4$ and $R \gg \delta$, we can find the expansion of $r(z)$ and hence of entanglement entropy (2.70) in inverse powers of R/δ.

We checked that the leading and next-to-leading terms match equation (2.66), which was based on our general geometric formula (2.52).

However, in general, we had to resort to numerical methods to solve for the profile and the entanglement entropy. Further, one must integrate the profile from $z = 0$ to $z = \delta$ to determine the relation between R and $\tilde{R}$.

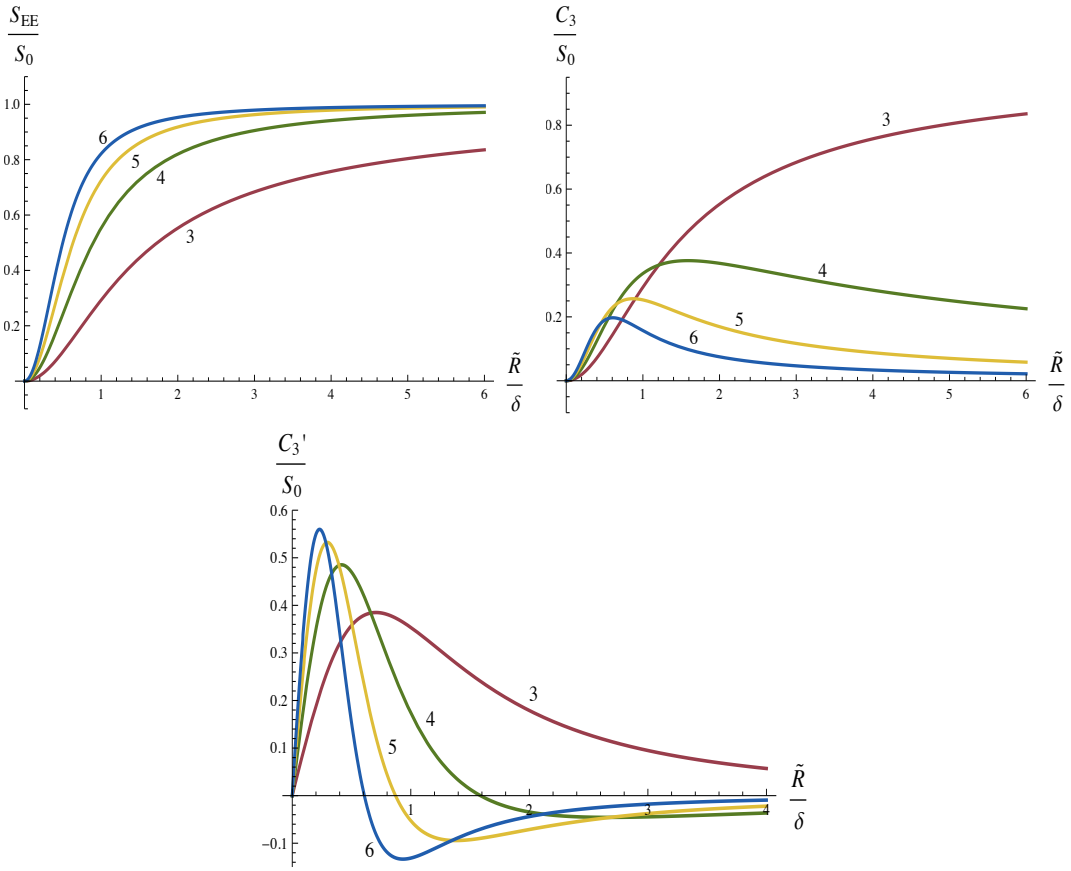

Figure 2.4: $S_{\rm EE}$, C_3 and $C_3' = \delta\partial_{\tilde{R}} C_3$ as a function of $\tilde{R}$ for $d = 3, 4, 5, 6$. The vertical axes are normalized with $S_0 = \mathcal{A}(\tilde{\Sigma})/(4G_d)$. The plot of $S_{\rm EE}$ confirms that for $\tilde{R} \gg \delta$, the dominant contribution is the BH term, *i.e.*, S_0. The last plot reveals that for $d = 4, 5, 6$, C_3' becomes positive for $\tilde{R} \lesssim \delta$. Also note that for $d = 3$, C_3' is positive for all $\tilde{R}$.

Figure 2.4 shows plots of S_{EE}, C_3 and its derivative as functions of $\tilde{R}$ for $d = 3$, 4, 5, and 6. The entropy plot confirms that entanglement entropy is always positive and finite in terms of the radius of the circle on the brane. It goes to zero at $\tilde{R} = 0$, as expected since the

interior region shrinks to zero, and it is bounded from above by the leading BH contribution shown in equation (2.66). Moreover, for $d \geq 4$, C_3 is increasing when the radius of the circle is small relative to the cut-off scale, *i.e.,* $\tilde{R} \lesssim \delta$, while it starts to decrease when the radius is large. Hence, we find $\partial_{\tilde{R}} C_3 < 0$ for large $\tilde{R}$, as required, but $\partial_{\tilde{R}} C_3$ becomes positive for $\tilde{R} \lesssim \delta$. However, this problematic behaviour can be explained, as before, by the finite resolution intrinsic to the RS2 model. Our results for the entanglement entropy are not meaningful when $\tilde{R} \lesssim \delta$ because the model cannot effectively distinguish the degrees of freedom inside and outside of the cylinder. Note, however, that $d = 3$ is a special case with $\partial_{\tilde{R}} C_3 > 0$ for all values of $\tilde{R}$. Clearly, this case requires further explanation, which we reserve for the following section.

2.4.3 Results for $d = 2$ and 3

Both the slab geometry for $d = 2$ and the cylindrical geometry for $d = 3$ are special cases. In particular, both cases appear to be problematic from the point of view of the analysis in this section. We found above that $\partial_{\tilde{R}} C_3 > 0$ for all radii in $d = 3$ and below we will show that $\partial_{\tilde{\ell}} C_2 > 0$ for all separations in $d = 2$. Another distinctive feature of these two cases is that the calculations can be done completely analytically, as they are both special cases of the analysis given in section 2.6.3.

Hence let us present the analytic results. For $d = 2$, the entanglement entropy for the slab geometry becomes

$$\begin{aligned} S_{\text{EE}} &= \frac{8}{\pi} C_T \log\left(\frac{\tilde{\ell}}{2\delta} + \sqrt{1 + \frac{\tilde{\ell}^2}{4\delta^2}}\right) \\ &\simeq \frac{8}{\pi} C_T \left[\log\left(\tilde{\ell}/\delta\right) + \frac{\delta^2}{\tilde{\ell}^2} + \cdots\right] \quad \text{for } \tilde{\ell} \gg \delta\,, \end{aligned} \tag{2.72}$$

where C_T is the central charge given by equation (2.86). Given this result for S_{EE}, we find

$$C_2 = \frac{8C_T}{\pi} \frac{\tilde{\ell}}{\sqrt{\tilde{\ell}^2 + 4\delta^2}} \simeq \frac{8C_T}{\pi}\left[1 - \frac{2\delta^2}{\tilde{\ell}^2} + \cdots\right], \tag{2.73}$$

$$\partial_{\tilde{\ell}} C_2 = \frac{32C_T}{\pi} \frac{\delta^2}{\left(\tilde{\ell}^2 + 4\delta^2\right)^{3/2}} \simeq \frac{32C_T}{\pi} \frac{\delta^2}{\tilde{\ell}^3} + \cdots, \tag{2.74}$$

where the approximate expressions apply for $\tilde{\ell} \gg \delta$. Similarly, we obtain a simple expression for entanglement entropy for cylindrical geometry in $d = 3$

$$\begin{aligned} S_{\rm EE} &= 8C_T \left(\sqrt{\frac{\tilde{R}^2}{\delta^2} + 1} - 1 \right) \\ &\simeq 8C_T \left[\frac{\tilde{R}}{\delta} - 1 + \frac{\delta}{2\tilde{R}} + \cdots \right] \quad \text{for } \tilde{R} \gg \delta \,. \end{aligned} \tag{2.75}$$

We use this expression for $S_{\rm EE}$ to calculate

$$C_3 = 8C_T \left(1 - \frac{\delta}{\sqrt{\tilde{R}^2 + \delta^2}} \right) \simeq 8C_T \left[1 - \frac{\delta}{\tilde{R}} + \cdots \right] , \tag{2.76}$$

$$\partial_{\tilde{R}} C_3 = 8C_T \frac{\tilde{R}\,\delta}{\left(\tilde{R}^2 + \delta^2\right)^{3/2}} \simeq 8C_T \frac{\delta}{\tilde{R}^2} + \cdots . \tag{2.77}$$

We have again also presented the leading terms in an expansion for $\tilde{R} \gg \delta$.

Since the expressions in equations (2.74) and (2.77) are both positive, it is evident that the inequalities in equations (2.57) and (2.59) are never satisfied in these two cases. Further, as noted before, it is clear the finite resolution δ will not resolve this discrepancy since these violations occur for arbitrarily large regions. A common feature of both of these cases is that the gravity theory on the brane is somewhat unusual, *i.e.,* for $d = 2$ and 3, there will be no propagating graviton modes on the brane. While this feature may make these theories seem somewhat pathological, we do not believe that the failure of the inequalities is tied to this peculiar property. In particular note that, with the slab geometry, we still found that equation (2.57) is satisfied for $d = 3$.

Instead, examining the large size expansions in equations (2.72–2.77), we find that in these two special cases, the inequalities are probing contributions to the entanglement entropy that contain positive powers of the cut-off (in the long-distance expansion). That is, equation (2.74) is controlled by the $\delta^2/\tilde{\ell}^2$ term in equation (2.72) for large $\tilde{\ell}$, while the $\delta/\tilde{R}$ term in equation (2.75) dominates the result in equation (2.77) at large $\tilde{R}$. This contrasts to the cases where equations (2.57) and (2.59) were satisfied. As shown in equation (2.61) for the slab geometry, we found the leading contribution to C_2 was independent of δ. For the cylindrical entangling surface, equation (2.67) shows that the leading contribution to C_3 is controlled by κ_3, which is proportional to $1/\delta^{d-4}$ for $d > 4$ and to $\log \delta$ for $d = 4$. Further, we might note that such contributions with positive powers of δ would be dropped

in standard AdS/CFT calculations because they vanish in the limit $\delta \to 0$. Let us also observe that similar terms are also becoming important where the previous calculations fail to satisfy the desired inequalities, *i.e.,* when $\tilde{\ell}, \tilde{R} \lesssim \delta$.

Hence the calculations of $\partial_{\tilde{\ell}} C_2$ for $d = 2$ and $\partial_{\tilde{R}} C_3$ for $d = 3$ are scrutinizing the RS2 model in an essentially different way from the previous calculations. In particular, the problems with equations (2.57) and (2.59) indicate that we are probing the RS2 model beyond its proper regime of validity. We expect that the culpable feature in our framework responsible for this bad behaviour is the superficial treatment of the cut-off δ as a discrete surface in the AdS bulk. For example, in a stringy construction [238, 237, 152, 149, 6], the AdS space would extend smoothly into some complex UV geometry. Of course, understanding the dual description of such a construction would also be more difficult. In particular, an interesting question would be finding the appropriate definition of the holographic entanglement entropy to replace equation (2.9). Given the conjecture of [19], it seems that one should simply consider applying the BH formula (2.1) to some surface in the extended geometry. However, it remains to find some principle that would select the appropriate surface in the UV geometry. Given this reasoning, another perspective on our problems with equations (2.57) and (2.59) would to say that the standard holographic prescription (2.9) for the entanglement entropy must be supplemented by order δ corrections when calculating S_{EE} in the RS2 braneworld — not a particularly surprising conclusion.

2.5 Discussion

In this chapter, we used the Randall-Sundrum II braneworld as a framework to study the conjecture [19] that in quantum gravity, the entanglement entropy of a general region should be finite and the leading contribution is given by the Bekenstein-Hawking area law (2.1). As this braneworld model has a dual description in terms of gravity in an AdS bulk, we were able to apply the usual prescription for holographic entanglement entropy to show that this conjecture is realized in this model. The validity of this result required that the curvatures of the brane geometry were small relative to the cut-off scale, as in equation (2.14). Further, the geometry of the entangling surface, *i.e.,* the boundary of the region for which S_{EE} is being calculated, must also be sufficiently smooth as expressed in equation (2.19).

The entanglement entropy of general regions also shows interesting structure beyond the area law term. In section 2.3, we extended our holographic calculations to find the leading corrections to the BH term, which involve integrals of background and extrinsic curvatures over the entangling surface. One notable feature of the general result shown in

equation (2.3) is that the (dimensionful) coefficients of these correction terms in $S_{\rm EE}$ can be expressed in terms of the gravitational couplings of the curvature-squared coefficients in the induced gravity action. The latter action was derived in section 2.6.1 and the general form of our results is given in equation (2.2). It is natural to compare the Wald entropy (2.28) of this gravity action with the entanglement entropy and we found

$$S_{\rm EE} = S_{\rm Wald} - \int_{\tilde{\Sigma}} d^{d-2}y\sqrt{\tilde{h}}\left[\kappa_1\, K^i K_i + 4\,\kappa_2\left(K^i_{ab}K_i{}^{ab} - \frac{1}{d-2}K^i K_i\right)\right] + \cdots\,. \tag{2.78}$$

That is, $S_{\rm Wald}$ and $S_{\rm EE}$ match except that the extrinsic curvature terms appearing in the entanglement entropy are absent in the Wald entropy. However, since the extrinsic curvatures of a Killing horizon vanish, this means that we will find $S_{\rm EE} = S_{\rm Wald}$ if the entanglement entropy is evaluated on such a horizon, *e.g.,* of a stationary black hole. Of course, this conclusion reinforces the results of [70, 113] that horizon entropy can be interpreted as entanglement entropy in the RS2 model. Further, our result is perhaps natural given that the 'off-shell' approach [40, 224] to evaluating horizon entropy is constructed to take the form of an entanglement entropy calculation and further when this approach is applied in a higher curvature gravity theory, it reproduces precisely the Wald entropy [185, 186]. Given that the extrinsic curvature terms in $S_{\rm EE}$ also appear multiplied by the gravitational couplings, it would be interesting to construct an analogous 'derivation' which also produces these terms for a general horizon or a generic entangling surface.

As an indication of the robustness of these results, we compare equation (2.3) with a perturbative calculation of the holographic entropy functional for a general curvature-squared gravity action in the bulk [124]. Following the reasoning of [19], this entropy functional should represent the leading contribution to the entanglement entropy for general regions in the AdS spacetime. Hence it is interesting to compare the result emerging from the two different calculations for consistency. Their analysis begins with a general curvature-squared action for a five-dimensional gravity action, which for convenience we write as

$$I = \frac{1}{16\pi G_5}\int \mathrm{d}^5x\,\sqrt{-g}\,\left[\frac{12}{L^2} + R + L^2\left(\lambda_1\, C_{ijkl}C^{ijkl} + \lambda_2\, R_{ij}R^{ij} + \lambda_3\, R^2\right)\right]\,. \tag{2.79}$$

The (dimensionless) couplings of the curvature-squared terms were assumed to be small, *i.e.,* $\lambda_{1,2,3} \ll 1$, and the calculations were only carried to out to linear order in these couplings. Note that the action above contains a negative cosmological constant term and so the vacuum solution is an AdS_5 spacetime. Considering the AdS/CFT correspondence in this context, the objective in [124] was to determine the appropriate prescription for holographic entanglement entropy. By demanding that this prescription produce the correct

universal contribution to the entanglement entropy in the dual four-dimensional CFT, as appears in equation (2.55), the following entropy functional was constructed

$$S_{\rm EE} = \frac{\mathcal{A}(\sigma)}{4G_5} + \frac{L^2}{4G_5}\int_\sigma d^3x\sqrt{h}\,\Big[2\lambda_1\left(h^{ac}h^{bd}\,C_{abcd} - K^i_{ab}K_i{}^{ab}\right) + \lambda_2\,R^{ij}g^\perp_{ij} + 2\lambda_3\,R + \alpha\,K^iK_i\Big]\,, \tag{2.80}$$

where σ denotes the extremal surface in the AdS bulk. Now comparing this result with equation (2.3) with $d = 5$, we find agreement for the leading area term, of course, and further the terms involving the background curvatures match the Wald entropy in both expressions. A more interesting observation is that the coefficient of the $K^i_{ab}K_i{}^{ab}$ term precisely matches in both expressions, *i.e.,* this coefficient is the same as that of the Weyl curvature term but with the opposite sign. Unfortunately, no comparison can be made for the K^iK_i term because the coefficient α above remains undetermined in equation (2.80). This ambiguity arises because the calculations yielding equation (2.80) were only linear in the higher curvature couplings, whereas fixing α would require a higher order calculation because the leading order equations extremizing the surface set $K^i = 0$.[18] However, the fact that the two independent calculations agree on the coefficient of the $K^i_{ab}K_i{}^{ab}$ term seems to hint at the universal structure of the extrinsic curvature contributions in $S_{\rm EE}$. It is also revealing that there are no additional contributions to $S_{\rm EE}$ of this form for the action (2.79) where the couplings λ_2 and λ_3 are completely independent, whereas with $d = 5$, we have $\lambda_3 = -\frac{5}{16}\lambda_2$ in equation (2.2).

Given equation (2.78), it is interesting to examine the sign of the extrinsic curvature corrections to $S_{\rm EE}$. For simplicity, let us assume that we are considering the entangling surface on a fixed time slice in a stationary background, *i.e.,* the time-like normal will not contribute to the extrinsic curvatures. In this case, both of the geometric expressions in equation (2.78) are positive (or vanishing).[19] Hence the sign of the extrinsic curvature term depends on the sign of the gravitational couplings, κ_1 and κ_2. In particular, $S_{\rm EE} \leq S_{\rm Wald}$ for $\kappa_1, \kappa_2 \geq 0$. Hence this inequality is satisfied for the RS2 model constructed with Einstein gravity and also $f(\mathcal{R})$ gravity in the AdS bulk — see equations (2.108) and (2.39). However, the couplings for the RS2 model with GB gravity in the bulk are given in equations (2.104) and (2.105) and in this case, it is clear κ_2 will be negative when the GB coupling λ is negative. A closer examination also shows that κ_1 will become negative in $d \geq 5$ if λ

[18] The suggestion was made in [124] to set $\alpha = 2\lambda_1$ in order to simplify the equations determining the extremal bulk surfaces. Of course, this choice would disagree with the results in equation (2.3).

[19] If we denote the eigenvalues of K^i_{ab} for the space-like normal as k_α, then $K^iK_i = (\sum_\alpha k_\alpha)^2$ and $K^i_{ab}K_i{}^{ab} - \frac{1}{d-2}K^iK_i = \sum_\alpha k_\alpha^2 - \frac{1}{d-2}(\sum_\alpha k_\alpha)^2$. The latter can be shown to be positive or zero using Lagrange's identity.

becomes sufficiently positive. Hence for these models, the extrinsic curvature corrections in equation (2.78) do not have a definite sign. Of course, in dynamical circumstances, *e.g.,* in a cosmological setting or for an expanding black hole, the time-like normal will also generically contribute nonvanishing K^t_{ab} and in such a situation, the geometric expressions in equation (2.78) are no longer guaranteed to be positive. Hence it does not possible to make a general statement about the sign of the extrinsic curvature corrections and hence about the relative magnitude of S_{EE} and S_{Wald}.

It may seem desirable to establish an inequality of the form $S_{\text{EE}} \leq S_{\text{Wald}}$ as this would be inline with the intuitive statement that 'black holes are the most entropic objects' in the corresponding gravity theory, as might arise in discussions of the Bekenstein bound [15] or holographic bounds [28, 29] on the entropy. Hence although the conjecture of [19] suggests that in theories of quantum gravity, S_{EE} is finite and closely related to the Bekenstein-Hawking entropy (2.1), the previous discussion seems to indicate that entanglement entropy alone is not the correct quantity in which to frame such discussions. In particular, in examining entropy bounds, it seems crucial to relate the appropriate entropy density to the stress-energy tensor [90], which would not be achieved by, *e.g.,* quantum correlations in the vacuum. Hence it seems a more refined measure of the entropy is required for such discussions [45, 21].

As an aside, let us add that [95, 96] suggested that extremal surfaces should play an important role in combining entanglement entropy and quantum gravity. That is, the leading contribution to entanglement entropy should be given by the BH formula (2.1) but only when the entangling surface is an extremal surface. This contrasts with the present perspective [19] where extremal surfaces do not seem to play a special role. Certainly, our calculations in the RS2 model establish $S_{\text{EE}} = \mathcal{A}/(4G_d) + \cdots$ for arbitrary surfaces, not only event horizons. Further, while $K^i = 0$ for an extremal surface, this does not eliminate all of the extrinsic curvature corrections in equation (2.78).

As a final note, we remind the reader of the various limitations appearing in our calculations. First of all, our results in equations (2.2) and (2.3) rely on the geometries of both the background and the entangling surface being weakly curved, as described by the constraints in equations (2.14) and (2.19). Further, the calculations in section 2.4 for $d = 2$ and 3 revealed new limitations, in that, contributions to the entanglement entropy at $O(\delta/R)$ appear unreliable. It would appear that this problem could be resolved by considering a stringy construction [238, 237, 152, 149, 6] which emulates the RS2 model. In particular, such a construction would give a better understanding of the geometric cut-off in the AdS geometry. It would be interesting if this approach also gave some new insights into the standard holographic prescription (2.9) for entanglement entropy. The discussion in section 2.4 also showed that there are basic limitations to assigning an entanglement

entropy to spacetime regions, which are generic rather than being specific to the RS2 model. In particular, one expects that any theory of quantum gravity will only distinguish different regions of spacetime with some finite resolution and so one will not be able to meaningfully assign an entanglement entropy to arbitrarily small regions (or regions defined by geometric features which are arbitrarily small). We note that the assumptions of strong subadditivity, Lorentz symmetry and causality lead one to conclude that if the entanglement entropy of any arbitrary region in flat space is finite then it must be given by precisely $S_{\rm EE} = c_0 \mathcal{A} + c_1$, where c_0 and c_1 are universal constants [44]. Hence the 'failure' of the putative entanglement entropy for arbitrarily small regions in section 2.4 is actually an essential ingredient to providing a nontrivial result (2.3) at large scales.

2.6 Supplementry material for chapter 1

2.6.1 Induced Gravity Action

In this section, we use the Fefferman-Graham expansion given in equations (2.10) and (2.11) to explicitly evaluate the first few contributions in the derivative expansion of the induced gravity action (2.6) on the brane. In the following, we consider a bulk theory with higher curvature interactions, namely Gauss-Bonnet (GB) gravity [167, 166]. One should regard this theory as a toy model which may provide some insights into more general holographic CFT's. In particular, having a curvature-squared term in the bulk results in the boundary theory having two independent central charges [189, 22]. In part, this feature motivated several recent holographic studies of GB gravity, *e.g.,* [34, 30, 35, 57, 41, 58, 122, 42]. Of course, the results for Einstein gravity (2.22) are easily obtained from the following by taking the limit where the higher curvature coupling vanishes.

The GB gravity action in the bulk takes the form[20]

$$I^{\rm GB}_{bulk} = \frac{1}{16\pi G_{d+1}} \int d^{d+1}x \sqrt{-G} \left[\frac{d(d-1)}{L^2} + \mathcal{R} + \frac{L^2\,\lambda}{(d-2)(d-3)}\,\chi_4 \right] + I^{\rm GB}_{surf}\,. \tag{2.81}$$

where χ_4 is proportional to the four-dimensional Euler density,

$$\chi_4 = \mathcal{R}_{\mu\nu\rho\sigma}\mathcal{R}^{\mu\nu\rho\sigma} - 4\,\mathcal{R}_{\mu\nu}\mathcal{R}^{\rho\sigma} + \mathcal{R}^2\,. \tag{2.82}$$

[20] As in the main text, calligraphic $\mathcal{R}$ and $\mathcal{K}$ are used to denote bulk curvature and the second fundamental form of the brane, respectively. Recall that there are two copies of the AdS geometry and so implicitly, we assume that bulk integral runs over both copies and surface integral is carried over both sides of the brane.

This curvature-squared interaction in the bulk requires higher curvature contributions in the surface action [179, 192], which appears along with the standard Gibbons-Hawking-York term for the Einstein-Hilbert action,

$$I^{\rm GB}_{surf} = \frac{1}{16\pi G_{d+1}}\int d^dx\,\sqrt{-\tilde{g}}\,\Big[2\mathcal{K}+\frac{L^2\,\lambda}{(d-2)(d-3)}\Big(4R\,\mathcal{K}-8R_{ij}\mathcal{K}^{ij} \\ -\frac{4}{3}\mathcal{K}^3+4\mathcal{K}\mathcal{K}_{ij}\mathcal{K}^{ij}-\frac{8}{3}\mathcal{K}_{ij}\mathcal{K}^{jk}\mathcal{K}^{i}{}_{k}\Big)\Big]\,, \tag{2.83}$$

where $\tilde{g}_{ij}$ corresponds to the induced metric on the brane.

While L sets the scale of the cosmological constant in equation (2.81), one easily finds that the AdS curvature scale is actually given by

$$\delta^2=\tilde{L}^2=\frac{L^2}{f_\infty} \qquad \text{where} \quad f_\infty=\frac{1-\sqrt{1-4\lambda}}{2\lambda}\,. \tag{2.84}$$

Here we are using the relation $\delta=\tilde{L}$ which holds for the RS2 model, as discussed in section 2.2. Note that we chosen f_∞ such that with $\lambda\to 0$, $f_\infty=1$ and so we recover $\tilde{L}=L$ in this limit. Implicitly, f_∞ is determined as the root of a quadratic equation and we are discarding the other root since with this choice, the graviton would be a ghost and hence the dual CFT would not be unitary [27, 183, 180]. Further, constraints on the holographic construction limit the GB coupling to lie in the following range, *e.g.,* [34]

$$-\frac{(3d+2)(d-2)}{4(d+2)^2}\le\lambda\le\frac{(d-2)(d-3)(d^2-d+6)}{4(d^2-3d+6)^2} \tag{2.85}$$

for $d\ge 4$. As noted above, one interesting feature of GB gravity (2.81) is that the dual boundary theory will have two distinct central charges. Following [185, 186, 34], we define these charges as:[21]

$$C_T = \frac{\pi}{8}\frac{\delta^{d-1}}{G_{d+1}}\left[1-2\lambda f_\infty\right]\,, \tag{2.86}$$

$$a^*_d = \frac{\pi}{8}\frac{\delta^{d-1}}{G_{d+1}}\left[1-2\frac{d-1}{d-3}\lambda f_\infty\right]\,. \tag{2.87}$$

The first charge C_T controls the leading singularity of the two-point function of the stress tensor. The second central charge a^*_d can be determined by calculating the entanglement

[21] For convenience, our normalizations of C_T and a^*_d are slightly different here than originally appears in *e.g.,* [185, 186, 34].

entropy across a spherical entangling surface [185, 186]. In even dimensions, a_d^* is also proportional to the central charge appearing in the A-type trace anomaly [185, 186]. Note that in the limit $\lambda \to 0$, $C_T = a_d^*$.

For GB gravity as presented in equation (2.81), the two unknown coefficients k_1 and k_2 in equation (2.13) are given by [124]

$$\begin{aligned} k_1 &= \frac{3}{4(d-1)(d-2)(d-3)(d-4)} \frac{\lambda f_\infty}{(1-2\lambda f_\infty)} \,, \\ k_2 &= -\frac{4}{3}(d-1)\, k_1 \,. \end{aligned} \tag{2.88}$$

Now the equations of motion for the metric in the bulk are given by

$$\begin{aligned} &\mathcal{R}_{\mu\nu} - \frac{G_{\mu\nu}}{2}\left(\mathcal{R} + \frac{d(d-1)}{L^2} + \frac{L^2\lambda}{(d-2)(d-3)}\chi_4\right) \\ &\quad + \frac{2L^2\,\lambda}{(d-2)(d-3)}\left(\mathcal{R}_{\mu\sigma\rho\tau}\mathcal{R}_\nu{}^{\sigma\rho\tau} - 2\mathcal{R}_{\mu\rho}\mathcal{R}_\nu{}^{\rho} - 2\mathcal{R}_{\mu\rho\nu\sigma}\mathcal{R}^{\rho\sigma} + \mathcal{R}\mathcal{R}_{\mu\nu}\right) = 0\,. \end{aligned} \tag{2.89}$$

Taking trace of these equations then yields

$$\frac{L^2\lambda}{(d-2)(d-1)}\,\chi_4 = -\mathcal{R} - \frac{d(d+1)}{L^2}\,. \tag{2.90}$$

Hence, the on-shell bulk action can be written as follows

$$2I^{\rm GB}_{bulk} = -\frac{1}{4\pi G_{d+1}(d-3)}\int d^{d+1}x\,\sqrt{-G}\Big[\frac{2d(d-1)}{L^2} + \mathcal{R}\Big] + 2I^{\rm GB}_{surf}\,, \tag{2.91}$$

where $I^{\rm GB}_{surf}$ is given in equation (2.83). We have included an extra factor of two above, as in equation (2.4), since we are assuming that the integrals above run over one copy of the AdS space.

The outward-pointing unit normal at the cut-off surface, $\rho = 1$, is given by $n_\mu = -\sqrt{G_{\rho\rho}}\,\delta^\rho_\mu$. Now one can readily evaluate derivative expansion of the second fundamental form at this surface

$$\mathcal{K}_{ij} = \nabla_i n_j|_{\rho=1} = -\frac{\rho}{\delta}\frac{\partial G_{ij}}{\partial\rho}\Big|_{\rho=1} = \frac{1}{\delta}\sum_{n=0}^{\infty}(1-n)\overset{(n)}{g}_{ij} = \frac{1}{\delta}\Big(\tilde{g}_{ij} - \sum_{n=1}^{\infty} n\overset{(n)}{g}_{ij}\Big)\,, \tag{2.92}$$

where we are using $\tilde{L} = \delta$. Recall that equation (2.15) gives the induced metric $\tilde{g}_{ij}$ on the brane in terms of the FG expansion coefficients (2.11).

Now, the general expansion of the curvature scalar requires rather tedious computations. However, we employ a shortcut since we will only carry the derivative expansion to fourth order. In this case, we need only $\overset{(1)}{g}_{ij}$ and $\overset{(2)}{g}_{ij}$ in the FG expansion (2.11). The main observation for our shortcut is to exploit Einstein gravity in order to argue that for any gravity theory in the bulk only terms proportional to k_1 and k_2 in equation (2.13) contribute nontrivially at fourth order in the derivative expansion of the curvature scalar while the second order term in such expansion vanishes independently of the details of the bulk gravity theory.

Indeed, in the case of Einstein gravity (for which $\delta = \tilde{L} = L$), the Ricci scalar is constant by the equations of motion, *i.e.,* equation (2.90) yields $\mathcal{R} = -d(d+1)/\delta^2$ (with $\lambda = 0$). Therefore in the derivative expansion, coefficients of all higher order corrections vanish. Furthermore, we observe that $k_1 = k_2 = 0$ from equation (2.88) with $\lambda = 0$. Hence we may deduce that in the absence of k_1 and k_2, the contributions that originate from $\overset{(1)}{g}_{ij}$ and $\overset{(2)}{g}_{ij}$ cancel each other. Therefore with a general theory for bulk gravity, only Weyl-squared terms in equations (2.12) and (2.13) can contribute in a nontrivial way at the fourth order in the derivative expansion of the curvature scalar, whereas second order must vanish identically. Now since the Weyl-squared terms already possess four derivatives, it is enough to perform linear analysis to find the desired contributions in the expansion of $\mathcal{R}$. That is, first we rewrite equation (2.10) as

$$ds^2 = G_{\mu\nu}\, dx^\mu dx^\nu = \frac{\delta^2}{4}\frac{d\rho^2}{\rho^2} + \frac{1}{\rho}\ \overset{(0)}{g}_{ij}(x)\, dx^i dx^j + \delta G_{ij}(x,\rho)\, dx^i dx^j\,, \tag{2.93}$$

where, in principle, one has

$$\delta G_{ij}(x,\rho) = \overset{(1)}{g}_{ij}(x) + \overset{(2)}{g}_{ij}(x)\rho + \cdots = \sum_{n=1}^{\infty} \overset{(n)}{g}(x)\, \rho^{n-1}\ . \tag{2.94}$$

Then we can evaluate linear correction to $\mathcal{R}$ associated with δG_{ij}, however, for the present purposes, we do not use the entire expression (2.94) but rather we keep only contributions of the Weyl-squared terms appearing in $\overset{(2)}{g}_{ij}$.

The first variation of the curvature scalar under $G_{\mu\nu} \to G_{\mu\nu} + \delta G_{\mu\nu}$ is given by

$$\delta\mathcal{R} = -\mathcal{R}^{\mu\nu}\delta G_{\mu\nu} + \nabla^\mu(\nabla^\nu \delta G_{\mu\nu} - \nabla_\mu \delta G^\nu{}_\nu)\ , \tag{2.95}$$

where covariant derivative ∇_μ is compatible with unperturbed metric $G_{\mu\nu}$ which is also used to raise and lower the indices in the above expression. In our case, the unperturbed

Ricci tensor is given by

$$\mathcal{R}^{\rho\rho} = -\frac{4d}{\delta^4}\rho^2 \ , \quad \mathcal{R}^{ij} = \rho\left(\rho\, R^{ij}[\overset{(0)}{g}] - \frac{d}{\delta^2}\,\overset{(0)}{g}{}^{ij}\right) \ , \tag{2.96}$$

where indices in parenthesis are raised and lowered with $\overset{(0)}{g}_{ij}$. Combining the above results altogether, we find the following expansion for the curvature scalar to fourth order in the derivative expansion:

$$\mathcal{R} = -\frac{d(d+1)}{\delta^2} + 4(d-3)(d\,k_1 + k_2)\,\delta^2\rho^2\, C_{mnkl}C^{mnkl} + \cdots \ . \tag{2.97}$$

In particular, in the special case of GB gravity (2.46), it follows from equation (2.88) that

$$\mathcal{R} = -\frac{d(d+1)}{\delta^2} - \frac{1}{(d-1)(d-2)}\,\frac{\lambda f_\infty}{(1-2\lambda f_\infty)}\,\delta^2\rho^2\, C_{mnkl}C^{mnkl} + \cdots \ . \tag{2.98}$$

Next we substitute equations (2.92) and (2.98) into equations (2.83) and (2.91) and then integrate over the extra dimension ρ in equation (2.91). The final result takes the form

$$\begin{aligned} 2I^{\rm GB}_{bulk} \;=\; & \frac{\delta}{8\pi(d-2)G_{d+1}}\int d^dx\sqrt{-\tilde{g}}\Bigg[\frac{2(d-1)(d-2)}{\delta^2}\big(1-\frac{2}{3}\lambda f_\infty\big) \\ & + (1+2\lambda f_\infty)R + \frac{1-6\lambda f_\infty}{(d-2)(d-4)}\,\delta^2\left(R_{ij}R^{ij} - \frac{d}{4(d-1)}R^2\right) \\ & + \frac{\lambda f_\infty}{(d-3)(d-4)}\,\delta^2\, C_{ijkl}C^{ijkl} + \mathcal{O}(\partial^6)\Bigg] \ . \end{aligned} \tag{2.99}$$

Note that implicitly the above expression only contains the contribution from the lower limit of the ρ integration, *i.e.,* from $\rho = 1$. Our result coincides with the $I^{(n)}$ terms in equation (2.6) for $n = 0$, 1 and 2. Up to the Weyl-squared term, this boundary action is identical to that found in [242] for GB gravity. However, the Weyl-squared term was absent in [242] simply because the analysis there only considers conformally flat boundaries. To get the full induced gravity action (2.6) on the brane, we need to add I_{brane} to the above expression. In the absence of any matter fields, the latter has the simple form

$$I_{brane} = -T_{d-1}\int d^dx\sqrt{-\tilde{g}}\,. \tag{2.100}$$

Now for simplicity, we tune the brane tension to be

$$T_{d-1} = \frac{d-1}{4\pi G_{d+1}\delta}\left(1-\frac{2}{3}\lambda f_\infty\right) \ , \tag{2.101}$$

so that it precisely cancels the cosmological constant contribution in equation (2.99). Combining these expressions together, we finally obtain

$$I_{ind}^{\rm GB} = \int d^dx\sqrt{-\tilde{g}}\left[\frac{R}{16\pi G_d} + \frac{\kappa_1}{2\pi}\left(R_{ij}R^{ij} - \frac{d}{4(d-1)}R^2\right) + \frac{\kappa_2}{2\pi}\,C_{ijkl}C^{ijkl} + \mathcal{O}(\partial^6)\right] . \tag{2.102}$$

where the effective d-dimensional Newton's constant is given by

$$\frac{1}{G_d} = \frac{2\,\delta}{d-2}\frac{1+2\lambda f_\infty}{G_{d+1}} = \frac{16}{\pi(d-2)}\,\frac{(d-2)C_T - (d-3)a_d^*}{\delta^{d-2}}\,, \tag{2.103}$$

and the couplings for the curvature-squared terms can be written as

$$\kappa_1 = \frac{\delta^3}{4(d-2)^2(d-4)}\,\frac{1-6\lambda f_\infty}{G_{d+1}} = \frac{2}{\pi(d-2)^2(d-4)}\,\frac{(d-3)a_d^* - (d-4)C_T}{\delta^{d-4}}\,, \tag{2.104}$$

$$\kappa_2 = \frac{\delta^3}{4(d-2)(d-3)(d-4)}\,\frac{\lambda f_\infty}{G_{d+1}} = \frac{1}{2\pi(d-2)(d-4)}\,\frac{C_T - a_d^*}{\delta^{d-4}}\,. \tag{2.105}$$

Now setting $\lambda = 0$ above, we recover the induced action for Einstein gravity (2.22) in the bulk

$$I_{ind}^{\rm E} = \int d^dx\sqrt{-\tilde{g}}\left[\frac{R}{16\pi G_d} + \frac{\kappa_1}{2\pi}\left(R_{ij}R^{ij} - \frac{d}{4(d-1)}R^2\right) + \mathcal{O}(\partial^6)\right] , \tag{2.106}$$

where the induced couplings can be written as

$$\frac{1}{G_d} = \frac{2\,\delta}{d-2}\,\frac{1}{G_{d+1}} = \frac{16}{\pi(d-2)}\,\frac{C_T}{\delta^{d-2}}\,, \tag{2.107}$$

$$\kappa_1 = \frac{\delta^3}{4(d-2)^2(d-4)}\,\frac{1}{G_{d+1}} = \frac{2}{\pi(d-2)^2(d-4)}\,\frac{C_T}{\delta^{d-4}}\,. \tag{2.108}$$

Note that in this case, induced gravity action does not contain a term proportional to the square of the Weyl tensor, *i.e.*, $\kappa_2 = 0$.

2.6.2 Codimension-two Bulk Surfaces

In this section, we consider various curvatures associated with codimension-two surface σ in the bulk and evaluate their derivative expansion up to second order. The formulae that we obtain here are useful in the derivation of equation (2.50).

Recall that FG-like expansion of the induced metric on σ was given in equation (2.17). Let us rewrite its components in the following way

$$h_{\rho\rho} = \frac{\delta^2}{4\rho^2} + \delta h_{\rho\rho}\,, \qquad h_{ab} = \frac{\overset{(0)}{h}_{ab}}{\rho} + \delta h_{ab}\,. \tag{2.109}$$

Here, we are again using $\tilde{L} = \delta$, as is appropriate for calculations in the RS2 model, and further we have defined

$$\delta h_{\rho\rho} = \frac{\delta^2}{4}\sum_{n=1}^{\infty} \overset{(n)}{h}_{\rho\rho}\,\rho^{n-2}\,, \qquad \delta h_{ab} = \sum_{n=1}^{\infty} \overset{(n)}{h}_{ab}\,\rho^{n-1}\,. \tag{2.110}$$

As in equation (2.96), the Ricci tensor of the leading order metric $\overset{(0)}{h}_{\alpha\beta}$ is given by[22]

$$\mathcal{R}^{\rho\rho} = -\frac{4(d-2)}{\delta^4}\rho^2\,, \quad \mathcal{R}^{ij} = \rho\big(\rho\, R^{ij}[\overset{(0)}{h}] - \frac{(d-2)}{\delta^2}\,\overset{(0)}{h}{}^{ij}\big)\,, \tag{2.111}$$

Now applying equation (2.95) for the full induced metric (2.109) yields

$$\begin{aligned}\mathcal{R} &= -\frac{(d-1)(d-2)}{\delta^2} + \rho\bigg(R_\Sigma + \frac{(d-2)(d-3)}{\delta^2}\,\overset{(1)}{h}_{\rho\rho} + \frac{2(d-3)}{\delta^2}\,\overset{(0)}{h}{}^{ab}\,\overset{(1)}{h}_{ab}\bigg) + \mathcal{O}(\partial^4)\\ &= -\frac{(d-1)(d-2)}{\delta^2} + \rho\bigg(R_\Sigma - \frac{d-3}{d-2}\Big[2\,\overset{(0)}{h}{}^{ab}R_{ab} - \frac{d-2}{d-1}\,R + K^i K_i\Big]\bigg) + \mathcal{O}(\partial^4)\,,\end{aligned} \tag{2.112}$$

where we have explicitly substituted for $\overset{(1)}{h}_{\alpha\beta}$ using equations (2.12) and (2.18) in the second line. Here R_Σ denotes intrinsic curvature scalar for Σ. However, note that to the order that we are working the latter is indistinguishable from the intrinsic Ricci scalar evaluated for $\tilde{\Sigma}$, the entangling surface on the brane, *i.e.,* using equation (2.21), $R_\Sigma = R_{\tilde{\Sigma}} + O(\partial^4)$.

To evaluate the holographic entanglement entropy in section 2.3.3, it is useful to apply further geometric identities to re-express the first order term in equation (2.112). In particular, we use the Gauss-Codazzi equation

$$[R_{\tilde{\Sigma}}]_{abcd} = R_{abcd} + K^i_{ac}K_{i\,bd} - K^i_{ad}K_{i\,bc} \tag{2.113}$$

along with

$$\tilde{h}^{ac}\tilde{h}^{bd}C_{abcd} = \tilde{h}^{ac}\tilde{h}^{bd}R_{abcd} - \frac{2(d-3)}{d-2}\tilde{h}^{bd}R_{bd} + \frac{d-3}{d-1}R\,, \tag{2.114}$$

[22] Indices of Ricci tensor $R^{ij}[h^{(0)}]$ are raised and lowered with $\overset{(0)}{h}_{ij}$.

where C_{ijkl} denotes the Weyl tensor evaluated with the brane metric. Combined these identities allow us to re-express equation (2.112) as

$$\mathcal{R} = -\frac{(d-1)(d-2)}{\delta^2} + \rho\left(\tilde{h}^{ac}\tilde{h}^{bd}C_{abcd} - K^i_{ab}K_i{}^{ab} + \frac{1}{d-2}K^iK_i\right) + \mathcal{O}(\partial^4)\,. \tag{2.115}$$

For the present purposes, the entangling surface $\tilde{\Sigma}$ is the boundary of the extremal surface σ and so we now turn to evaluate the second fundamental form with the above asymptotic expansion. The outward normal vector of $\tilde{\Sigma}$ imbedded into σ is $n_\alpha = -\sqrt{h_{\rho\rho}}\,\delta^\rho_\alpha$. Hence, extrinsic curvature tensor takes the following form

$$\mathcal{K}_{ab} = \nabla_a n_b = -\frac{1}{2\sqrt{h_{\rho\rho}}}\frac{\partial h_{ab}}{\partial\rho}\Big|_{\rho=1} = \frac{\overset{(0)}{h}_{ab}}{\delta}\big(1 - \frac{1}{2}\overset{(1)}{h}_{\rho\rho}\big) + \mathcal{O}(\partial^4)\,, \tag{2.116}$$

whereas its trace is given by

$$\begin{aligned}\mathcal{K} &= \frac{d-2}{\delta}\big(1 - \frac{1}{2}\overset{(1)}{h}_{\rho\rho}\big) - \frac{1}{\delta}\overset{(0)}{h}^{ab}\overset{(1)}{h}_{ab} + \mathcal{O}(\partial^4)\\ &= \frac{d-2}{\delta} - \frac{\delta}{2(d-2)}\left(2R^{ij}\,\tilde{g}^\perp_{ij} - \frac{d}{d-1}\,R - K^iK_i\right) + \mathcal{O}(\partial^4)\,.\end{aligned} \tag{2.117}$$

In the second line, we have explicitly substituted for $\overset{(1)}{h}_{\alpha\beta}$ using equations (2.12) and (2.18). We have also simplified the resulting expression using $R = R^{ab}\,\tilde{h}_{ab} + R^{ij}\,\tilde{g}^\perp_{ij}$.

2.6.3 Spherical Entangling Surfaces

In this section, we compare our perturbative results for the entanglement entropy in section 2.3 with those for a simple case where the entire holographic result can be calculated analytically, namely a spherical entangling surface in flat space. For this purpose, we consider the case where the bulk is pure AdS space and the brane geometry is flat. In this situation, we have $g_{ij}(x,\rho) = \eta_{ij}$ in equation (2.10) and the full metric coincides with the standard Poincaré patch metric upon substituting $z^2 = \delta^2\rho$. Further, choosing the entangling surface Σ in the AdS boundary to be a $(d-2)$-dimensional sphere of radius R, then the extremal surface σ is given by [204, 203]

$$\delta^2\,\rho + r^2 = R^2 = \tilde{R}^2 + \delta^2\,, \tag{2.118}$$

where r is the radial coordinate in the boundary geometry. Here we have also introduced $\tilde{R}$, which corresponds to the radius of the spherical entangling surface $\tilde{\Sigma}$ on the brane, *i.e.*,

at $\rho = 1$. In fact, the derivation of [49] shows that this same surface will be the appropriate extremal surface, independently of the bulk gravity theory. As it will prove useful below, let us write the induced metric on σ

$$ds^2 = \frac{\delta^2}{4}\frac{d\rho^2}{\rho^2}\left(1+\frac{\delta^2}{r^2}\,\rho\right) + \frac{r^2}{\rho}\,d\Omega_{d-2}^2\,. \tag{2.119}$$

Now in the case of Einstein gravity in the bulk, the holographic prescription (2.9) yields the following [204, 203]

$$\begin{aligned} S_{\rm EE} &= 2\,\frac{\mathcal{A}(\sigma)}{4G_{d+1}} = \frac{\delta^{d-1}}{2G_{d+1}}\,\Omega_{d-2}\int_{\frac{\delta}{\sqrt{\delta^2+\tilde{R}^2}}}^{1} dy\frac{(1-y^2)^{\frac{d-3}{2}}}{y^{d-1}} \\ &= \frac{\delta^{d-1}\Omega_{d-2}}{2G_{d+1}}\left[\frac{(1+\tilde{R}^2/\delta^2)^{\frac{d-2}{2}}}{d-2}\,{}_2F_1\left(\frac{2-d}{2},\frac{3-d}{2},\frac{4-d}{2},\frac{1}{1+\tilde{R}^2/\delta^2}\right)+\frac{\Gamma\left(\frac{2-d}{2}\right)\Gamma\left(\frac{d-1}{2}\right)}{2\sqrt{\pi}}\right], \end{aligned} \tag{2.120}$$

where we have again introduced a factor of two above to account for the two copies of the AdS geometry and Ω_{d-2} is the surface area of a $(d-2)$-dimensional sphere of unit radius, *i.e.*, $\Omega_{d-2} = 2\pi^{(d-1)/2}/\Gamma\left(\frac{d-1}{2}\right)$. Now to satisfy the constraint (2.19), we consider a large sphere with $\tilde{R} \gg \delta$. In this case, we may expand the result in equation (2.120) to find

$$S_{\rm EE} = \frac{\mathcal{A}(\tilde{\Sigma})}{4G_d}\left(1-\frac{d-2}{2(d-4)}\left(\frac{\delta}{\tilde{R}}\right)^2+\cdots\right)\,, \tag{2.121}$$

where we substituted for the d-dimensional Newton's constant using equation (2.107) and we wrote $\mathcal{A}(\tilde{\Sigma}) = \Omega_{d-2}\tilde{R}^{d-2}$ for the area of the entangling surface. Hence we again find the leading term takes precisely the form of the BH entropy (2.1). Further let us match the first correction to that in equation (2.27). First, we calculate the extrinsic curvatures of the sphere of radius $\tilde{R}$ as

$$K^{\hat{t}}_{ab} = 0 \qquad \text{and} \qquad K^{\hat{r}}_{ab} = \frac{\delta_{ab}}{\tilde{R}}\,, \tag{2.122}$$

where the first is associated with a time-like normal vector $n^{\hat{t}}_i = \delta^t_i$ and the second with the radial normal $n^{\hat{r}}_i = \delta^r_i$. Now using equation (2.108), we find there is a precise agreement between the first corrections appearing in equations (2.27) and (2.121).

Let us now turn to the case of Gauss-Bonnet gravity (2.46). Now for the holographic calculation of entanglement entropy, we extremize the new entropy functional in equation (2.49). However, as noted above, for a spherical entangling surface $\tilde{\Sigma}$ in the boundary

theory, the extremal surface σ in the bulk is again given by equation (2.118). Hence we must examine the geometry of this surface somewhat more closely to evaluate the desired S_{JM}. First of all, although it is not immediately evident from equation (2.119), σ is a constant curvature surface with

$$\mathcal{R} = -(d-1)(d-2)/\delta^2 \,. \tag{2.123}$$

Next, the extrinsic curvature of the boundary $\partial\sigma$ on the brane, *i.e.,* $\rho = 1$ is given by

$$\mathcal{K}_{ab} = -\frac{1}{2\sqrt{h_{\rho\rho}}}\left.\frac{\partial h_{ab}}{\partial \rho}\right|_{\rho=1} = \frac{\tilde{h}_{ab}}{\delta}\sqrt{1+\frac{\delta^2}{\tilde{R}^2}}\,. \tag{2.124}$$

As shown in [124], combining these results yields

$$S_{JM} = \left[1 - 2\frac{d-1}{d-3}\lambda f_\infty\right]\frac{\mathcal{A}(\sigma)}{2G_{d+1}} + \frac{2\lambda f_\infty}{d-3}\frac{\delta}{G_{d+1}}\sqrt{1+\frac{\delta^2}{\tilde{R}^2}}\;\Omega_{d-2}\tilde{R}^{d-2}\;, \tag{2.125}$$

where the formula for $\mathcal{A}(\sigma)$ is the same as in the case of Einstein gravity equation(2.120). As above, we expand this expression for $\tilde{R} \gg \delta$ and the result may be written as

$$S_{\text{EE}} = \frac{\mathcal{A}(\tilde{\Sigma})}{4G_d}\Big(1 - \frac{1-6\lambda f_\infty}{1+2\lambda f_\infty}\frac{d-2}{2(d-4)}\left(\frac{\delta}{\tilde{R}}\right)^2 + \cdots\Big)\;, \tag{2.126}$$

after substituting with equation (2.103). Now examining the previous result in equation (2.50), we first note that the combination of extrinsic curvatures appearing in the κ_2 term vanishes if we substitute with equation (2.122). However, using equations (2.104) and (2.122), we find an exact agreement between the κ_1 term appearing in equation (2.50) and the first correction appearing above in equation (2.126).

Chapter 3

A Holographic Quantum Hall Ferromagnet

3.1 Introduction and Summary

The quantum Hall effect is one of the most dramatic phenomena in condensed matter physics [8, 81]. At particular values of its charge density and magnetic field, a two-dimensional electron gas exhibits incompressible charge-gapped states. These states can be robust and persist over a range of the ratio of density to field, that is, over a Hall plateau on which the Hall conductivity is a constant ν times the elementary unit of conductivity $\frac{e^2}{h}$ ($= \frac{1}{2\pi}$ in the natural units which we shall use in this chapter),

$$\sigma_{xy} = \frac{\nu}{2\pi}. \tag{3.1}$$

The same electron gas can exhibit an array of such states, where ν is generally an integer, for the integer quantum Hall effect, or a rational number for the fractional quantum Hall effect.

What is more, the integer quantum Hall effect has a beautiful and simple explanation as a single-particle phenomenon. When a charged particle moving in two dimensions is exposed to a magnetic field, its spectrum is resolved into discrete Landau levels. Landau levels are flat, dispersionless bands with gaps between them. Fermi-Dirac statistics dictates that the low energy states of a many-electron system are obtained by filling the lowest energy single-electron states, with one electron per state. When a Landau level is completely filled with electrons, the next electron one inserts into the system must go to

the next higher level which is separated from the ones that are already occupied by a gap. The result is a jump in the chemical potential. Alternatively, when the chemical potential is in the gap between levels, it can be varied with no change of the charge density. Such a state is said to be incompressible. This effect is enhanced by disorder induced localization which forms a mobility gap and results in the Hall plateau.

In the absence of disorder, for free electrons, the Hall conductivity is given by equation (3.1) with ν equal to the filling fraction. The filling fraction is defined as the ratio of the number of electrons to the number of states in the Landau levels which are either completely or partially occupied (see equation (3.3) below). When a number of Landau levels are completely filled, ν is an integer which coincides with the number of filled levels and the Hall conductivity is quantized. It is given by the formula (3.1). Moreover, for completely filled energy bands, the Hall conductivity is a topological quantum number insensitive to smooth alterations of the energy band [160, 231, 188], such as those caused by changes in the environment of the single electrons. We can turn on lattice effects and disorder with the Hall conductivity remaining unchanged, and can thus conclude that, when ν is an integer, the quantized Hall conductivity is robust for a large range of single-particle interactions including the effects of disorder which are responsible for forming the Hall plateaus.

In addition to this, there are good theoretical arguments for the persistence of the integer Hall effect in the presence of electron-electron interactions, at least when the interactions are weak enough that perturbation theory can be applied. An easy way to understand this is by noting that, at the level of a low energy effective action, the Hall effect is encoded in a Chern-Simons term for the photon field,

$$S_{\mathrm{CS}} = \frac{\sigma_{xy}}{2} \int d^3x \, \epsilon^{\mu\nu\lambda} A_\mu \partial_\nu A_\lambda \ . \tag{3.2}$$

The coefficient of the Chern-Simons term is proportional to the Hall conductivity. Moreover, there is a theorem which states that the Chern-Simons term does not renormalize beyond one-loop order in either a relativistic or non-relativistic field theory [54, 209, 169]. The theorem depends on the existence of a charge gap in the spectrum. If the gap closes it is known that either scalar or fermion charged matter can renormalize the Chern-Simons term [209]. Thus, as far as perturbation theory is valid, the existence of the integer quantum Hall effect after interactions are turned on is intimately tied to the question of whether the incompressible nature of the state due to the energy gap between Landau levels survives in the interacting theory.

In this chapter, we shall discuss the question as to whether any features of the integer Hall effect can persist when the coupling is strong, beyond the reach of perturbation

theory. The development of AdS/CFT duality between certain gauge field theories and certain string theories has given us a tool for solving the strong coupling limit of some quantum systems. In a recent paper [158], two of the authors have found an example of a strongly coupled quantum field theory which, in a state with non-zero charge density and when subject to an external magnetic field, exhibits incompressible states with integer quantized Hall conductivity. It occurs in a non-Abelian gauge field theory that has a well-established string theory dual, the D3-D5 system [151, 150]. The string theory is quantitatively tractable in its semi-classical low energy limit, and a further probe limit where the number of D5 branes is much smaller than the number of D3 branes. These limits coincide with the strong coupling and quenched planar limit of the quantum field theory and its solution yields information about the latter at strong coupling. The behavior of the theory when a charge density and magnetic field are added can readily be studied there. In that system, it was shown that there exist exotic states of the D3-D5 system where it becomes incompressible. These states occur at precisely integer values of the filling fraction ν, where

$$\nu \equiv \frac{2\pi\rho}{NB}, \tag{3.3}$$

with ρ the particle density, B the external field and N the number of colors of quarks in the non-Abelian gauge theory. These states were argued to be the natural strong coupling manifestation of some incompressible integer quantum Hall states which appear in the weak coupling limit of that theory.

Aside from a manifestation of an integer quantum Hall state, the incompressible states of the strongly coupled system found in reference [158] have an interesting analog in the observed quantum Hall states of graphene. Graphene is a two-dimensional semi-metal where the electron obeys an emergent massless Dirac equation with four flavors of the fermion field and an effective SU(4) symmetry [208, 99]. This fact leads to the anomalous quantum Hall effect [111] where the Hall conductance is quantized as

$$\sigma_{xy}^{\text{graphene}} = \frac{e^2}{h} \cdot 4 \cdot \left(n + \frac{1}{2} \right). \tag{3.4}$$

The factor of 4 in this expression arises from the four-fold degeneracy of the low energy fermions and the offset of $1/2$ in $n + 1/2$ is a result of the spectrum of the massless Dirac fermions in a magnetic field. The Dirac Hamiltonian in a magnetic field has zero energy modes which form a Landau level at the apex of the Dirac cones. Particle-hole symmetry dictates that, in the ground state of the many-electron system, when it is charge neutral, as well as all of the negative energy single electron states of the Dirac Hamiltonian, half of

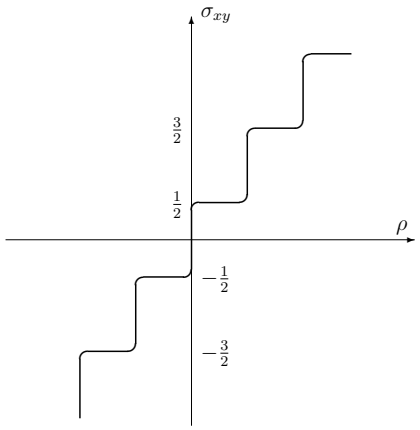

Figure 3.1: Integer quantum Hall effect in graphene. The vertical axis is the Hall conductivity in units of $4\frac{e^2}{h}$. The horizontal axis is the charge density at fixed magnetic field. The plateaus occur at the anomalous integer Hall conductivities $\sigma_{xy} = 4\,\frac{e^2}{h}(n + \frac{1}{2})$.

the zero modes should be filled . The neutral state is therefore not a Hall plateau. It has a half-filled Landau level and it is in the middle of a Hall step, as depicted in figure 3.1. These features were observed in the initial experiments which were performed soon after graphene was discovered in 2004 [247, 191].

Later, with stronger magnetic fields and cleaner samples, the formation of new plateaus were discovered at all of the integer steps. The four-fold degeneracy of the Landau levels is partially or completely lifted, depending on the filling fraction [246, 244]. The new plateaus are depicted in figure 3.2. In particular, the states which originate from the zero mode Landau level have interesting properties [1, 52, 53].

The mechanism for formation of these additional plateaus is thought to be spontaneous symmetry breaking and, like the integer Hall effect itself, it has a beautiful and elegant explanation at weak coupling. Here, we will focus on the charge neutral Landau level (near ρ=0 in figures 3.1 and 3.2). As we have already noted, in an external magnetic field, the single electron spectrum has zero modes and, when we construct the many-electron state in a certain range of densities, these single-electron zero modes must be partially filled. If electrons are non-interacting, a partially filled Landau level is a highly degenerate state, as any partial filling has the same energy as any other partial filling. In this circumstance, an interaction, no matter how weak, will generically

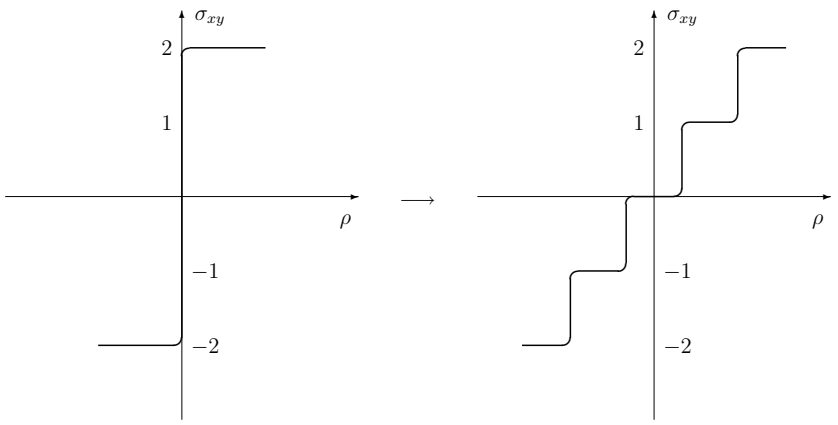

Figure 3.2: Quantum Hall Ferromagnetism/Magnetic Catalysis of chiral symmetry breaking in graphene. The four-fold degeneracy of all Landau levels is seen to be completely resolved in experiments with sufficiently clean samples with strong enough magnetic fields [246]. The vertical axis is the Hall conductivity in units of $\frac{e^2}{h}$. The horizontal axis is charge density at fixed magnetic field.

split the degeneracy of these states. The most important electron-electron interaction in graphene is the Coulomb interaction. There are good arguments that suggest that, for the quarter-, half- or three-quarters filled zero mode Landau level, the Coulomb exchange interaction is minimized by states which resolve the four-fold degeneracy by spontaneously breaking the SU(4) symmetry. Once the symmetry is broken, energy gaps and Hall plateaus emerge at all integer filling fractions. This phenomenon is known in the condensed matter literature as quantum Hall ferromagnetism [84, 147, 80, 177, 175, 190, 101, 11] and in the particle physics literature as magnetic catalysis of chiral symmetry breaking [156, 109, 110, 211, 212, 153, 89, 210, 24, 74, 23, 215, 20, 86].[1] In experiments, this resolution is now seen for all of the integer Hall states [244] as well as the zero modes. In a clean system, the argument for symmetry breaking that we have reviewed here works at arbitrarily weak coupling and gives a candidate for an explanation of this interesting phenomenon.

[1] These mechanisms usually focus on different order parameters and are sometimes thought to be mutually exclusive. In the present case, they are indistinguishable as a nonzero value of one order parameter will lead to a nonzero value of the other, and in fact the order parameters are equal in the weak coupling limit [210].

However, graphene is not weakly coupled. The Coulomb interaction in graphene is putatively strong.[2] In fact, the magnitude of the energy gaps due to symmetry breaking that are seen in experiments is of order the Coulomb energy and they are already large enough to conclude that the system is strongly coupled. At a first pass, to understand the occurrence of this symmetry breaking in graphene, it is necessary to understand whether it can also happen in a strongly coupled system, that is, whether the features of quantum Hall ferromagnetism survive as the coupling constant is increased to large values. Reference [158] gives an affirmative answer to this question in the context of a certain quantum field theory. To be precise, the supersymmetric large N gauge field theory that is considered there cannot be regarded as a model of graphene in all of its details. On the other hand, as we shall outline below, it may be entirely possible that it does model some of the physics of the charge neutral Landau level in graphene. For this reason, among others, it is important to have an improved picture of the predictions of the model.

In this chapter, we shall present a significant elaboration on the work in reference [158]. That work considered the D3-D5 system which is dual to a superconformal defect quantum field theory which has $\mathcal{N} = 4$ supersymmetric Yang-Mills theory living in the bulk of 3+1-dimensional spacetime. The 3+1-dimenisonal spacetime is bisected by an infinite, flat 2+1-dimensional defect. A 2+1-dimensional hypermultiplet field theory resides on the defect and interacts with the $\mathcal{N} = 4$ degrees of freedom in the 3+1-dimensional bulk. The defect field theory preserves half of the supersymmetry of the bulk $\mathcal{N} = 4$ theory and is conformally symmetric for all values of its coupling constant. The field theory living on the defect has both scalar and spinor fields and the Lagrangian is known explicitly [63][75]. At weak coupling, its action contains massless fermions and bosons,

$$\mathcal{S} \sim \int d^3x \sum_{\alpha=1}^{N} \sum_{\gamma=1}^{N_5} \left[\bar{\psi}_a^{\alpha\gamma} i\partial\!\!\!/ \psi_{\alpha\gamma}^a - \partial_\mu \bar{\phi}_{\dot{a}}^{\alpha\gamma} \partial^\mu \phi_{\alpha\gamma}^{\dot{a}} \right] + \ldots, \tag{3.5}$$

which are fundamental representations of the gauged $SU(N)$ color and the global $U(N_5)$ flavor symmetries and are $(0, \frac{1}{2})$ and $(\frac{1}{2}, 0)$ representations of an $SO(3) \times SO(3)$ R-symmetry,

[2] The Coulomb energy of an electron-hole pair on neighboring sites is approximately 10 eV, whereas the tunnelling energy between the sites is about 2.7 eV. This is in line with the rough argument that the graphene fine structure constant which controls the quantum fluctuations of the photon is large: $\alpha_{\text{graphene}} = \frac{e^2}{4\pi\hbar v_F} = \frac{e^2}{4\pi\hbar c}\frac{c}{v_F} \approx \frac{300}{137}$ where we have used graphene's emergent speed of light which is a factor of 300 less than the speed of light in vacuum, $v_F \approx c/300$. This suggests that the Coulomb interaction in graphene is strongly coupled and out of the range of perturbation theory. Other indications such as the approximate perfect conical shape of Dirac cones seen in ARPES measurements [216] suggest that graphene dynamics is approximately scale invariant and has 2+1-dimensional Lorentz invariance over a significant range of energy scales. There is no known truly quantitative mechanism which would explain this.

respectively. The masslessness of the fermions is protected by symmetry as there are no possible time reversal invariant mass operators which preserve all of the $SU(N)$, $U(N_5)$ and $SO(3) \times SO(3)$ symmetries. All solutions that we consider are invariant under color $SU(N)$, the $U(1)$ subgroup of $U(N_5)$ and the first $SO(3)$. We will consider solutions which break either the second $SO(3)$ or the $SU(N_5)$ subgroup of $U(N_5)$ or both, and we will call this "chiral symmetry breaking" . This terminology will apply to any solution where the constant c_2 defined in equation (3.39) in section 3 is nonzero. This constant is called the "chiral condensate". The three dots in the action (3.5) indicate the action of $\mathcal{N} = 4$ Yang-Mills theory and interaction terms.

A constant $U(1) \subset U(N_5)$ external magnetic field, B, breaks supersymmetry. The free fermions and free bosons have different Landau level energies, $\omega_n = \pm\sqrt{2nB}$ and $E_n = \pm\sqrt{(2n+1)B}$, respectively, with $n = 0, 1, 2, ...$ The boson energies have a gap, $\sqrt{B}$. At energies lower than this gap, only the bosonic vacuum is relevant. On the other hand, the fermions have zero modes with degeneracy $2NN_5\frac{B}{2\pi}$. For states with filling fraction $\nu \leq N_5$ (with ν defined in equation (3.3) [3]), the lowest energy modes of the sufficiently weakly interacting theory are governed by the problem of populating the fermion zero modes. The arguments for quantum Hall ferromagnetism should apply to the $\mathcal{N} = 4$ gluon-mediated color interaction. In the large N planar limit in particular, the exchange interaction is emphasized and minimizing it should lead to breaking of the $SO(3)$ chiral symmetry and, depending on the filling fraction, various symmetry breaking patterns for the $U(N_5)$ flavor symmetry. The states with integer filling fractions $\nu = 0, \pm1, \pm2, ..., \pm N_5$ should be gapped, incompressible states with integer quantized Hall conductivities, though the series could truncate before it gets to $\pm N_5$ if the splitting of the states begins to compete with the energy of bosons, which begins at $\sqrt{B}$.[4] Also, the higher fermionic Landau levels are at energies greater than the threshold for creating bosons, so one would expect that they lead to no further incompressible states. We will see shortly that the counting of possible incompressible states is matched on the strong coupling side which is described by string theory.

The strongly coupled system is described by the embedding of N_5 coincident D5-branes

[3]Note that there is a factor of the number of colors, N, in the denominator of that equation. We are assuming that the SU(N) color symmetry remains unbroken. Thus, we take for candidate states only those which are singlets of the global color symmetry. For a many-body state of quarks to be a color singlet, the number of quarks must be an integer multiple of N. Therefore we consider states where the quarks come in multiples of N only. The filling fraction defined in equation (3.3) is the fractional occupancy of a Landau level where this natural N-fold degeneracy is taken into account.

[4]In addition, once supersymmetry and scale symmetry are broken by introduction of a magnetic field, there is no symmetry which prevents a boson mass term $m^2\bar{\phi}^{\alpha\gamma}_{\dot{a}}\phi^{\dot{a}}_{\alpha\gamma}$ from appearing in effective field theory. This would further isolate the fermion zero modes.

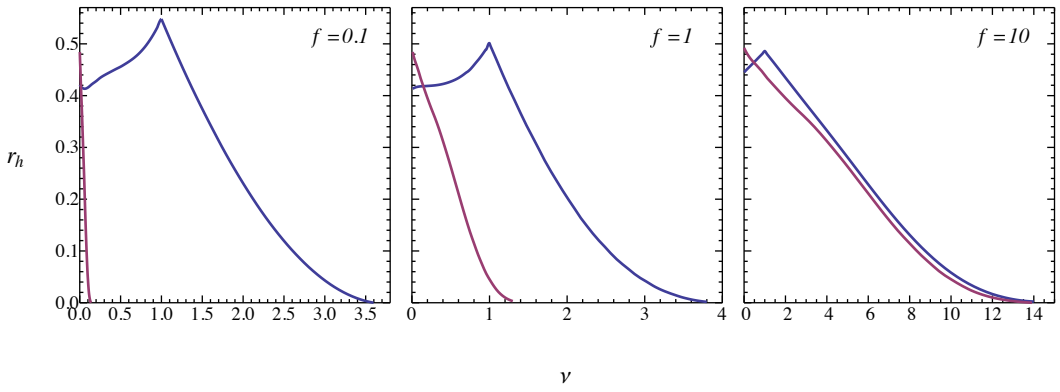

Figure 3.3: Chiral Symmetry Breaking: The wedge in the lower left below the red and blue lines are the regions where the Abelian D5-brane and the D7-brane, respectively, have lower energies than the chiral symmetric D5-brane. The horizontal axis is the filling fraction $\nu = \frac{2\pi\rho}{NB}$ and the vertical axis is the horizon radius (which is proportional to the temperature), in units of magnetic field. The parameter $f = \frac{2\pi N_5}{\sqrt{\lambda}}$ is proportional to the number of D5-branes. Plots for three different values of f are shown.

in the $AdS_5 \times S^5$ background. At zero charge density and in the absence of magnetic fields, the D5-brane geometry is $AdS_4 \times S^2$, which has superconformal symmetry. The AdS_4 is a subspace of AdS_5. The S^2 is the maximal volume S^2 which can be embedded in S^5. The embedding position has an $SO(3)$ symmetry so that an $SO(3) \times SO(3)$ subgroup of the $SO(6)$ symmetry of S^5 survives.

Here, and everywhere in the following, we are considering boundary conditions for the embedding problem which do not violate the chiral symmetry of the gauge theory. This means that, even for other solutions, the worldvolume geometry must approach this maximally symmetric $AdS_4 \times S^2$ geometry sufficiently rapidly as the D5-brane worldvolume approaches the boundary of $AdS_5 \times S^5$. In particular, the S^2 must become the $SO(3) \times SO(3)$ symmetric maximal S^2 and the N_5 multiple D5-branes must become coincident. The latter condition makes their boundary condition symmetric under $SU(N_5)$. If the chiral symmetry is broken, it must be by spontaneous symmetry breaking. This symmetry breaking occurs if, as the D5-brane worldvolume stretches into the bulk of $AdS_5 \times S^5$, either the S^2 which the D5-brane wraps deviates at all from the maximal one of the most symmetric embedding, or the D5-branes spread apart, breaking the global $SU(N_5)$ symmetry. We will encounter both of these behaviors shortly.

If we keep the charge density and the temperature at zero and introduce a constant external magnetic field, the D5-brane geometry changes drastically [89]. Near the boundary of $AdS_5 \times S^5$, the D5-brane is still $AdS_4 \times S^2$. However, as it enters the bulk of AdS_5, it pinches off and ends before it reaches the Poincare horizon of AdS_5, forming what is called a Minkowski embedding. It can pinch off smoothly without creating a boundary when a cycle shrinks to zero size. It is the S^2 which shrinks and chiral symmetry is spontaneously broken. Moreover, a Minkowski embedding has a charge gap due to the fact that charged excitations are open strings which must be suspended between the worldvolume and the Poincare horizon. When the worldvolume does not reach the Poincare horizon, these strings have a minimal length and therefore a gap in their energy spectrum. Thus, the strong coupling limit at $\nu = 0$ has an incompressible, charge-gapped state. This phenomenon is interpreted as the strong coupling manifestation of magnetic catalysis of chiral symmetry breaking. It is reasonable to conjecture that it is precisely the continuation to strong coupling of the formation of a gap at $\nu = 0$ in the neutral Landau level which we discussed at weak coupling. The symmetry breaking pattern is $SO(3) \times SU(N_5) \to SO(2) \times SU(N_5)$. When a charge density and a temperature are turned on the chiral symmetry breaking phase survives for some range of these parameters, but it is eventually restored if the density or temperature become large enough.[5] The chiral symmetric phase of the D5-brane which is found at large enough temperature or density is simply one where the worldsheet is a product metric of the maximal S^2 embedded in S^5 and an asymptotically AdS_4 space, together with a configuration of worldvolume electro-magnetic fields which are needed to create the dual of the field theory with nonzero density and magnetic field.

The simple chiral symmetry breaking solutions of the D3-D5 system have been studied extensively in a number of contexts [79, 85, 76, 140, 77, 78, 104, 87, 105]. Their distinguishing feature can be characterized as "Abelian", in that the dynamics of each D5-brane in the stack of D5-branes is treated independently and their behaviors are all identical. The non-Abelian nature of the worldvolume theory does not play a role. The D5-branes remain coincident and have unbroken $SU(N_5)$ symmetry. The phase diagram of these Abelian solutions is well known. It is reproduced in the numerical results of the present work and corresponds to the red curves in figure 3.3, 3.4, and 3.8. More specifically, the lower-left-hand wedge in figure 3.3 is the region where the "Abelian" chiral symmetry breaking solutions of the D5-brane are stable. At the red line, the chiral symmetric competitor takes over, in the sense that it has lower energy. (The same red curve re-appears in figure 3.4 and figure 3.8.) A more detailed discussion with more details about this phase transition

[5] The fact that the spontaneous breaking of a continuous symmetry in 2+1-dimensions survives at finite temperature would seem to contradict the Coleman-Mermin-Wagner theorem in the field theory. This is a typical artifact of the large N limit.

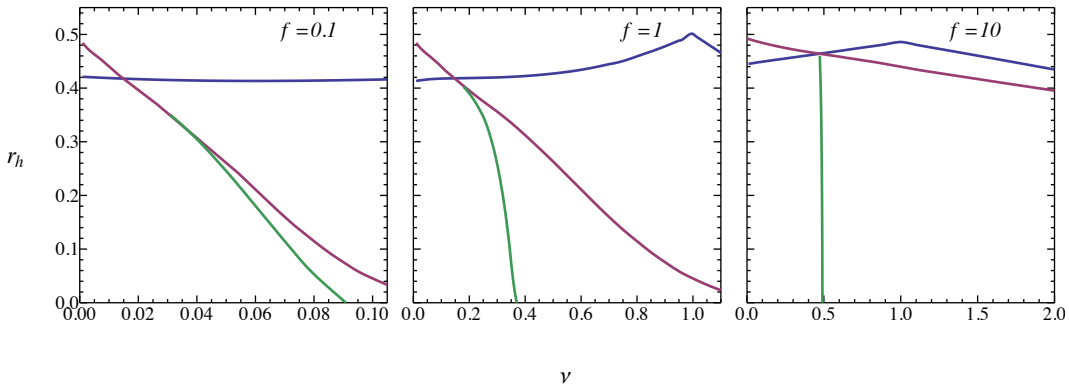

Figure 3.4: Phase diagram extracted from numerical data: The red and blue lines are taken from figure 3.3. They are lines where the chiral symmetric D5-brane has the same energy as the D5 brane (red) and the D7-brane (blue). The chiral symmetric phase is always more stable to the right and toward the top of the figure. The green line is where the Abelian D5-brane and the D7-brane have the same energy with the Abelian D5 preferred to the left and the D7 preferred to the right. The axes and values of f are as in figure 3.3.

is given by Evans et. al. [77].

The D7-brane is an alternative solution of the D5-brane theory.[6] It can be thought of as a "non-Abelian" configuration of D5 branes which is approximated by a D7-brane [158]. The stability region for the D7-brane in the temperature-density plane is similar to that of the Abelian D5-brane, but somewhat larger. It has less energy than the chiral symmetric competitor (the same competitor as for the Abelian D5 brane) to the lower left of the blue line in figure 3.3. The reader should beware that figure 3.3 does not compare the relative energies of the Abelian D5 and the D7-branes. This will be done in figure 3.4.

We now know of three competing solutions of the D3-D5 system, the Abelian D5-brane, the D7-brane and the chiral symmetric solution. (As we shall see later, for $\nu > 1$ we will in addition have the possibility of composite solutions.) To decide which is the preferred one at a given value of the temperature and filling fraction, we must compare their free energies. The free energy is a function of the temperature, the charge density, the magnetic

[6] An alternative solution of a D7-brane theory, called D7', has been studied extensively [17, 144, 142, 18, 143, 145]. It also exhibits incompressible Hall states but with Hall conductivities that are given by irrational numbers. The main difference between that solution and the one that we study here is the behavior at the boundary of AdS_5. The D7 that we consider collapses to a D5-brane there, and should therefore be thought of as a solution of the D3-D5 system whereas D7' remains a D7-brane.

field and the number of D5-branes, N_5. We will use a system of units where the magnetic field is equal to one. This leaves a normalized temperature, the filling fraction ν and the parameter

$$f \equiv \frac{2\pi N_5}{\sqrt{\lambda}}, \tag{3.6}$$

as the variables which define the thermodynamic problem. We have done a numerical calculation of the energies of the three competing solutions. Before we begin to describe it, we warn the reader that, later on, we will find a completely different structure that takes over when the filling fraction ν is greater than or equal to one, and where the temperature is low. Thus, in the end, the following discussion will only apply to the region $0 < \nu < 1$. We will ignore this fact for now and will pursue the following discussion of the relative stabilities of the three solutions that we know about so far for all values of ν.

In figure 3.4, the regions where the Abelian D5-brane and the D7-brane are more stable than the chiral symmetric solution are displayed for three values of f. In all cases, the chiral symmetric solution is stable in the upper right-hand part of the diagram. The Abelian D5-brane is stable in the lower left, below the green line, that is, in all cases, for sufficiently small filling fraction and low temperature. As we increase temperature or filling fraction to the green line, there is a phase transition and, beyond the green line, the D7-brane becomes the energetically preferred solution. It remains so until we approach the blue line where the chiral symmetric phase becomes more stable and chiral symmetry is restored. This part of the blue line is beyond the edge of the figures in 3.4 but can be seen in figure 3.3. In summary, at low temperatures, as we increase the filling fraction from zero, generically there are three phases. First, at low density is the Abelian D5-brane. At some value of the density, there is a phase transition to the D7-brane. Then, at a larger density yet, there is a phase transition to the chiral symmetric state.

At low temperatures, the phase transition at the blue line in figures 3.3 and 3.4 is likely always of first order. At zero temperature, the chiral symmetric phase can be shown analytically to be meta-stable beyond a critical density, which is also known analytically [140]

$$\nu_{\text{crit}} \approx 1.68 f. \tag{3.7}$$

In all of the cases where we have computed it, the blue line always occurs at higher values of ν.[7] This means that there is always a region where the D7-brane has lower energy

[7]For very large values of f, we have observed that the red and blue lines come closer together and it is possible that, for sufficiently large f, they will coincide. In that case, there could be a large f region where the the BKT-like transition from either the abelian D5 or D7-brane to the chiral symmetric phase would still exist.

than a meta-stable chiral symmetric phase. In this region, there must be an energy barrier between the phases. This indicates a first order phase transition. In the case of the Abelian solution at zero temperature, it is known that the transition to the chiral symmetric phase occurs precisely at $\nu_{\rm crit}$ and it is BKT like [140]. This is the intersection of the red line with the horizontal axis in figures 3.3 and 3.4. It is a beautiful and rare example of a non-mean-field phase transition for probe D branes. However, in all of the cases that we have studied, including those in figure 3.4, the green line occurs at values ν smaller than $\nu_{\rm crit}$ and the D7-brane is more stable than either the Abelian D5 or the chiral symmetric D5 in this region - there is no BKT-like transition in these cases.

The three phases that we have discussed so far have distinct symmetry breaking patterns. The Abelian D5-brane phase breaks the $SO(3)$ symmetry to $SO(2)$, but preserves the $SU(N_5)$ flavor symmetry. The D7-brane phase breaks both the $SO(3)$ symmetry and the $SU(N_5)$ leaving only a subgroup of simultaneous transformations in $SO(3)$ and an $SO(3)$ subgroup of $SU(N_5)$. Then the chiral symmetric phase retains both the $SO(3)$ and the $SU(N_5)$. This pattern of symmetry breaking is one of the predictions of the holographic model. However, as we have warned the reader. further developments that we shall outline below will cut this scenario off when the filling fraction reaches $\nu = 1$. It is only the behavior which occurs in the interval where $0 < \nu < 1$ which will turn out to be a prediction of what we have done so far.[8] As we can see by inspecting figures 3.3 and 3.4, the first transition from Abelian D5 to D7 typically occurs in this interval whereas the second, from D7 to chiral symmetric D5 does not.

The Abelian D5-brane has the feature that, once a non-zero charge density is turned on, it can no longer have a Minkowski embedding. This means that the theory no longer has a charge gap. Without a magnetic field, this would be natural. The analog at weak coupling is a finite density of fermions which create a Fermi surface. There are always low energy excitations of a Fermi surface. Such a system is not gapped, and this is also what is seen for the Abelian D5-brane. However, the Abelian D5-brane also remains ungapped in an external magnetic field, for any value of the magnetic field and any nonzero density. In other words, besides the $\nu = 0$ state, the Abelian D5-brane solutions contain no incompressible states at non-zero filling fractions, even in arbitrarily strong magnetic fields.

The D7-brane, on the other hand, can have incompressible states at special nonzero values of the charge density [158]. The D7-brane should properly be regarded as a non-Abelian configuration of D5-branes. It arises in the D5-brane theory when the transverse

[8] Of course, in a real two dimensional electron gas, the physics of some of the region that we are talking about here is dominated by other effects such as impurities and localization. Our prediction could still appy to the symmetries of the Hall plateaus which are formed by these other effects. The other possibility is the clean limit which is thus far proven difficult to achieve, even in graphene.

coordinates of the N_5 embedded D5-branes, which are $N_5 \times N_5$ matrices, form a fuzzy sphere.[9] It would be interesting to understand this "non-Abelian" configuration of the D5-brane better from this point of view. We shall not do this in the following. Instead, we simply approximate it by a classical D7-brane which wraps both of the S^2's in S^5. The second S^2 is the classical limit of the fuzzy sphere. The D7-brane remembers its origin as N_5 D5 branes by supporting a magnetic flux with Dirac monopole number N_5 on the second S^2. This approximation should be good when the number of D5-branes, N_5, is much greater than one, but still much less than N. In the asymptotic region near the boundary of $AdS_5 \times S^5$ the D7-brane has geometry $AdS_4 \times S^2 \times S^2$ where one S^2, the same one which is wrapped by the Abelian D5-brane, is nearly maximal and the other S^2 shrinks to zero size as the boundary is approached. This sphere has magnetic flux and when it shrinks to zero size it leaves a singular magnetic source. This can be regarded as a point where a D5-brane is attached to the D7-brane and it occurs precisely at the boundary of AdS_5.

In figures 3.3 and 3.4 there are peaks of the blue curves at $\nu = 1$. This is the special state of the D7 brane, where it has a Minkowski embedding and is incompressible with a charge gap. At low enough temperature, this state is energetically preferred over its competitors in the entire range of the parameter f that we have been able to study. Its existence also allows us to find an incompressible state for higher integer values of ν. This is gotten by simply taking ν D7-branes, each with filling fraction equal to one. As well as the charge density, which they share equally, the D7-branes must share the N_5 D5-branes between them. A numerical computation in reference [158] indicated that, at least for $\nu = 2$, first of all, the energy is minimized when the D5-branes are shared equally and secondly, the energy of two gapped $\nu = 1$ D7-branes with f shared equally between them is less than the energy of one ungapped $\nu = 2$ D7-brane or Abelian D5-brane. The

[9] S^5 is the locus of $n_1^2 + \ldots + n_6^2 = 1$ for real numbers $(n_1, ..., n_6)$. The two S^2's are loci of $n_1^2 + n_2^2 + n_3^2 = \sin^2\psi$ and $n_4^2 + n_5^2 + n_6^2 = \cos^2\psi$. All D5 and D7-brane solutions which we discuss wrap the first sphere, (n_1, n_2, n_3), and its $SO(3)$ isometry is preserved. For the D5-brane, (n_1, n_2, n_3) are longitudinal coordinates and (n_4, n_5, n_6) are transverse coordinates. The chiral symmetric D5-brane sits at a higher symmetry point $n_4 = n_5 = n_6 = 0$ (or $\psi = \frac{\pi}{2}$) and preserves the second $SO(3)$ symmetry. The Abelian D5 solution has some of the (n_4, n_5, n_6) non-zero. This breaks the second $SO(3)$ (and preserves $SU(N_5)$). The D7-brane is a non-Abelian D5-brane where (n_4, n_5, n_6) are $N_5 \times N_5$ matrices in the $SU(N_5)$ Lie algebra and which form an irreducible representation of an $SO(3)$ subalgebra of $SU(N_5)$,

$$[n_a, n_b] = i\epsilon_{abc} n_c \ . \tag{3.8}$$

The D7-brane preserves an $SO(3)$ which is a combination of the $SO(3)$ of the second S^2 and the $SO(3)$ subgroup of $SU(N_5)$. A time reversal invariant fermion mass operator (and order parameter for chiral symmetry breaking) which is invariant under the residual symmetry would be $m\bar{\psi} n_a \sigma^a \psi$. In the classical description as a D7-brane wrapping the second S^2 with N_5 units of monopole flux, the unbroken symmetry is the magnetic translation group on the S^2.

second of these results tells us that the $\nu = 2$ gapped state with 2 D7-branes is preferred over the other possible ungapped states. The first one tells us that the gapped state is a state with two coincident gapped D7-branes. We conjecture but have not checked that this pattern persists to higher values of ν. Here, we shall assume that when the charge density is shared equally, the branes also prefer to share N_5 D5-branes equally. Indeed, this state has more symmetry than the alternatives, since the ν D7-branes are identical and coincident, and therefore have an unbroken internal gauge symmetry $SU(\nu)$. This would be an unbroken global symmetry of the field theory dual. Of course, in the strict sense, it can only happen if ν is an integer divisor of N_5. However, in the large N_5 limit that we are considering, the N_5 D5-branes can always be split equally to precision $\frac{1}{N_5}$ and the residual symmetry would be there to a very good approximation. This symmetry would be a subgroup $SU(\nu) \subset SU(N_5)$ which (in addition to some $SO(3)$'s), survives dynamical symmetry breaking by D7-branes. Its existence can be regarded as a prediction of our hypothesis for finding the charge gapped state with integer filling fraction ν.

Now, we are ready to take the next step and understand the ungapped states in the region between integer filling fractions, say the region $1 \leq \nu \leq 2$. At $\nu = 1$ the stable state is the gapped D7-brane. If we increase ν slightly, we might expect that the lowest energy state is a composite brane made from the same gapped D7-brane and either an ungapped Abelian D5-brane or an ungapped D7-brane where, in both cases, the second, ungapped brane takes on a share of the filling fraction, $\nu - 1$. In addition to this, the gapped and ungapped branes must share the N_5 D5-branes between them. Exactly how N_5 is distributed between the branes in the composite system is a dynamical question which we shall solve numerically in a few cases.[10]

Our investigation shows that, which ungapped brane is stable depends on the total N_5 through the parameter f defined in equation (3.6). If f is big enough, the Abelian D5 brane wins, and the state just above $\nu = 1$ is a hybrid of the gapped D7-brane and the ungapped Abelian D5-brane. Then, there is a phase transition in this intermediate region $\nu \in [1, 2]$, at a critical value of ν, to a state which is a composite of the gapped D7 and an ungapped D7-brane. As ν is increased further, and $\nu = 2$ approached from smaller values

[10] In the non-Abelian picture, the transverse matrix-valued coordinates of the gapped D7-ungapped D7-brane composite would have the n_a in equation (3.8) block-diagonal,

$$n_a = \begin{bmatrix} L_a^{(1)} & 0 \\ 0 & L_a^{(2)} \end{bmatrix}$$

where $L_a^{(1)}$ is a $n \times n$ and $L_a^{(2)}$ is an $(N_5 - n) \times (N_5 - n)$ irreducible representation of $SO(3)$, respectively. For the gapped D7-ungapped Abelian D5-brane composite, $L_a^{(2)}$ is replaced by 0.

of ν, the state should be the gapped D7-ungapped D7-brane composite. When $\nu = 2$ is reached, as we have discussed above, it becomes two coincident gapped D7-branes, each with $\nu = 1$. At smaller values of f, our results indicate that the state just above $\nu = 1$ is immediately a composite of the gapped D7-brane and the ungapped D7-brane. The Abelian D5-brane does not appear at all in the interval $1 \leq \nu \leq 2$.

A similar pattern of composite branes is repeated in the intervals between larger integer values of ν. We have investigated this by numerical computation and have found that it is indeed the case. We have explicit numerical solutions up to the interval $8 \leq \nu \leq 9$. We currently have no evidence that the pattern stops. We also find that, even when f is large enough that the Abelian D5-brane phase exists just above the lower integer ν's, this is so only of the smaller values of ν. At higher integers, the Abelian D5 phase ceases to occur and integer ν D7-branes immediately become a composite of the gapped D7-branes and an ungapped D7-brane when ν is increased beyond the integer value.

In summary, in the defect quantum field theory that we are studying, when the magnetic field is turned on, for any value of the field strength, the chiral symmetry is broken in that there is always a chiral condensate. However, there is a charge gap only when ν is an integer, either positive or negative, and for values of ν with magnitude no bigger than N_5. The series could truncate before it gets to $\nu = \pm N_5$. We have not seen numerical evidence for this truncation, mainly due to the fact that our analysis considers very large N_5 and smaller values of ν. Between the integer values of ν, even though there is a nonzero chiral condensate, there is no charge gap.

The symmetry breaking patterns are then quite interesting. Let us begin with the case where f is small enough that the only composite branes are gapped D7-ungapped D7-branes. Let us begin at $\nu = 0$. There, at $\nu = 0$, as soon as the magnetic field is turned on, the SO(3) is spontaneously broken to an $SO(2)$ subgroup. The full $SU(N_5)$ symmetry is preserved there. As ν is increased, this symmetry breaking pattern persists up to a phase transition at a critical value of ν between zero and one, where there is a phase transition. At that phase transition, the system goes to a phase where the only symmetry which survives is in a diagonal subgroup of $SO(3)$ and an $SO(3)$ subgroup of $SU(N_5)$. This symmetry breaking pattern then persists until we reach $\nu = 1$, where it is also the symmetry of the charge gapped state which appears at $\nu = 1$. Then, when we increase ν beyond one, the pattern changes again. The composite gapped D7-ungapped D7-brane that is stable there preserves two diagonal $SO(3)$'s, one for each D7-brane. These consist of $SO(3)$ rotations combined with rotations in two commuting $SO(3)$ subgroups of $SU(N_5)$. When we reach $\nu = 2$, this symmetry is enhanced once again. The diagonal $SO(3)$'s become degenerate and they are transformed into each other by an additional $SU(2)$ subgroup of $SU(N_5)$. That is, at $\nu = 2$, out of the original $SO(3) \times SU(N_5)$, the symmetry which survives is

$[SO(3)]^2 \times SU(2)$. When we increase ν to values just above two, the stable solution being a two gapped D7-one ungapped D7 composite, the symmetries that existed at filling fraction two are still there and, in addition, another new diagonal $SO(3)$ emerges so that the total is $[SO(3)]^2 \times SO(3) \times SU(2)$. The latter is the symmetry of the third, gapped D7-brane. When we reach $\nu = 3$, the third diagonal $SO(3)$ becomes degenerate with the first two, so that $[SO(3)]^2 \times SO(3) \times SU(2)$ becomes $[SO(3)]^3 \times SU(3)$. As far as we have investigated, this pattern repeats itself as we proceed to higher values of ν. At $\nu = n$, out of the original $SO(3) \times SU(N_5)$, the symmetry which survives is $[SO(3)]^n \times SU(n)$. When ν is just above n, this gets an additional $SO(3)$ to become $[SO(3)]^n \times SO(3) \times SU(n)$. When we reach $\nu = n + 1$ this is enhanced again to $[SO(3)]^{n+1} \times SU(n + 1)$. Of course, we know this reliably only when $n << N_5$. To study what happens for larger values of n is beyond our current ability, but would indeed be very interesting.

If the parameter f is larger, the additional composite phase, where there are n gapped D7-branes and an Abelian D5-brane, inserts itself in some of the regions just above $\nu = n$. We find that this is so, at least for big enough values of f and for small enough values of n. We have seen that, for $f = 10$, this happens for $\nu = 1, 2, 3$ and it ends at $\nu = 4$. Thereafter the states are always composites of D7-branes. This phase involving D5-branes breaks the $SO(3)$ of the second S^2 to $SO(2)$, and it leaves its share of the $SU(N_5)$ symmetry intact. It therefore has residual symmetry $[SO(2)]^n \times SU(n) \times SU(N_5 - N_5^0)$ where N_5^0 is the number of D5-branes that are absorbed by the n gapped D7-branes in the composite, leaving a stack of $N_5 - N_5^0$ D5-branes for the Abelian D5-brane part of the composite. Then, somewhere in the interval $\nu = [n, n + 1]$ we expect a phase transition where the ungapped Abelian D5-brane blows up to an ungapped D7-brane, so that $[SO(2)]^n \times SU(n) \times SU(N_5 - N_5^0) \rightarrow [SO(3)]^n \times SO(3) \times SU(n)$. At some big enough value of n, the intermediate composites with Abelian D5-branes cease to exist and the pattern of the preceding paragraph takes over.

These symmetry breaking patterns can be considered a prediction of our holographic model and it is interesting to ask whether they are relevant to any realistic system. Aside from the supersymmetric system that is modelled directly, there is some hope that the model also captures some of the physics of any electronic system with degenerate Landau levels and a strong repulsive interaction. If interactions are ignored entirely, $2N_5$ degenerate Landau levels have an effective $SU(2N_5)$ symmetry. In our model, the interactions on the other hand, have only a smaller symmetry, $SO(3) \times SU(N_5)$. (We are also ignoring the other, first $SO(3)$, which transforms the first S^2 in the string theory and acts on the scalar fields in the weakly coupled field theory.) We are only able to analyze the situation where N_5 is large. We might wonder whether some aspect of the symmetry breaking pattern survives for small values of N_5. Then, the generic prediction is that the $\nu = 0$ state, that

is the one where half of the states are filled, has distinctly different symmetry from all of the others.

The most realistic possibility is $N_5 = 2$ which could match the symmetries (spin times valley) of graphene or the a bilayer quantum Hall system where the SO(3) is spin symmetry and the SU(2) transforms the layer index. In both of these cases, the valley/layer symmetry is only approximate. In graphene, the long ranged Coulomb interaction is $SU(4)$ symmetric and short ranged parts reduce this symmetry to $SO(3) \times Z_2$, which is sometimes approximated by $SO(3) \times SU(2)$ where further, weaker interactions break the $SU(2)$ [175].

We could ask how our symmetry breaking patterns would be seen in the weak coupling states where the charge neutral Landau level is fractionally filled. Let us go back to weak coupling for a moment. Denote the completely empty four-fold degenerate Landau level as $|0>$ and the electron creation operator as $\psi^\dagger_{Pab}$ where P denotes a state in some basis of the degenerate single-electron states of the Landau level and a, b, each taking values $\uparrow, \downarrow$ are valley/layer and spin indices. To get a translation invariant state, we must create an electron within each degenerate state of the Landau level, that is we must fill all of the states denoted by P. We begin by half-filling the Landau level to get the $\nu = 0$ state. That state has $SO(3)$ symmetry broken to $SO(2)$, but still has good $SU(2)$ symmetry. This should be the symmetry pattern of the $\nu = 0$ plateau. The weak coupling state that does this is

$$\prod_P \psi^\dagger_{P\uparrow\uparrow}\psi^\dagger_{P\uparrow\downarrow}\ |0>$$

which is, for each state P in the Landau level, a valley triplet and spin singlet. It thus breaks the valley symmetry and preserves the spin symmetry. (The inverse is also possible, where the spin symmetry is broken and the valley symmetry survives. Here we are not distinguishing spin and valley symmetries.)

Then, consider the one-quarter and three-quarter filled states. For graphene, these are the $\nu = -1$ and $\nu = 1$ states, respectively. Quarter filling is achieved by creating an electron in one quarter of the zero mode states. A simple candidate for such a state is

$$\prod_P \psi^\dagger_{P\uparrow\uparrow}\ |0>$$

which is both spin and valley polarized. [11] This state breaks both the spin and valley

[11] If graphene, say, were fully $SU(4)$ symmetric, the $SU(4)$ could be used to rotate this state to any other choice, so if the dynamics were $SU(4)$ invariant, this would be the most general state. However, if the interactions are not fully $SU(4)$ invariant, but are symmetric under $SO(3) \times SU(2)$ instead, this state would break both the $SO(3)$ and $SU(2)$ symmetries. What is more, it is not the unique choice for a quarter filled state. The holographic states suggest the alternative state (3.9).

symmetry. This is a different symmetry breaking pattern than we found for our holographic state with $\nu = 1$. We can make a many body state with a symmetry breaking pattern which matches the holographic state. It would be the state

$$\prod_P \frac{1}{\sqrt{2}} \epsilon^{ab} \psi^\dagger_{Pab} \; |0> = \prod_P \frac{1}{\sqrt{2}} (\psi^\dagger_{P\uparrow\downarrow} - \psi^\dagger_{P\downarrow\uparrow}) \; |0> \tag{3.9}$$

This state is neither spin nor valley polarized. It is a singlet under a simultaneous spin and valley rotation, and a triplet under a spin rotation and a simultaneous valley inverse rotation. Since, for the fermion zero mode Landau level that we are discussing, the wave-function of the zero modes in a specific valley also occupy only one of the graphene sublattices [209], the other valley occupying the other sublattice, a flip of the valley index corresponds to a translation which interchanges the sublattices. Since the state (3.9) is left unchanged by a simultaneous flip of valley and spin indices, this state is then an anti-ferromagnet.

There is a state at three-quarters filling that has similar symmetries,

$$\prod_P \frac{1}{\sqrt{8}} \epsilon^{fa} \psi^\dagger_{Pab} \epsilon^{bc} \psi^\dagger_{Pcd} \epsilon^{de} \psi^\dagger_{Pef} \; |0>$$

This state is also spin and valley unpolarized. The fact that the integer $\nu \neq 0$ states are that way is a generic feature of the holographic model. Here, we see that it suggests a particular state for both $\nu = -1$ and $\nu = 1$. It would be interesting to see if this suggestion is realized in graphene or multilayer Hall systems. Recent experimental results seem consistent with this picture [244].

The remainder of this chapter discusses the details of the work that has been summarized in this introduction. In section 2 we discuss the mathematical problem of embedding D5 and D7-branes in $AdS_5 \times S^5$. In section 3, we discuss the boundary conditions and the asymptotic behavior of the solutions that we are looking for. In section 4 we discuss the details of both the technique and results of our numerical computations. In section 5 we conclude and we discuss directions for further work.

3.2 The geometric set-up

We shall study D5 and D7 probe branes at finite temperature and density. We will embed them in the asymptotically $AdS_5 \times S^5$ black hole background using coordinates where the

metric has the form

$$ds^2 = \sqrt{\lambda}\alpha' \Big[r^2(-h(r)dt^2 + dx^2 + dy^2 + dz^2) + \frac{dr^2}{h(r)r^2} + \\ + d\psi^2 + \sin^2\psi(d\theta^2 + \sin^2\theta d\phi^2) + \cos^2\psi(d\tilde{\theta}^2 + \sin^2\tilde{\theta} d\tilde{\phi}^2) \Big] , \tag{3.10}$$

Here, the coordinates of S^5 are a fibration of the 5-sphere by two 2-spheres over the interval $\psi \in [0, \pi/2]$. Furthermore, (t, x, y, z, r) are coordinates of the Poincare patch of AdS_5 and

$$h(r) = 1 - \frac{r_h^4}{r^4} ,$$

with r_h the radius of the event horizon. The Hawking temperature is $T = r_h/\pi$. The Ramond-Ramond 4-form of the IIB supergravity background takes the form

$$C^{(4)} = \lambda\alpha'^2 \left[h(r) r^4 dt \wedge dx \wedge dy \wedge dz + \frac{c(\psi)}{2} d\cos\theta \wedge d\phi \wedge d\cos\tilde{\theta} \wedge d\tilde{\phi} \right] , \tag{3.11}$$

Here, $\partial_\psi c(\psi) = 8\sin^2\psi\cos^2\psi$ and for later convenience we choose

$$c(\psi) = \psi - \frac{1}{4}\sin 4\psi - \frac{\pi}{2}. \tag{3.12}$$

The choice of integration constant is a string theory gauge choice and our results will not depend on it.

We will study D5 and D7-branes as well as some composite systems thereof in this background using the probe approximation where the number of probe branes N_5 and N_7 is much smaller than the number, N, of D3-branes. The world volume coordinates of our probe branes will be as given in the table below.

(3.13)

	t	x	y	z	r	ψ	θ	ϕ	$\tilde{\theta}$	$\tilde{\phi}$
$D3$	×	×	×	×						
$D5$	×	×	×		×		×	×		
$D7$	×	×	×		×		×	×	×	×

(3.14)

Table 1 : D3, D5 and D7 world volume coordinates

3.2.1 Probe D5-branes

Probe D5-branes are described by the DBI plus WZ actions, *i.e.,*

$$S_5 = \frac{T_5}{g_s} N_5 \int d^6\sigma \left[-\sqrt{-\det(g + 2\pi\alpha' \mathcal{F}_5)} + 2\pi\alpha' C^{(4)} \wedge \mathcal{F}_5 \right], \tag{3.15}$$

where g_s is the closed string coupling constant, which is related to the $\mathcal{N} = 4$ Yang-Mills coupling by $4\pi g_s = g_{YM}^2$, σ^a are the coordinates of the D5-brane worldvolume, $g_{ab}(\sigma)$ is the induced metric of the D5 brane, $\mathcal{F}_5$ is the worldvolume gauge field and

$$T_5 = \frac{1}{(2\pi)^5 \alpha'^3}, \tag{3.16}$$

is the D5-brane tension. The Wess-Zumino action will not contribute to the D5-brane equations of motion for the types of embeddings that we will discuss here. The overall factor of N_5 denotes the number of D5-branes. We are here assuming that the non-Abelian $U(N_5)$ gauge symmetry structure of multiple N_5 branes plays no role. We shall take the world volume gauge field strength to be of the form

$$2\pi\alpha' \mathcal{F}_5 = \sqrt{\lambda}\alpha' \left[\frac{d}{dr} a(r) dr \wedge dt + b dx \wedge dy \right]. \tag{3.17}$$

Hence, we have a constant external magnetic field

$$B = \frac{\sqrt{\lambda}}{2\pi}\, b, \tag{3.18}$$

and a charge density ρ

$$\rho = \frac{1}{V_{2+1}} \frac{2\pi}{\sqrt{\lambda}} \frac{\delta S_5}{\delta \frac{d}{dr} a(r)}.$$

It is well known that there exists an embedding of the D5-brane with the world volume coordinates $(t, x, y, r, \theta, \phi)$ for which $\tilde{\theta}$, $\tilde{\phi}$ and z are constant and for which $\psi = \psi(r)$ depends only on r. For this embedding the world volume metric can be written as

$$ds^2 = \sqrt{\lambda}\alpha' \left[r^2(-h(r)dt^2 + dx^2 + dy^2) + \sin^2\psi(d\theta^2 + \sin^2\theta d\phi^2) \right. . \\ \left. + \frac{dr^2}{h(r) r^2} \left(1 + h(r) \left(r \frac{d\psi}{dr} \right)^2 \right) \right], \tag{3.19}$$

and the DBI action becomes

$$S_5 = -\mathcal{N}_5 N_5 \int_0^\infty dr\ 2\sin^2\psi\sqrt{b^2+r^4}\sqrt{1+h(r)\left(r\frac{d\psi}{dr}\right)^2-\left(\frac{da}{dr}\right)^2}, \tag{3.20}$$

where, using equation (3.16),

$$\mathcal{N}_5 = \frac{T_5}{g_s}(\sqrt{\lambda}\alpha')^3(2\pi)V_{2+1} = \frac{2\sqrt{\lambda}N}{(2\pi)^3}V_{2+1}. \tag{3.21}$$

The factor $(\sqrt{\lambda}\alpha')^3$ comes from the overall factor in the worldvolume metric in equation (3.19), the factor of (2π) is from the integral over the worldvolume two-sphere.[12] and the integral over (x, y, t) produces the volume factor V_{2+1}. To finalize the description of the embedding of the D5-brane we should determine the functions $\psi(r)$ and $a(r)$ by varying the action above. In the process of variation one can use the boundary condition

$$\lim_{r\to\infty}\psi(r) = \frac{\pi}{2}, \tag{3.22}$$

which, as we shall see later, is compatible with the equation of motion for ψ. Since the variable $a(r)$ enters the Lagrangian only via its derivative, $a(r)$ is cyclic and can be eliminated in favor of an integration constant using its equations of motion. The corresponding integration constant is (up to another constant factor) equal to the charge density ρ, hence

$$\rho = const.$$

Eliminating $a(r)$ via a Legendre transform, following the steps of reference [158], gives us the Routhian,

$$\mathcal{R}_5 = -\frac{\mathcal{N}_5 N_5}{f}\left(\frac{2\pi B}{\sqrt{\lambda}}\right)^{\frac{3}{2}}\int_0^\infty dr\ \mathcal{L}_5, \tag{3.23}$$

where

$$\mathcal{L}_5 = \sqrt{4\sin^4\psi f^2(1+r^4)+(\pi\nu)^2}\sqrt{1+h(r)\left(r\frac{d\psi}{dr}\right)^2}. \tag{3.24}$$

[12]It is half of the volume of the 2-sphere. The other factor of 2 is still in the action in front of $\sin^2\psi$. This notation is designed to match with the D7 brane, which we shall study in the next section, and to coincide with notation in reference [158].

Here r is a dimensionless variable, obtained by rescaling $r \to r\sqrt{b}$, the quantity f is related to the total number of D5-branes, i.e

$$f = \frac{2\pi}{\sqrt{\lambda}} N_5, \tag{3.25}$$

and finally ν is the filling fraction

$$\nu = \frac{2\pi}{N}\frac{\rho}{B}. \tag{3.26}$$

To determine $\psi(r)$ we should now finally extremize the Routhian keeping ν fixed. This leads to the following equation of motion for $\psi(r)$

$$\begin{aligned} &\frac{h\left(r\frac{d}{dr}\right)^2\psi}{1+h\left(r\frac{d}{dr}\psi\right)^2} + hr\frac{d}{dr}\psi\left[1+\frac{8r^4\sin^4\psi f^2}{4\sin^4\psi f^2(1+r^4)+(\pi\nu)^2}\right] \\ -2\frac{r_h^4}{r^4}r\frac{d}{dr}\psi&\left[1+\frac{1}{1+h\left(r\frac{d}{dr}\psi\right)^2}\right] - \frac{8\sin^3\psi\cos\psi f^2(1+r^4)}{4\sin^4\psi f^2(1+r^4)+(\pi\nu)^2} = 0. \end{aligned} \tag{3.27}$$

where, now r_h is in magnetic units, *i.e.,* it has been rescaled $r_h \to r_h/b^{\frac{1}{2}}$ so that

$$r_h^2 = \pi^2 T^2 \frac{\sqrt{\lambda}}{2\pi B}. \tag{3.28}$$

Note that the D5-brane solutions will depend only on the ratio $\frac{\nu}{f}$ and on the temperature T in magnetic units.

3.2.2 Probe D7-branes

For probe D7-branes the DBI plus WZ action reads

$$S = \frac{T_7}{g_s}\int d^8\sigma\left[-\sqrt{-\det(g+2\pi\alpha'\mathcal{F}_7)} + \frac{(2\pi\alpha')^2}{2}C^{(4)}\wedge\mathcal{F}_7\wedge\mathcal{F}_7\right], \tag{3.29}$$

where

$$T_7 = \frac{1}{(2\pi)^7\alpha'^4}, \tag{3.30}$$

is the D7-brane tension. Notice that here we are considering a single D7-brane. The world volume gauge field strength we take to be of the form

$$2\pi\alpha'\mathcal{F}_7 = \sqrt{\lambda}\alpha'\left(\frac{d}{dr}a(r)dr\wedge dt + bdx\wedge dy + \frac{f}{2}d\cos\tilde{\theta}\wedge d\tilde{\phi}\right). \tag{3.31}$$

The flux parameter, f, is the parameter defined in equation (3.25). It corresponds to N_5 Dirac monopoles on $\tilde{S}^2$. The magnetic field and the charge density are again given by expressions (3.18) and (3.2.1). We will now be interested in the embedding of the D7-brane with world volume coordinates $(t, x, y, r, \theta, \phi, \tilde{\theta}, \tilde{\phi})$ and we know that there exists an embedding for which z is a constant and $\psi = \psi(r)$ is a function of ψ only. The corresponding D7 brane world volume metric reads

$$\begin{aligned} ds^2 = \sqrt{\lambda}\alpha'\Bigg[r^2(-h(r)dt^2 + dx^2 + dy^2) + \frac{dr^2}{h(r)r^2}\left(1 + h(r)\left(r\frac{d\psi}{dr}\right)^2\right) + \\ + \sin^2\psi(d\theta^2 + \sin^2\theta d\phi^2) + \cos^2\psi(d\tilde{\theta}^2 + \sin^2\tilde{\theta}d\tilde{\phi}^2)\Bigg], \end{aligned} \tag{3.32}$$

and the action becomes

$$\begin{aligned} S_7 = -\mathcal{N}_7\int_0^\infty dr\Bigg[2\sin^2\psi\sqrt{(f^2 + 4\cos^4\psi)(b^2 + r^4)}\sqrt{1 + h(r)\left(r\frac{d\psi}{dr}\right)^2 - \left(\frac{da}{dr}\right)^2} \\ + 2\frac{da}{dr}bc(\psi)\Bigg], \end{aligned} \tag{3.33}$$

where, using equation (3.30),

$$\mathcal{N}_7 = \frac{2\lambda N}{(2\pi)^4}V_{2+1}. \tag{3.34}$$

Again to finalize the embedding we have to determine the functions $\psi(r)$ and $a(r)$ by varying the action. We will use the same boundary condition as before, *i.e.,* the one given in equation (3.22) which again will indeed be compatible with the equations of motion for $\psi(r)$. In this connection it is convenient that we have chosen $c(\psi)$ as in equation (3.12). Similarly to before $a(r)$ is a cyclic variable which can be eliminated using its equation of motion and the corresponding integration constant is again equal to the charge density up to a constant factor (different from the one of the D5 case). We will be interested in the situation where we fix the integration constants so that the charge density, ρ, is the

same for D5-branes and D7-branes. After eliminating $a(r)$ via a Legendre transformation as before we find the following Routhian

$$\mathcal{R}_7 = -\mathcal{N}_7 \left(\frac{2\pi B}{\sqrt{\lambda}}\right)^{\frac{3}{2}} \int_0^\infty dr \mathcal{L}_7, \tag{3.35}$$

with

$$\mathcal{L}_7 = \sqrt{4\sin^4\psi(f^2+4\cos^4\psi)(1+r^4)+(\pi(\nu-1)+2\psi-\frac{1}{2}\sin 4\psi)^2}\ \times \\ \sqrt{1+h(r)\left(r\frac{d\psi}{dr}\right)^2}, \tag{3.36}$$

where we have rescaled r in the same way as before $r \to r\sqrt{b}$ and where ν is defined in equation (3.26). From the Routhian we derive the following equation of motion for $\psi(r)$

$$\begin{aligned} 0 =& \frac{h\left(r\frac{d}{dr}\right)^2\psi}{1+h\left(r\frac{d\psi}{dr}\right)^2} - 2\frac{r_h^4}{r^4} r\frac{d}{dr}\psi\left[1+\frac{1}{1+h\left(r\frac{d}{dr}\psi\right)^2}\right] \\ &+ hr\frac{d\psi}{dr}\left[1+\frac{8r^4\sin^4\psi(f^2+4\cos^4\psi)}{4\sin^4\psi(f^2+4\cos^4\psi)(1+r^4)+(\pi(\nu-1)+2\psi-\frac{1}{2}\sin 4\psi)^2}\right] \\ &- \frac{8\sin^3\psi\cos\psi f^2(1+r^4)+4\sin^3 2\psi\cos 2\psi r^4+4\sin^2 2\psi(\pi(\nu-1)+2\psi)}{4\sin^4\psi(f^2+4\cos^4\psi)(1+r^4)+(\pi(\nu-1)+2\psi-\frac{1}{2}\sin 4\psi)^2}. \end{aligned} \tag{3.37}$$

The main difference between the Routhian for the D5 and D7-branes is the term arising from the charge density, it is $(\pi\nu)^2$ for the D5-brane and $(\pi(\nu-1)+2\psi-\frac{1}{2}\sin 4\psi)^2$ for the D7-brane. This difference comes from the presence of Wess-Zumino terms in the action for the D7-brane.

3.3 Characteristics of solutions

3.3.1 Asymptotic behaviour as $r \to \infty$

Looking at the equations of motions for $\psi(r)$ for the $D5$ branes and the D7-branes respectively, *i.e.,* equations (3.27) and (3.37), one can check that the asymptotic behaviour

$\psi(r) \to \frac{\pi}{2}$ as $r \to \infty$, assumed in their derivation, is indeed compatible with these. Expanding $\psi(r) = \frac{\pi}{2} + \delta\psi$ for large r one furthermore finds the following differential equation both for D5 and D7

$$\left(r\frac{d}{dr}\right)^2 \delta\psi + 3\left(r\frac{d}{dr}\right)\delta\psi + 2\delta\psi = 0. \tag{3.38}$$

This equation has the solution $\delta\psi(r) = \frac{c_1}{r} + \frac{c_2}{r^2}$ and hence for large r

$$\psi(r) = \frac{\pi}{2} + \frac{c_1}{r} + \frac{c_2}{r^2} + \dots. \tag{3.39}$$

Since the full equations of motions for $\psi(r)$ are second order differential equations the two integration constants c_1 and c_2 completely characterize the solution. In the dual field theory language c_1 is a quantity proportional to the bare mass of the fundamental representation fields and c_2 is proportional to the chiral condensate. In this chapter we will always be dealing with the massless case, *i.e.*, $c_1 = 0$.

It is easy to see that the constant function $\psi(r) = \frac{\pi}{2}$ is a solution of the equations of motion for all $r \in [r_h, \infty]$ both for the D5-brane and the D7-brane case. For zero temperature, $r_h = 0$, one can show that there is a certain critical value of ν/f below which the constant solution is unstable, more precisely[13]

$$\left(\frac{\nu}{f}\right)_{crit} = \frac{2\sqrt{7}}{\pi} \approx 1.68, \quad \text{for} \quad r_h = 0. \tag{3.40}$$

For $(\nu/f) < (\nu/f)_{crit}$ the stable solution of the equations of motion should hence be an r-dependent solution. When $r_h > 0$ we expect that $(\nu/f)_{crit}$ becomes smaller. A solution with $c_1 = c_2 = 0$ must necessarily be the constant solution. A solution with $c_1 = 0$ and $c_2 \neq 0$ can be viewed as showing spontaneous breaking of chiral symmetry. The phase transition which occurs when $(\nu/f) = (\nu/f)_{crit}$ is thus interpreted as a chiral symmetry breaking/restoring phase transition. This phase transition was found for the D5-brane in reference [140] and was shown to exhibit Berezinsky-Kosterlitz-Thouless scaling. For the D7 case numerical investigations have shown that there are r-dependent solutions even in some part of the region where the constant solution is supposed to be stable and that these solution are energetically favoured compared to the constant one [158].

Finally, let us highlight that the Routhians become identical for the D5-branes and the D7-brane as $r \to \infty$ due to the identity

$$\mathcal{N}_7 = \frac{\mathcal{N}_5 N_5}{f}. \tag{3.41}$$

[13]Note that even though the D7-brane equations of motion depend on ν and f separately, the prediction for the location of the phase transition depends only on their ratio.

3.3.2 Asymptotic behaviour as $r \to r_h$

Let us consider first the zero temperature case, $r_h = 0$. Looking at the equation of motion for $\psi(r)$ for the D5-brane we see that for $r = r_h = 0$, the equation of motion for $\psi(r)$ reduces to

$$\left.\frac{\partial_\psi V_5}{2V_5}\right|_{r=r_h=0} = 0, \tag{3.42}$$

where the "potential" V_5 is given by

$$V_5 = 4\sin^4\psi f^2(1+r^4) + (\pi\nu)^2. \tag{3.43}$$

The angle ψ must hence come to an extremum of the potential V_5, *i.e.,* we need that

$$\partial_\psi V_5|_{r=r_h=0} = 16\sin^3\psi\cos\psi f^2 = 0. \tag{3.44}$$

There are only two possible solutions, $\psi = 0$ and $\psi = \frac{\pi}{2}$. The solution $\psi = 0$ corresponds to a minimum of the potential and the solution $\psi = \frac{\pi}{2}$ to a maximum. A minimum is preferred since the second derivative of is positive there. When $r_h = 0$, if we assume that $\psi \to \psi_0$ as $r \to 0$, the linearized equation in the vicinity of $r = 0$ is

$$\left(r\frac{d}{dr}\right)^2\delta\psi + r\frac{d}{dr}\delta\psi - \frac{\partial_\psi^2 V_5(\psi_0)}{2V_5(\psi_0)}\delta\psi = 0$$

and the solution has the form

$$\psi \sim \psi_0 + \alpha_+ r^{-\frac{1}{2}\left[1+\sqrt{1+\frac{2\partial_\psi^2 V}{V}}\right]} + \alpha_- r^{-\frac{1}{2}\left[1-\sqrt{1+\frac{2\partial_\psi^2 V}{V}}\right]} + \ldots$$

If ψ_0 is at a maximum of the potential, so that $\frac{2\partial_\psi^2 V_5(\psi_0)}{V_5(\psi_0)} < 0$, both exponents are negative or complex. To have a sensible solution, both α_+ and α_- must be zero. This means that, if we begin integrating the nonlinear ordinary differential equation for $\psi(r)$ from $r = 0$, the solution will be the constant, and this can only make sense if $\psi_0 = \frac{\pi}{2}$, which is the solution that we already know about. Coincidentally, $\frac{\partial_\psi^2 V_5(\pi/2)}{V_5(\pi/2)} < 0$, so this is a consistent picture. On the other hand, if ψ_0 is a minimum of the potential, $\frac{\partial_\psi^2 V_5(\psi_0)}{4V_5(\psi_0)} > 0$, and one exponent, α_+ is negative whereas the other α_- is positive. To have a sensible solution, α_+ must be zero. If, again we integrate the differential equation for ψ up from $r = 0$, some fixed value of α_- will lead to an asymptotic form (3.39) of $\psi(r)$ where both c_1 and c_2 are

nonzero. We would then have to adjust α_- so that $c_1 = 0$ to find the type of solutions that we are discussing. Then c_2 is completely fixed by the solution of the equation. There is the third possibility that the potential is flat, $\frac{\partial_\psi^2 V_5(\pi/2)}{V_5(\pi/2)} = 0$, which in fact happens at the other extremum, $\psi_0 = 0$. Then α_+ must again be set to zero. But the exponent multiplying α_- vanishes and it would seem that the linearized equation is solved by any constant fluctuation of ψ. In this case, one must appeal to nonlinear effects to see that the correct choice of minimum is still $\psi = 0$, although the flatness of the potential in the vicinity leads to a very slow evolution of ψ toward $\psi = 0$ as $r \to 0$. A similar argument to the above applied to the $r \to \infty$ regime shows that there exist two normalizable modes of the equation for fluctuations of the angle ψ only when ψ approaches a maximum of the potential, which is the large r limit of potential (3.43). The unique maximum is $\psi = \frac{\pi}{2}$ which is the asymptotic value that we are using.

For the D7-brane similar considerations apply but the relevant potential is different. More precisely,

$$V_7 = 4\sin^4\psi(f^2 + 4\cos^4\psi)(1 + r^4) + (\pi(\nu - 1) + 2\psi - \frac{1}{2}\sin 4\psi)^2, \tag{3.45}$$

for which

$$\partial_\psi V_7|_{r=r_h=0} = 8\sin^2\psi\cos\psi\left(2f^2\sin\psi + 4(\pi(\nu-1) + 2\psi)\cos\psi\right). \tag{3.46}$$

We observe that as in the D5-brane case the derivative of the potential vanishes for $\psi = 0$ and $\psi = \frac{\pi}{2}$. However, in this case there is a third zero of the derivative which satisfies

$$\frac{f^2}{2}\tan\psi_0 + \pi(\nu - 1) + 2\psi_0 = 0. \tag{3.47}$$

As long as $0 < \psi_0 < \frac{\pi}{2}$, $\partial_\psi^2 V(\psi_0) > 0$ and this point is the minimum of the potential. For $\nu < 1$ there is always a solution to equation (3.47) in the interval $[0, \frac{\pi}{2}]$ but for $\nu > 1$ there is never such a solution. In summary, for $\nu < 1$, ψ_0 is always the minimum. When $\nu > 1$, the minimum is at the extreme point of the interval, $\psi = 0$. Another way to see this is by looking at higher derivatives of the potential. We find

$$\partial_\psi^2 V_7(\psi)\big|_{\psi=0} = 0, \qquad \partial_\psi^3 V_7(\psi)\big|_{\psi=0} = \frac{32}{3}(\nu - 1)\pi. \tag{3.48}$$

The vanishing second derivative implies that $\psi = 0$ is an inflection point. Note that the sign of the third derivative is different if ν is greater or less than one. If $\nu > 1$, the potential is decreasing as ψ approaches zero and the endpoint of the interval is a global minimum

for the function restricted to the range $[0, \frac{\pi}{2}]$. On the other hand, if $\nu < 1$ it is increasing as ψ approaches zero, and the endpoint is a local maximum, the only minimum being at $\psi = \psi_0$.

The above applies for when $\nu > 1$ or $\nu < 1$. However, for the D7-brane, $\nu = 1$ is a special place. For $\nu = 1$ the potential $V_7(\psi)$ vanishes for $\psi = 0$ and the last term in eqn. (3.37) diverges. The equation can still be fulfilled if ψ becomes zero at some value of $r = r_0 > r_h$ and if $d\psi/dr$ simultaneously diverges at r_0. This type of embedding of the D7-brane is known as a Minkowski embedding, the D7-brane pinches off at AdS radius r_0 and does not reach the horizon. It is not possible to have a Minkowski embedding for the D7-brane for other values of ν. For the D5-brane a Minkowski embedding would only be possible for vanishing charge density, *i.e.,* for $\nu = 0$, a case we shall not be interested in here.

For $r_h \neq 0$, the equation of motion evaluated at $r = r_h$ is

$$0 = -4r_h \frac{d}{dr}\psi + \frac{\partial_\psi V(\psi)}{2V(\psi)} \tag{3.49}$$

This no longer requires that ψ goes to an extremum of the potential, but it determines the derivative of ψ at the horizon once a value of ψ is specified there.

3.3.3 Composite systems

As explained above the parameters of our N_5 probe D5-branes and our single probe D7-brane are adjusted in a particular way in order to allow the interpretation of the probe D7-brane as a blown up version of the N_5 D5-branes. More precisely we fix the flux through the extra 2-sphere wrapped by the D7-brane to fulfill the relation (3.25) and we adjust the charge density and the magnetic field so that it is the same for the D5-branes and the D7 brane. Starting from N_5 D5-branes with a given charge density one can, however, imagine other scenarios than all of them blowing up to a single D7-brane.

For instance n_5 D5-branes could blow up to a D7-brane and the rest remain D5-branes. The resulting brane configuration in the interior of AdS_5 would then be a single D7-brane with flux $f = \frac{2\pi}{\sqrt{\lambda}} n_5$ and $(N_5 - n_5)$ D5-branes. The charge density would have to be shared between the D5-branes which would remain D5-branes and those which would blow up, resulting in, for instance for initial filling fraction ν, the D7-branes having filling fraction $\nu - \nu_0$ and the remaining $D5$ branes having filling fraction ν_0.

Similarly, the N_5 D5-branes could blow up to a larger number of D7-branes with different charge densities. In the most general case, starting from N_5 D5-branes with filling

fraction ν we could have $N_5 - n_5$ D5-branes remaining D5-branes with filling fraction ν_0 and n_5 D5-branes blowing up to n_7 D7-branes with flux values $\{f_i\}_{i=1}^{n_7}$, and filling fractions $\{\nu_i\}_{i=1}^{n_7}$ where the parameters would have to fulfill

$$\nu = \nu_0 + \sum_{i=1}^{n_7} \nu_i, \qquad n_5 = \frac{\sqrt{\lambda}}{2\pi} \sum_{i=1}^{n_7} f_i. \tag{3.50}$$

Notice in particular that this implies that the Routhian of the composite system (assuming the components to be non-interacting) becomes identical to the simple D5-brane Routhian as $r \to \infty$.

We shall not study this most general composite system but limit ourselves to the case where $\nu_i = 1$, for all i, except possibly for one, and $0 \leq \nu_0 < 1$. The reason for this is that the $\nu = 1$ gapped D7-brane has a special status, being particularly favoured energetically and according to our previous studies [158] having the interpretation of a first quantized Hall level. Composite systems will be investigated in detail in section 3.4.4. .

3.4 Numerical Investigations

We wish first in subsection 3.4.1-3.4.3 to consider a situation where a single D7-brane can be viewed as a blown up version of N_5 D5-branes. Accordingly, we chose the same value of the B-field, the charge density and hence the filling fraction ν for the two systems. Obviously, r_h is also chosen to be the same for the two systems. Furthermore, we choose the flux of the D7-brane on the second two-sphere, $\tilde{S}^2$, to be given as $f = \frac{2\pi}{\lambda} N_5$. Subsequently, in subsection 3.4.4 we turn to considering the types of composite systems mentioned above. I all cases we will restrict ourselves to the massless case, *i.e.*, $c_1 = 0$, cf. section 3.3.1.

3.4.1 Characteristic solutions

To generate a non-constant solution for $\nu \neq 1$ we generate from the differential equation a Taylor series for ψ as a function of r for r in the vicinity of r_h assuming some value ψ_0 for $\psi(r_h)$. This series expansion is then used to generate the initial data needed for the integration procedure. We finally determine the value of ψ_0 by demanding that the solution has $c_1 = 0$.

To generate a non-constant solution for $\nu = 1$ we generate from the differential equation a Taylor series solution for $r(\psi)$ for small ψ assuming some value r_0 for $r(\psi = 0)$. Then we

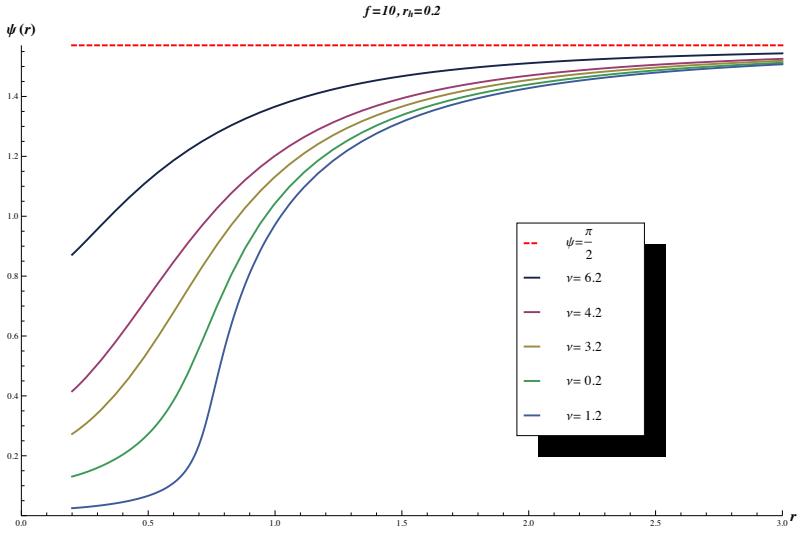

Figure 3.5: D7-brane solutions for $f = 10$ and $r_h = 0.2$ for various values of ν.

use the value of $r(\psi)$ and $r'(\psi)$ as generated by this Taylor series expansion as input to our integration procedure. Analogously to above we determine the value of r_0 by demanding that the solution has $c_1 = 0$. In figure 3.5 we have plotted some solutions for $\psi(r)$ for $f = 10$ and $r_h = 0.2$ and various values of ν.

3.4.2 The stability lines for D5 and D7

As explained in subsection 3.3.1 the constant solution $\psi = \frac{\pi}{2}$ solves the equation of motion both for D5 branes and D7-branes for all values of the parameters but this solution is expected to be unstable when ν/f is small. For $r_h = 0$ the critical point below which the constant solution is unstable is given by $(\nu/f)_{crit} = \frac{2\sqrt{7}}{\pi}$. In this case, however, numerical studies show, that the non-constant D7-brane solution remains energetically favoured even in a part of the parameter space where the constant solution is stable [158].

One would expect that also for $r_h \neq 0$ one would have a region for small values of ν/f where the non-constant solution is energetically favoured. We have investigated this by comparing the energies of constant and non-constant solutions as determined from (minus) the corresponding values of the Routhian for various values of our parameters. Notice that whereas the total energy of any of the systems considered diverges (cf. equations (3.24)

and (3.36)) energy differences between systems with identical values of the parameter f are finite.

In figure 3.3 we have shown the transition lines separating the region where the non-constant solution is energetically favoured from the region where the constant solution is the favoured one. The red curves correspond to D5-branes and the blue ones to D7-branes. Notice that non-constant D5-brane solutions depend only on ν/f whereas non-constant D7-brane solutions depend on ν and f separately. (The phase diagram for the D5-brane appeared already in [77].)

As for the zero-temperature case the D7-brane seems to have a much bigger region where the non-constant solution is favoured and very likely the non-constant solution again co-exists with the stable constant solution in a large part of the parameter space. The end point of the transition lines at $r_h = 0$ coincide with our previous zero-temperature estimates [158].

It is interesting to notice that the plots all have a peak corresponding to $\nu = 1$ which shows that this value of the filling fraction is particularly favoured. This is in agreement with our earlier interpretation of this state as the first quantum Hall level [158]. The special status of the $\nu = 1$ state implies that it is advantageous for the D-branes to organize into composite systems for $\nu > 1$. We shall discuss this in detail in section 3.4.4.

3.4.3 Crossover between D5 and D7 for $\nu < 1$

To the left of the blue curves in figure 3.3 the D5-branes and the corresponding D7-brane both have lower energy than the constant solution. It is thus interesting to investigate which one of these two has the lowest energy in the region $0 < \nu < 1$. (As already mentioned, when we pass the line $\nu = 1$, we in addition have composite systems to worry about and this case will be discussed in the following subsection.) We have earlier pointed out that the Routhians for the D5-branes and the D7-branes become identical when $r \to \infty$. We notice that for $r \to r_h$ the Routhians would coincide for $\nu = 1/2$ if for both systems the angle ψ would tend to zero at the horizon and a reasonable first guess for the location of the transition point could be at $\nu = 1/2$. (We know, however, that for the D7-brane when $r_h \neq 0$ and $\nu < 1$ the angle ψ does not tend to zero at the horizon, cf. section 3.3.2.)

In figure 3.4 we show in green the line of transition between D5 and D7 for $0 < \nu < 1$ for various values of f. The curve lies somewhat displaced from $\nu = \frac{1}{2}$ but approaches this line when f becomes larger.

3.4.4 Composite systems

As discussed above the gapped D7-brane with $\nu = 1$ is particularly energetically favoured. One can hence wonder whether composite systems could start playing a role when $\nu > 1$. Let us consider $\nu = 1 + \nu_0$, where $\nu_0 < 1$. For this value of ν one could imagine that n_5 of the N_5 D5-branes would blow up to a D7-brane with $\nu = 1$ and the rest either remain D5-branes with $\nu = \nu_0$ or blow up to another D7-brane with $\nu = \nu_0$. To see if this possibility is realized we have to compare the energy of the composite system with that of the simple D7-brane and D5-brane solution. The energy of the composite solution will of course depend on how many D5-branes blow up to gapped D7-branes and how many remain ungapped branes. The distribution of the D5 branes is reflected in the parameter f of the two components of the composite system. Let us denote the the flux of the gapped brane as f_0, *i.e.,*

$$f_0 = \frac{2\pi}{\sqrt{\lambda}} n_5. \tag{3.51}$$

Then the f-parameter of the ungapped branes becomes $f_{tot} - f_0$ where f_{tot} is the f-parameter of the initial D5-branes. What we are interested in is the composite system for which the energy is the smallest possible one so for a given initial number N_5 of D5-branes and hence a given initial value of $f_{tot} = \frac{2\pi}{\sqrt{\lambda}} N_5$ we will have to find the value of f_0 which minimizes the energy of the composite systems. Naively one would expect that as many D5-branes as possible would blow up to gapped D7-branes but there are many dynamical issues which must be taken into account and we have to determine the minimum energy solution numerically.

In figure 3.6 we show an example for $f_{tot} = 1$ and $r_h = 0.2$ of how we sweep over different values of f_0 to determine the minimum possible energy for the composite system. Here we are considering a composite system consisting of a gapped D7-brane with $\nu = 1$ and a number of un-gapped D7-branes with $\nu = 0.3$. A similar sweep over values of f_0 must be done for the competing system consisting of gapped D7-branes supplemented with D5-branes. Subsequently, we can compare the minimum energies of the the two composite systems and in addition we should compare these to the energy of the non-constant D7-brane solution with $\nu = 1.3$ and $f = 1$. (Had there been a non-constant D5-brane solution with similar parameters we would also have had to compare to the energy of this one but there is not.) In this way, *i.e.,* by comparing energies, we are able to tell which system is the favoured one.

The case we have discussed pertains to the situation $1 < \nu < 2$. Let us now discuss what happens when we vary ν in this range. What we find is that when f is small the

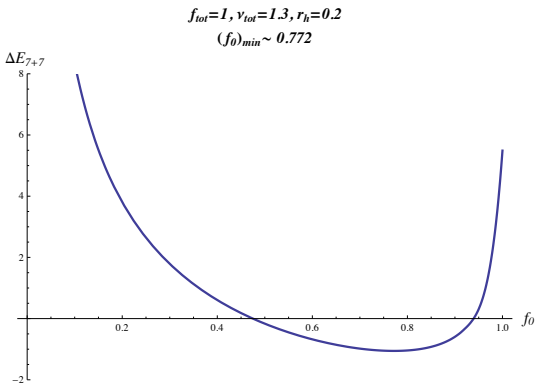

Figure 3.6: Plot for $f_{tot} = 1$ and $r_h = 0.2$ showing the energy of a composite system consisting consisting of a gapped *i.e.,* $\nu = 1$ D7-brane with flux f_0 and ungapped D7 branes with $\nu = 0.3$ and $f = 1 - f_0$ minus the energy of the constant solution with $\nu = 1.3$. The energetically favoured solution corresponds to $f_0 = 0.772$.

composite system consisting of gapped D7-branes plus un-gapped D7-branes is always the favoured one. However when f becomes larger, there appears at a certain value of ν a crossover between a region where the favoured composite system is D7 plus D5 and a region where the favoured composite system is D7 plus D7. In figure 3.7 we show for $r_h = 0.2$ and $f_{tot} = 1$ the energy difference between the D7-D5 system and the constant solution (red curves) and the energy difference between the D7-D7-brane system and the constant solution (blue curves) for $f_{tot} = 1$ and for $f_{tot} = 10$ as a function of ν where $\nu \in [1, 2]$. Notice that to generate a given data point on each of these curves we first have to go through the minimization procedure described above and illustrated in figure 3.6. The curves tell us that for $f_{tot} = 1$ and $r_h = 0.2$ the composite D7-D7 system is always the favoured one but for $f_{tot} = 10$ and $r_h = 0.2$ there is a crossover between D5-D7 and D7-D7 at $\nu \approx 1.41$. We have repeated the analysis for different values of r_h and found that the crossover point does not show strong dependence on r_h.

Now we can move on to considering the interval $2 < \nu < 3$, *i.e.,* a ν on the form $\nu = 2 + \nu_0$ where $0 < \nu_0 < 1$. In this interval we can have composite systems consisting of two gapped D7 branes with $\nu = 1$ in combination with either ungapped D7-branes or D5-branes. Again we have to determine by numerical investigations how many D5-branes blow up to gapped D7-branes and how many do not. In addition, we now in principle have the option that the two gapped D7-branes can have different values for the flux. However, we know from our previous analysis of the zero temperature case [158] that for a collection

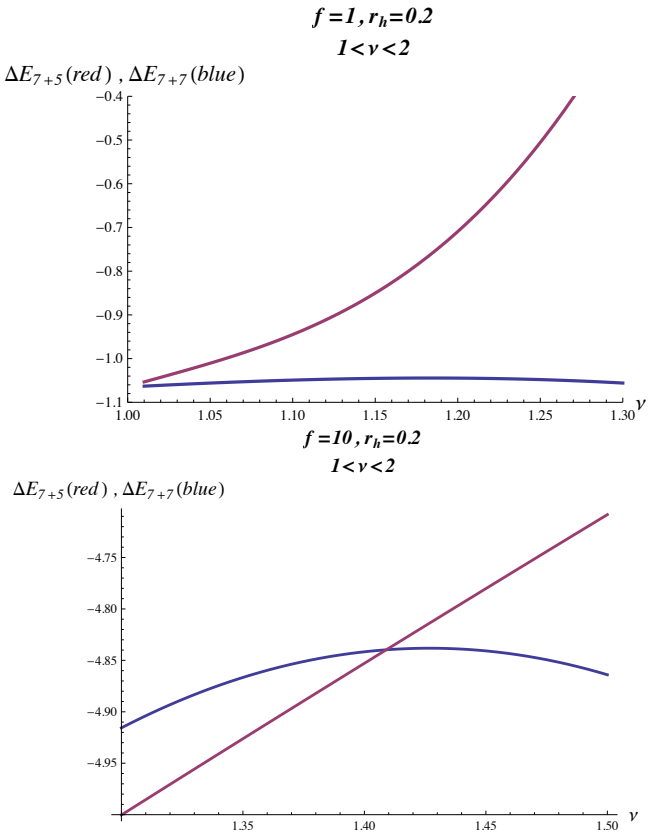

Figure 3.7: The difference between the energy of the composite D7-D5 system and the constant solution (red curves) and the difference between the energy of the composite D7-D7 system and the constant solution (blue curves) for $r_h = 0.2$ and $f = 1$ and $f = 10$ respectively. Notice the crossover at $\nu \approx 1.41$ for $f = 10$.

of gapped D7-branes with total flux f the energetically favoured situation is the one where the flux is equally shared between the D7-branes. If we denote the flux for each of the gapped D7-branes as f_0 the f-parameter for the un-gapped branes now becomes $f_{tot} - 2f_0$. Again we have to sweep over f_0 to determine how precisely the branes of the composite systems organize themselves into gapped branes and ungapped ones. After having found the most favourable configuration for each of the two types of composite systems we can again compare their energies to each other and to the energy of the constant solution with $\nu = 2 + \nu_0$. What we find is that the pattern seen in the interval $1 < \nu < 2$ repeats itself. For small values of f the composite D7-D7 system always wins but when f becomes larger

there starts to appear a cross over between D7-D5 and D7-D7. Again the cross over point does not depend very much on r_h.

It is obvious that we can now repeat the whole procedure again in the interval $3 < \nu < 4$ and in all the following intervals of the type $n < \nu < n+1$ where we could have composite systems with n gapped D7-branes in combination with an ungapped D7-brane or with D5-branes. We have done the analysis for $r_h = 0.2$ and for intervals up to and including $\nu \in [8, 9]$. We have found that up to and including $\nu \in [4, 5]$ there is in each interval a transition between a region where the D7-D5 system is the energetically favoured one and another region where the D7-D7 system is favoured. The region where the D7-D5 system is favoured diminishes as ν increases and for $\nu > 5$ the D7-D7 system always wins. In figure 3.8 we show the full phase diagram for $f = 10$. The red and the blue curves are the stability lines for the D5 and the D7-branes from figure 3.3 and the vertical green lines are the lines which separate the composite D5-D7 systems from the composite D7-D7 systems.

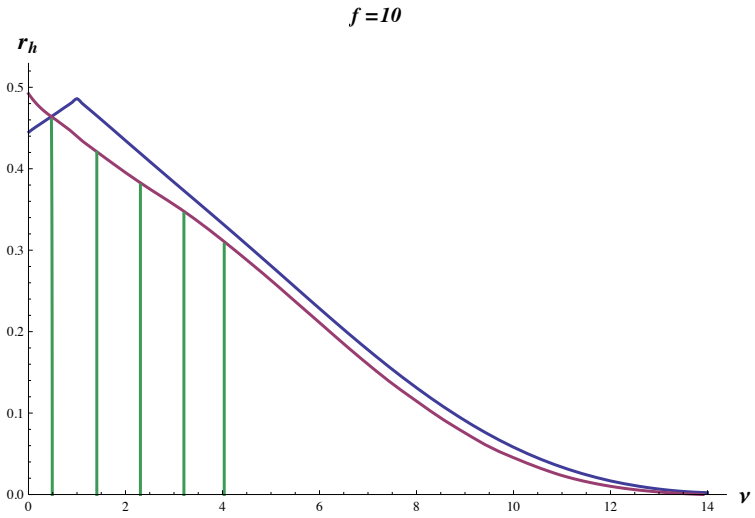

Figure 3.8: Plot for $f = 10$ showing a transition line (green) in each interval $[\nu, \nu+1]$ with $\nu \in \{0, 1, 2, 3, 4\}$ separating the composite D5-D7 system with ν gapped D7-branes from the composite D7-D7 system, likewise with ν gapped D7-branes. For $\nu > 5$, the D7-D7 system always wins.

3.5 Discussion

The results of our numerical investigations and the conclusions that can be drawn from there are reviewed in the first section of this chapter. In this concluding section, we wish to point out some interesting directions for further work on this subject, including some speculations about possible new results.

We have not explored the blown up solutions of the D5-brane from the D5-brane point of view where it would be a non-Abelian configuration of D5-branes. There are a number of obstacles to this approach, one being that the full generalization of the Born-Infeld action is not known when the embedding coordinates of the D-brane are matrices. It would nevertheless be interesting to ask whether some of the features of the solution that we find are visible in the non-Abelian D5-brane theory. We expect that the approximation of the non-Abelian D5-brane as a classical D7 brane is good in the limit where the number of D5-branes is large. However, we also expect that the blow up phenomenon at $\nu = 1$ should also be there for a small number of branes and the only way to see it is from the non-Abelian D5-brane point of view.

We have done extensive numerical solutions of the embedding equations for the D5 and D7-branes. We have not analyzed the small fluctuations about these solutions. The spectrum of fluctuations would tell us, for example, if the solutions that we have found are stable or metastable. A search for further instabilities would be very interesting, especially considering that other D7-brane configurations are known to have instabilities to forming spatially periodic structures when the density is large enough.

Most excitingly, we have an observation about a possibly interesting electronic property of the ungapped D7-brane solutions. If we compare the numerical solutions of the ungapped Abelian D5-brane and the ungapped D7-brane, in the regions of the phase diagram where the D7-brane is favored, it has lower energy because it has an exceedingly narrow funnel. The funnel is the lower AdS radius part of the D-brane world volume which is in the region where the brane approaches the Poincare horizon. Numerical computation in reference [158] already found this narrow funnel and we have confirmed it here. As we have discussed in section 1, when the filling fraction is not an integer, it is necessary for the D-brane worldvolume to reach the Poincare horizon. This is due to the fact that the worldvolume electric fields that are needed to create the nonzero charge density state in the holographic theory need to end at a source, or else thread through the entire space. In a rough sense, the D brane creates the source in that it becomes narrow to emulate a group of suspended strings. In the case of the D7-brane, this funnel region is exceedingly narrow. In the dual field theory, this narrowness of the D-brane funnel implies a very small density of electronic

states at low energies. We liken this to the situation at weak coupling where localization due to impurities depletes the extended states, leading to a mobility gap. For the D7-brane, there is no mobility gap in the mathematical sense, but the density of conducting states is anomalously small. This scarcity of conducting states could lead to an approximate, dynamically generated quantum Hall plateau, a tantalizing possibility since the only other known mechanism for Hall plateaus is localization. This would give a strong coupling mechanism.

We have not found solutions of probe D5-brane theory which would be the holographic dual of fractional quantum Hall states. Such states are both predicted by theoretical arguments [232, 243, 194, 154, 214, 102] and found experimentally [25, 65, 176] in graphene and they are normally taken as evidence of strong electron-electron correlations. The strong coupling limit that we can analyze using holography should be expected to see such states. One might speculate that solutions corresponding to fractional Hall states could be obtained from the integer quantum Hall states that we have already found by SL(2,Z) duality which has a natural realization in three dimensional Abelian gauge theory [241] and also a natural action on quantum Hall states [37, 36]. In particular, it can map integer quantum Hall states to fractional quantum Hall states. Exactly how this would work in the context of this chapter certainly merits further careful study. In particular, it could elucidate the relationship of the current work with other known string theory and holographic constructions of fractional quantum Hall states [31, 120, 92, 161].

A beautiful aspect of the fractional Hall states found in reference [92] is the explicit construction of boundaries and the existence of boundary currents. In our construction, the Hall state has a charge gap and it must therefore be a bulk insulator. The Hall current should be carried by edge states. The edges must be at the asymptotic spatial boundaries. It would be interesting, following reference [92] to attempt to construct boundaries or domain walls which would carry the currents.

Another place that SL(2,Z) duality and alternative quantization have been exploited recently is in the holographic construction of an anyonic superfluid [146]. That construction was based on the D7' model which has non-integer quantized Hall states. It exploited the idea that, whcn the external magnetic field is made dynamical, so that it adjusts its own vacuum expectation value to the desired filling fraction, what was a quantum Hall state obtains a soft mode and becomes a compressible superfluid. It should be possible to apply similar reasoning to the construction that we have outlined in this chapter. In this case, it would describe anyons based on integer level Chern-Simons theory.

Chapter 4

Out of the white hole: a holographic origin for the Big Bang

4.1 Introduction

The scientific discipline of Physical Cosmology started as, and continues to be, an extremely ambitious attempt to summarize the physics of the entire universe within a handful of cosmological parameters. However, maybe the most surprising outcome of this enterprise has been how successful this naive approach has been in describing cosmological observations that are multiplying at an accelerating rate. This is exemplified by the spectacular data recently released by the Planck collaboration [3], and its remarkable agreement with the six-parameter ΛCDM paradigm. However, the experimental success of standard cosmology is overshadowed by fundamental existential questions: What is Dark Matter? Why Dark Energy? What is the nature of the Big Bang?

The starting point for this chapter was to ask whether a more satisfactory (or natural) understanding of these mysteries can come from an alternative description of the geometry. In particular, could these (seemingly unrelated) phenomena be manifestations of hidden spatial dimensions, that show up as "holographic fluid(s)" in our four-dimensional description?

Motivated by D-branes in ten-dimensional string theory, pure phenomenology, or a combination of the two, one way to describe our four-dimensional universe is through embedding it in a higher dimensional spacetime– with at least one more dimension– and investigate its gravitational and/or cosmological properties. This is known as the "*brane*

world" scenario, where the brane refers to our four-dimensional universe embedded in a bulk space-time with five or more dimensions, where only gravitational forces dare to venture. Well-known (and well-studied) examples of such scenarios are the Randall-Sundrum (RS) [201] model, where four-dimensional gravity is recovered through a compact volume bulk, or the Dvali-Gabadadze-Porrati (DGP) construction [55, 68], where our three-brane is equipped with its own induced gravity, competing with the bulk gravity via the so-called Vainshtein mechanism [235].

Radiation dominated cosmology has been studied in the context of RS model where FRW metric describing four-dimensional universe emerges as induced gravity on the brane in five-dimensional AdS/Shchwarzschild background, *e.g.,* [206, 108]. However in this chapter, we focus on the DGP model, which is defined by the following action:

$$\begin{aligned} S_{DGP} \equiv & \frac{1}{16\pi G_b}\int_{\text{bulk}} d^5x\sqrt{-g}R_5 + \frac{1}{8\pi G_b}\int_{\text{brane}} d^4x\sqrt{-\gamma}K \\ & + \int_{\text{brane}} d^4x\sqrt{-\gamma}\left(\frac{R_4}{16\pi G_N} + \mathcal{L}_{\text{matter}}\right), \end{aligned} \tag{4.1}$$

where g and γ are the bulk and brane metrics respectively, while K and R_4 are the mean extrinsic and Ricci intrinsic curvatures of the brane. G_b and G_N are then respectively the bulk and brane (*i.e.,* Newton's) gravitational constants. One may also express the gravitational constants in terms of the bulk and brane Planck masses:

$$M_4 = (16\pi G_N)^{-1/2} \qquad M_5 = (32\pi G_b)^{-1/3}, \tag{4.2}$$

which respectively describe the approximate energies at which the brane and bulk gravitons become strongly coupled. Moreover, the ratio $r_c \equiv G_b/G_N$ characterizes the length scale above where five-dimensional gravity becomes important.

Along with a great deal of attention, these models have received some criticism. The DGP model includes a de Sitter solution automatically, which is usually called a self accelerating (SA) branch. When first proposed, this gave rise to the hope of a consistent description of our accelerating universe without a cosmological constant. However, it turned out that SA solutions suffer from ghosts and tachyons [195, 168, 187, 51] as well as some pathological singularities [148]. Furthermore, the detailed predictions of the SA branch were inconsistent with cosmological observations [82]. Nevertheless, the normal (non-self-accelerating) branch of the DGP cosmology does not suffer from the same pathologies, and can be consistent with data, if one includes brane tension (which is the same as a four-dimensional cosmological constant) [9].

While most studies in the context of DGP have been made from the viewpoint of a four-dimensional observer living on the brane, the DGP model was reexamined [103] as a

theory of five-dimensional Einstein gravity coupled to four-dimensional DGP branes, using a Hamiltonian analysis. New pathologies were encountered in the model by generalizing the five-dimensional geometry from Minkowski space-time – as originally considered in the DGP model– to Schwarzschild. If the black hole mass in the bulk exceeds a critical value, a so called "*pressure singularity*" will arise at finite radius [103]. Furthermore, on the SA branch the five-dimensional energy is unbounded from below.

Here we study the DGP model around a five-dimensional black hole in greater detail to better understand its phenomenological viability. We relate bulk, brane, and black hole parameters and investigate constraints on them that allow one to avoid the pressure singularity. We find that viable solutions are indeed possible, leading us to propose a holographic description for the big bang, that avoids the big bang singularity. We further outline a novel mechanism through which the brane's atmosphere induces (near) scale-variant curvature perturbations on the brane, without any strong fine tuning (or need for additional processes, such as cosmic inflation), consistent with cosmic microwave background observations.

In Section 4.2, we introduce the induced gravity on the brane by solving the vacuum Einstein equations while we demand a Freedman-Robertson-Walker (FRW) metric on the brane. In Section 4.3, we describe the geometry in the bulk in more detail and clarify the holographic picture of the brane from the point of view of the five-dimensional observer. We then give our proposal for a holographic big bang as emergence from a collapsing five-dimensional black hole. Section 4.4 outlines a mechanism to generate cosmological curvature perturbations from thermal fluctuations in the brane atmosphere. Finally, Section 4.5 wraps up the chapter with a summary of our results and related discussions.

4.2 Universe with FRW metric

We start by introducing the standard form of the FRW line element:

$$ds^2 = -d\tau^2 + \frac{a^2(\tau)}{\mathcal{K}}\left[d\psi^2 + \sin\psi^2\left(d\theta^2 + \sin^2\theta d\phi^2\right)\right], \tag{4.3}$$

where $\mathcal{K} > 0$ is the curvature parameter whose dimensions are $(length)^{-2}$ and the scale factor a is dimensionless and normalized to unity at the present time, *i.e.,* $a(\tau_0) \equiv a_0 = 1$.

Using the metric (4.3) for the brane, we next turn to solving the Einstein equations on the brane

$$G_{\mu\nu} = 8\pi G_N(T_{\mu\nu} + \widetilde{T}_{\mu\nu}), \tag{4.4}$$

where G_N is the gravitational constant on the brane. We here include two types of energy-momentum tensor $T_{\mu\nu}$ and $\widetilde{T}_{\mu\nu}$. The former describes normal matter living on the brane in a form of a perfect fluid

$$T_{\mu\nu} = (P + \rho)u_\mu u_\nu + P g_{\mu\nu},$$

satisfying the continuity equation

$$\nabla^\mu T_{\mu\nu} = 0, \tag{4.5}$$

where $g_{\mu\nu}$ is the metric on the brane given by equation (4.3) and u^μ is the 4-velocity of the fluid normalized such that $u^\mu u_\mu = -1$. The latter stress-energy $\widetilde{T}_{\mu\nu}$ is the Brown-York stress tensor [32] induced on the brane, defined through the Israel junction condition [128, 12] from the extrinsic curvature $K_{\mu\nu}$ as

$$\widetilde{T}_{\mu\nu} \equiv \frac{1}{8\pi G_b}\left(K g_{\mu\nu} - K_{\mu\nu}\right), \tag{4.6}$$

where G_b is the gravitational constant in the bulk, and we have assumed Z_2 bulk boundary conditions on the brane. The vacuum Einstein equations in the bulk impose the following constraints on the brane

$$\nabla^\mu \left(K g_{\mu\nu} - K_{\mu\nu}\right) = 0\,, \tag{4.7}$$

$$R + K^{\mu\nu}K_{\mu\nu} - K^2 = 0\,, \tag{4.8}$$

where $R = -8\pi G_N(T + \widetilde{T})$ is the Ricci scalar on the brane. The first constraint is just the continuity equation for $\widetilde{T}_{\mu\nu}$ while the second one is the so called Hamiltonian constraint.

Without loss of generality, as a result of the symmetry of FRW space-time, we can write $\widetilde{T}_{\mu\nu}$ in a perfect fluid form *i.e.,*

$$\widetilde{T}_{\mu\nu} = (\widetilde{P} + \widetilde{\rho})u_\mu u_\nu + \widetilde{P} g_{\mu\nu}, \tag{4.9}$$

which we shall refer to as the induced (or holographic) fluid. Combining equations (4.6) and (4.9), we get:

$$K_{\mu\nu} = -8\pi G_b \left[(\widetilde{P} + \widetilde{\rho})u_\mu u_\nu + \frac{1}{3}\widetilde{\rho} g_{\mu\nu}\right]. \tag{4.10}$$

From equations (4.4), (4.5), (4.7) and (4.8) we respectively obtain

$$H^2 + \frac{\mathcal{K}}{a^2} = \frac{8\pi G_N}{3}(\rho + \widetilde{\rho})\,, \tag{4.11}$$

$$\dot{\rho} + 3H(\rho + P) = 0\,, \tag{4.12}$$

$$\dot{\widetilde{\rho}} + 3H(\widetilde{\rho} + \widetilde{P}) = 0\,, \tag{4.13}$$

$$\widetilde{\rho} + \rho - 3(P + \widetilde{P}) + \frac{8\pi G_b^2}{G_N}\left(\frac{2}{3}\widetilde{\rho}^2 + 2\widetilde{\rho}\widetilde{P}\right) = 0, \tag{4.14}$$

where the last equation follows from solving for $K_{\mu\nu}$ in terms of $(\widetilde{\rho}, \widetilde{P})$ using equation (4.10).

Combining equations (4.11-4.14) we get for $\widetilde{\rho}$ and $\widetilde{P}$:

$$\widetilde{\rho}_{\pm} = \widetilde{\rho}_s \left(1 \pm \sqrt{1 - \frac{\mu^2}{12\pi G_N \widetilde{\rho}_s} \frac{1}{a^4} + \frac{2\rho}{\widetilde{\rho}_s}} \right) , \tag{4.15}$$

$$\widetilde{P} = \frac{\widetilde{\rho}^2 + \widetilde{\rho}_s(\widetilde{\rho} - T)}{3(\widetilde{\rho}_s - \widetilde{\rho})} , \tag{4.16}$$

where

$$T = 3P - \rho \tag{4.17}$$

and we choose the constant of integration $-\mu^2$, of dimension $[\text{length}]^{-2}$, to be negative (see *e.g.,* [170], for a similar derivation of DGP cosmology). The choice of minus sign will be justified in the next section, where we introduce the holographic picture. Finally, we have also defined the characteristic density scale for the holographic fluid:

$$\widetilde{\rho}_s \equiv \frac{3G_N}{16\pi G_b^2} . \tag{4.18}$$

Equation (4.16) immediately implies that the pressure becomes singular at $\widetilde{\rho} = \widetilde{\rho}_s$. It is then of interest to investigate in whether this pressure singularity can happen at early or late times (if at all), in our cosmic history. We address this question in the next section.

Furthermore, we note that $\tilde{\rho}_s$ sets the characteristic density scale, below which the bulk gravity becomes important. Specifically, it is easy to see that both terms in the induced fluid density, $\tilde{\rho}$ (equation 4.15), become much smaller than the matter density, ρ, if $\rho \gg \tilde{\rho}_s$. Therefore, given the current lack of observational evidence for five-dimensional gravity (*e.g.,* [9]), it is safe to assume that $\rho(z) > \rho_{\text{now}} \gg \tilde{\rho}_s$, *i.e.,* the induced fluid has always had a negligible contribution to cosmic expansion, with the notable (possible) exception of the above-mentioned singularity.

4.3 Universe as a hologram for a Schwarzschild bulk

Consider our universe to be a (3+1)-dimensional holographic image [223] – call it a brane – of a (4+1)-dimensional background Schwarzchild geometry

$$ds^2_{\text{bulk}} = -f(r)dt^2 + \frac{dr^2}{f(r)} + r^2 d\Omega_3^2 , \tag{4.19}$$

with

$$f(r) = 1 - \frac{r_h^2}{r^2}\,, \tag{4.20}$$

and where $d\Omega_3$ is the metric of unit 3-sphere. We now assume a dynamical brane, i.e our universe, to be located at $r = a(\tau)/\sqrt{\mathcal{K}}$ described by the FRW metric (4.3), where τ is the proper time of the brane. Its unit normal vector is

$$n^\alpha = \varepsilon \left(\frac{\dot{a}}{\sqrt{\mathcal{K}} f(a)}, \sqrt{f(a) + \frac{\dot{a}^2}{\mathcal{K}}}, 0, 0, 0 \right)\,, \tag{4.21}$$

with $n^\alpha n_\alpha = 1$ and $\varepsilon = -1$ or $+1$, and we take

$$u^\alpha = \left(\frac{1}{f(a)} \sqrt{f(a) + \frac{\dot{a}^2}{\mathcal{K}}}, \frac{\dot{a}}{\sqrt{\mathcal{K}}}, 0, 0, 0 \right) \tag{4.22}$$

to be the unit timelike tangent vector on the brane, i.e $u^\alpha u_\alpha = -1$.

Recall that besides normal matter on the brane we also introduced an induced fluid denoted by $\widetilde{T}_{\mu\nu}$ on the brane, which is the imprint of the bulk geometry through the junction condition (4.6). Using

$$K_{ab} = n_{\alpha;\beta} e_a^\alpha e_b^\beta \tag{4.23}$$

with a, b and α, β labeling the brane and bulk coordinates respectively, it is just a matter of calculation to obtain

$$K_{ij} = \frac{\varepsilon\sqrt{\mathcal{K}}}{a} \sqrt{f(a) + \frac{\dot{a}^2}{\mathcal{K}}}\, \Omega_{ij}\,, \tag{4.24}$$

$$K_{\tau\tau} = -\frac{\varepsilon\left(\frac{\mathcal{K}^2 r_h^2}{a^4} + \frac{\ddot{a}}{a}\right)}{\sqrt{H^2 + \frac{\mathcal{K}}{a^2} - \frac{\mathcal{K}^2 r_h^2}{a^4}}}\,, \tag{4.25}$$

where i, j label the coordinates of the spatial section, with $H \equiv \dot{a}/a$ is the Hubble parameter. Ω_{ij} is the metric of the unit 3-sphere. Using expressions (4.24-4.25) for the extrinsic curvature in equation (4.6) and considering $\widetilde{T}_{\mu\nu}$ in a form of a perfect fluid on the brane we find

$$\widetilde{\rho}_\pm = \widetilde{\rho}_s \left(1 \pm \sqrt{1 - \frac{2(\rho_{\rm BH} - \rho)}{\widetilde{\rho}_s}} \right)\,, \tag{4.26}$$

$$\widetilde{P} = \frac{-(1+2\varepsilon)\,\widetilde{\rho}^2 + \widetilde{\rho}_s(\widetilde{\rho} - T)}{3(\widetilde{\rho}_s + \varepsilon\widetilde{\rho})}\,, \tag{4.27}$$

where $\rho_{\rm BH}$ is a characteristic 3-density, proportional to the density of the bulk black hole, averaged within our three-brane, defined as:

$$\rho_{\rm BH} \equiv \frac{3\Omega_k^2 H_0^4 r_h^2}{8\pi G_N a^4}\,, \tag{4.28}$$

while $\Omega_k \equiv -\mathcal{K}/H_0^2$. Comparing equations (4.15) with (4.26) we see that the integration constant μ from the previous section could be interpreted as the mass of the black hole in the bulk, given in terms of the horizon radius as

$$\mu = 3|\Omega_k| H_0^2 r_h\,, \tag{4.29}$$

with the comparison between equations (4.27) and (4.16) further indicating that $\varepsilon = -1$, and as a result, at $\widetilde{\rho} = \widetilde{\rho}_s$ the pressure becomes singular. Moreover, as promised in the previous section, $-\mu^2 \propto -r_h^2 < 0$, which is necessary for positive energy (or ADM mass) initial conditions.

We note that $\widetilde{\rho}_+$ is non-zero, even for $\rho = \rho_{\rm BH} = 0$, which is often known as the *self-accelerating* (SA) branch in the literature, as the universe can have acceleration, even in the absence of a cosmological constant (or brane tension). However, as discussed in the introduction, SA branch suffers from a negative energy ghost instability. On the other hand, $\widetilde{\rho}_-$, known as the *normal* branch, does not suffer from the same problems, and may well provide a healthy effective description of bulk gravity (*e.g.,* [187]). In what follows, we outline constraints on both branches for the sake of completeness.

In total, we have three adjustable parameters in our model: $\widetilde{\rho}_s$, $\mathcal{K}$, and r_h. We shall next consider the constraints on these parameters. We find two limits on $\widetilde{\rho}_s$. One is from demanding reality of all quantities in equation (4.26), *i.e.,*

$$\widetilde{\rho}_s \geq 2\,(\rho_{\rm BH} - \rho)\,. \tag{4.30}$$

where the equality indicates a pressure singularity. The other comes from the fact that, thus far, cosmological observations have not detected any effect of the induced fluid $\widetilde{\rho}$, which implies that the density of the induced matter on the brane should be small compared to normal matter in the universe. These constraints are often expressed in terms of the transition scale r_c [62], where

$$r_c \equiv \left(\frac{3}{16\pi G_N \widetilde{\rho}_s}\right)^{1/2} = \frac{G_b}{G_N}, \tag{4.31}$$

which is constrained to be bigger than today's cosmological horizon scale (*e.g.,* [9]). Therefore, we impose a conservative bound

$$|\,\widetilde{\rho}\,| \lesssim \epsilon\rho\,, \tag{4.32}$$

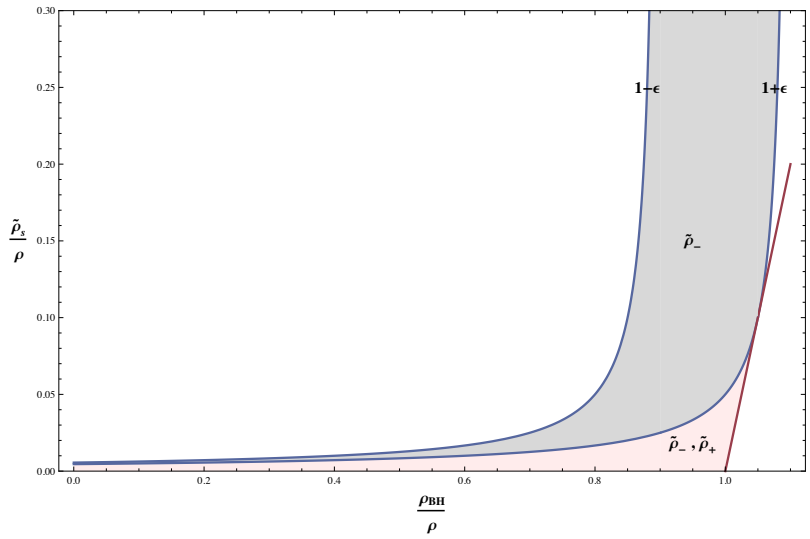

Figure 4.1: The shaded area shows the allowed values of $\widetilde{\rho}_s$ and $\rho_{\rm BH}$ for both branches (pink), and only $\widetilde{\rho}_-$ or the normal branch (gray). The red solid line indicates those values of $\widetilde{\rho}_s$ and $\rho_{\rm BH}$ for which pressure becomes singular. We have chosen $|\widetilde{\rho}/\rho| < \epsilon = 0.1$ in this figure.

where $\epsilon \ll 1$.

The two constraints (4.30) and (4.32) restrict the parameter space. To clarify this we employ equation (4.26), investigating the positive and negative branches separately. Consider first the positive branch. Solving equation (4.32) for $\widetilde{\rho}_+$ yields the upper bound

$$\frac{\widetilde{\rho}_s}{\rho} \leq \frac{\epsilon^2}{2}\left(1+\epsilon-\frac{\rho_{\rm BH}}{\rho}\right)^{-1}, \text{ for } \widetilde{\rho}_+ \text{ (self}-\text{accelearting branch)}, \tag{4.33}$$

which along with equation (4.30) bounds $\widetilde{\rho}_s$ within a certain range, *i.e.,* the pink shaded area in figure (4.1). The red line in this figure shows the values for which pressure becomes singular. Note that the lower bound (4.30) becomes important only if $\rho_{\rm BH} > \rho$; condition (4.30) is automatically satisfied for $\rho_{\rm BH} < \rho$, since $\widetilde{\rho}_s$ is always positive by definition. Both upper and lower limits coincide at $\rho_{\rm BH} = (1+\epsilon/2)\rho$; that is there are upper bounds for both $\rho_{\rm BH} \leq (1+\epsilon/2)\rho$ and $\tilde{\rho}_s \leq \epsilon\rho$.

Considering now the negative branch $\widetilde{\rho}_-$ in equation (4.32), we obtain upper and lower

limits on $\widetilde{\rho}_s$ as

$$\frac{\widetilde{\rho}_s}{\rho} \leq \frac{\epsilon^2}{2}\left(1-\epsilon-\frac{\rho_{\rm BH}}{\rho}\right)^{-1}, \text{ for } \frac{\rho_{\rm BH}}{\rho} < 1-\epsilon \ (\widetilde{\rho}_-, \text{ normal branch}), \tag{4.34}$$

$$\frac{\widetilde{\rho}_s}{\rho} \geq \frac{\epsilon^2}{2}\left(1+\epsilon-\frac{\rho_{\rm BH}}{\rho}\right)^{-1}, \text{ for } \frac{\rho_{\rm BH}}{\rho} > 1+\frac{\epsilon}{2} \ (\widetilde{\rho}_-, \text{ normal branch}). \tag{4.35}$$

This allowed region is shown in figure (4.1) with gray and pink shaded areas. Note that the red solid line representing the pressure singularity sets the lower bound for $\widetilde{\rho}_s/\rho$ within $(1-\epsilon/2)\rho < \rho_{\rm BH} < (1+\epsilon/2)\rho$.

So far we have found limits on $\widetilde{\rho}_s$ and $\rho_{\rm BH}$. Since the value of $\rho_{\rm BH}$ depends on the pair $\{\Omega_k, r_h\}$, it is interesting to consider possible limits on these parameters, and how they affect the cosmological evolution of our brane. This has been shown in a 3D plot in Figure 4.2. Note that any given value for $\rho_{\rm BH}$ in Figure 4.1 corresponds to a line in the $\{\Omega_k, r_h\}$ plane in Figure 4.2. Let us examine this figure more carefully:

First, note that the figure is plotted for the negative (or normal) branch, which, as discussed above, is physically more relevant. The empirical upper limit for the spatial curvature of the universe $-\Omega_k \lesssim 0.01$ (*e.g.,* [4]) is indicated by the purple vertical plane in the figure. The red surface represents those pairs of $\{\Omega_k, r_h\}$ for which $\rho_{\rm BH} = 1.05\rho(a)$ from present time ($\log a = 0$) back to Big Bang Nucleosynthesis (BBN; $a \sim 10^{-10}$). Here we have chosen the empirical bound $\epsilon \sim 0.1$ in equation (4.32), and have taken BBN as the earliest constraint on deviations from the standard cosmological model. As we noted before, according to the reality constraint (4.30) this is the maximum allowed value for $\rho_{\rm BH}$ at a given time. Therefore the whole area under the red surface is not allowed. Moreover, the red surface also shows the possible choices of the pairs $\{\Omega_k,\ r_h\}$ for which the pressure becomes singular for a given a. Consequently no pressure singularity could happen for pairs $\{\Omega_k,\ r_h\}$ chosen to be above the red plane at any given time.

The green plane indicates those pairs $\{\Omega_k,\ r_h\}$ for which the radius of our 4 dimensional universe coincides with the black hole horizon in the 5 dimensional bulk, *i.e.,* $r_h = r_3 = a/\sqrt{k}$. Therefore, for any $\{\Omega_k,\ r_h\}$ under the green plane, we have $r_3 < r_h$. For those pairs $\{\Omega_k,\ r_h\}$ chosen to be above this plane the radius of our holographic universe is larger than the horizon radius, meaning that our present cosmos lies outside the horizon of the black hole in the bulk, *i.e.,* $r_3 > r_h$. Subsequently, suppose we choose any pair of $\{\Omega_k,\ r_h\}$ above the green plane at the present time (the $\log a = 0$ plane) and move backwards in time. Let us assume that the universe today has its radius larger than the horizon in the bulk black hole. Moving backwards to early times ($\log a = -10$ plane), as the radius of the universe (proportional to scale factor a) decreases, it may or may not cross the green plane. This

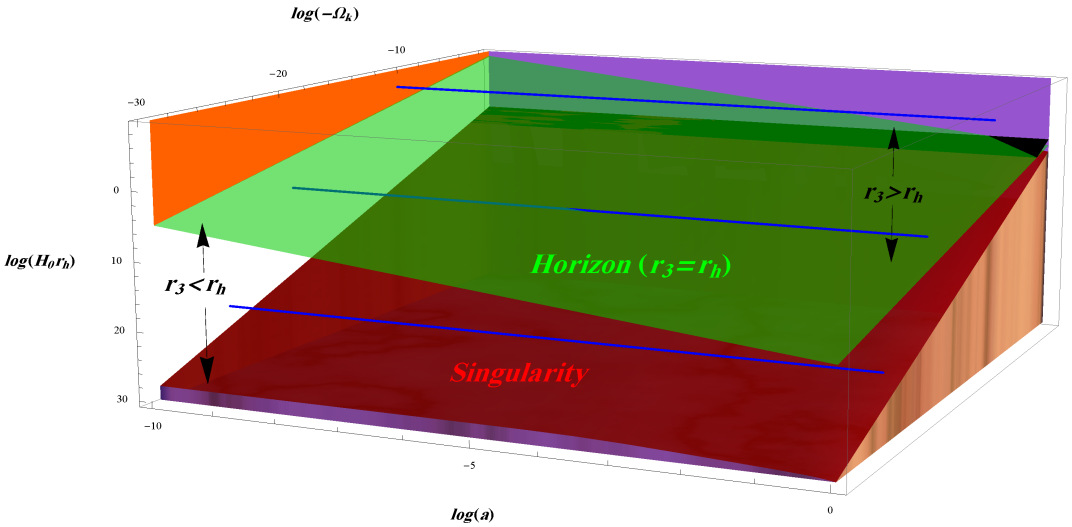

Figure 4.2: 3D plot for $-\Omega_k \leq 0.01$ versus $\log r_h$ from present time ($a = 1$) back to Big Bang Nucleosynthesis ($a \sim 10^{-10}$). The red plane indicates pressure singularity while the green plane is where $r_h = r_3 = a/\sqrt{k}$, *i.e.,* when our brane leaves the white hole horizon. The blue lines and the black strip (visible at the upper right as a triangle, and continuing underneath the green surface) dicate for a given $\{-\Omega_k,\, r_h\}$ how the radius of holographic universe evolves from BBN up to present time; *e.g.,* the black strip represents a holographic universe that emerges from the pressure singularity during the radiation era, passes through the white hole horizon at $a \sim 0.01 - 1$, and eventually is just outside the horizon at the present time.

has been illustrated with the upper two blue lines in Figure 4.2, the lower of which pierces the green plane at some value of r_h near $\log a \sim -5$.

Indeed, crossing the green plane means that at some early time the radius of the universe was smaller than the horizon radius. Since nothing can escape the horizon of a black hole, one would exclude those pairs of $\{\Omega_k,\, r_h\}$ for which their corresponding blue lines at some $a > 10^{-10}$ cross the green plane. Consequently the pairs highlighted with orange plane are possible choices of parameters $\{\Omega_k,\, r_h\}$ that satisfy $r_3 \geq r_h$ for $-\Omega_k \leq 0.01$ at $a = 10^{-10}$.

Consequently, one may interpret the crossing $r_3 = r_h$ before BBN ($0 < a < 10^{-10}$) as the emergence of the holographic universe out of a "collapsing star": this scenario replaces the Big Bang singularity. The overall picture of this proposal is shown in the Penrose diagram in figure (4.3)-left, which is reminiscent of the core-collapse of a supernova.

Another possibility is to consider a white hole in the bulk rather than a black hole.

With this scenario, it is possible for the universe to be inside the horizon at any time up to the present since all matter eventually emerges from the white hole horizon. Therefore the entire range of pairs $\{\Omega_k, r_h\}$ above the red surface is allowed; the lowest blue line in Figure 4.2 illustrates one such possible scenario. In this picture one may interpret the pressure singularity as a holographic description of the Big Bang that takes place at $a < 10^{-10}$. Hence those pairs $\{\Omega_k, r_h\}$ with $-\Omega_k \leq 0.01$ satisfying $\rho_{\rm BH} \lesssim \rho_r(a = 10^{-10})$, *i.e.,* lie above the intersection of the red surface and the $a = 10^{-10}$ plane are allowed[1]. For instance, choosing any value for $-\Omega_k$ in the range $10^{-4} \leq -\Omega_k \leq 10^{-2}$ with its corresponding horizon radius, *i.e.,* $r_h \simeq \sqrt{\Omega_r}/H_0\Omega_k$, represents a holographic universe that emerges from the pressure singularity during the radiation era, passes through the white hole horizon at $a \sim 0.01 - 1$, and eventually is just outside the horizon at the present time. This is illustrated with a black strip in Figure 4.2, visible at the upper right of the diagram and continuing underneath the green surface toward the upper left. For any $-\Omega_k < 10^{-4}$, the universe is inside the horizon at the present time but (given that its expansion is now dominated by the cosmological constant), it will expand indefinitely and eventually intersect the horizon in the future. The overall picture for this scenario has been shown in the Penrose diagram in figure (4.3)-right.

From the physical point of view, the former scenario, which we can dub the "black hole" universe is more plausible than the latter "white hole" universe. The reason is that the region inside a white hole horizon is to the future of a four-dimensional white hole naked singularity (Figure 4.3-right), which makes the brane dynamics, at best contrived, and at worst ill-defined. In particular, it is hard to physically justify why this singularity (*i.e.,* high curvature region) is preceded by a smooth "zero temperature" space-time. For example, it would be in contrast to (and thus more contrived than) the thermal bath that is the outcome of the big bang singularity.

4.4 Brane Atmosphere and Cosmological Perturbations

In this section, we introduce a mechanism to generate scale-invariant cosmological perturbations in our holographic big bang. As the holographic fluid is sub-dominant for most of the cosmic evolution, one expects the standard cosmological perturbation theory, that has been extremely successful in explaining cosmic microwave background observations (*e.g.,*

[1] We have chosen $\epsilon = 0.1$ in equation (4.32) and $\rho_r = \rho_0\Omega_r/a^4$.

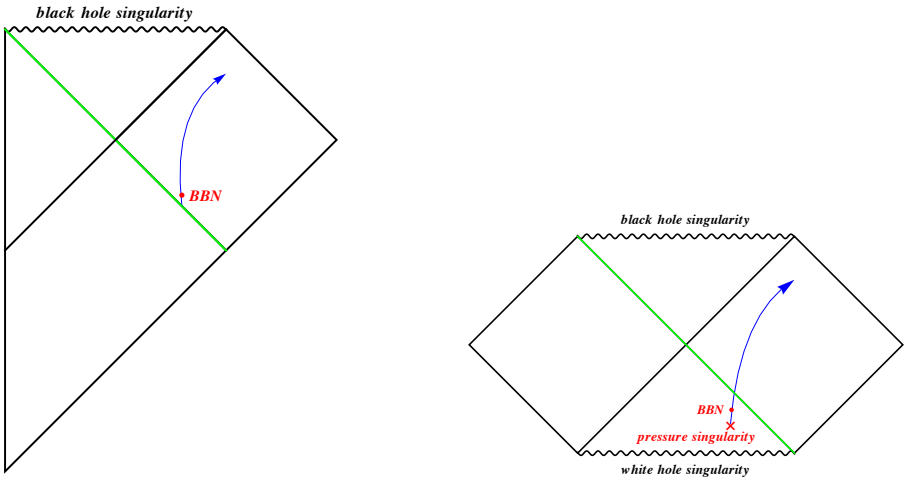

Figure 4.3: Penrose diagram for the dynamic brane (our universe) in blue for the black hole (left) or the white hole (right) in the bulk, where the green line indicates a collapsing shell (or "star"), or the white hole horizon respectively.

[3, 4], amongst other observational probes), to be applicable. The fluid will dominate cosmic evolution at very late times, but that can be avoided for sufficiently large r_c or small a.

For super horizon perturbations, general arguments based on locality and causality imply that one can use Friedmann equations with independent constants of motion, within independent Hubble patches. In the presence of adiabatic perturbations, which are currently consistent with all cosmological observations (*e.g.*, [3, 4]), these independent Hubble patches would only differ in their local value of comoving spatial curvature $\mathcal{K}$. This is often quantified using the Bardeen variable, ζ, where:

$$\delta\mathcal{K} \equiv \frac{2}{3}\nabla^2\zeta, \tag{4.36}$$

or equivalently the comoving gauge linearized metric takes the form

$$ds^2 = -N^2dt^2 + a(t)^2\left[(1+2\zeta)\delta_{ij} + h_{ij}\right]dx^i dx^j, \tag{4.37}$$

where h_{ij} is a traceless 3-tensor. Planck (+WMAP) observations [4] show that ζ has a near-scale-invariant spectrum of perturbations:

$$\frac{k^3}{2\pi^2}P_\zeta(k) = (2.196 \pm 0.059) \times 10^{-9}\left(\frac{k}{0.05\ \mathrm{Mpc}^{-1}}\right)^{-0.0397\pm0.0073}, \tag{4.38}$$

where k is the comoving wavenumber for spatial fluctuations.

Given that we assumed Z_2 (or mirror) boundary conditions for our three-brane, we can imagine an atmosphere composed of bulk degrees of freedom, which is stratified just outside the three-brane, due to the gravitational pull of the black hole. Here, we argue that the thermal fluctuations in the atmosphere of the three-brane induce a near-scale-invariant spectrum of curvature perturbations, *i.e.,* equation (4.38), on our cosmological brane.

Let us first compute the power spectrum of density fluctuations for a thermal gas of massless scalar particles in (4+1)-dimensional flat spacetime. The thermal two-point correlation function of a free scalar field is given in terms of the Bose-Einstein distribution:

$$\langle\varphi(x)\varphi(y)\rangle_T = \int \frac{d^4k_a}{(2\pi)^4}\left[\frac{2}{\exp(\omega/T)-1}+1\right]\frac{\exp[ik_a(x^a-y^a)-i\omega(x^0-y^0)]}{2\omega}, \tag{4.39}$$

where k_a is the spatial wave-number in 4+1D ($1 \leq a \leq 4$) , and we used $E = \omega = \sqrt{k^a k_a}$ for massless particles. Now, using the definition of energy density:

$$\rho(x) = \frac{1}{2}\dot{\varphi}^2 + \frac{1}{2}\partial_a\varphi\partial^a\varphi, \tag{4.40}$$

straightforward manipulations using equation (4.39) yield

$$\langle\rho(x)\rho(y)\rangle_T \simeq \frac{5}{8}\left|\int \frac{d^4k_a}{(2\pi)^4}\left[\frac{1}{\exp(\omega/T)-1}+\frac{1}{2}\right]\omega\exp[ik_a(x^a-y^a)-i\omega(x^0-y^0)]\right|^2. \tag{4.41}$$

Let us next consider how these density fluctuations affect metric fluctuations. As a first attempt, we focus on the linear scalar metric fluctuations in (4+1)-dimensions, which in the longitudinal gauge can be written as:

$$ds^2 = -(1+4\Phi_4)dt^2 + (1-2\Phi_4)\delta_{ab}dx^a dx^b, \tag{4.42}$$

where Φ_4 is the analog of the Newtonian potential. We can then use four-dimensional Poisson equation $\nabla_4^2\Phi_4 \simeq \frac{8\pi G_b}{3}\rho$ to find the statistics of scalar metric fluctuations. Using equation (4.41), we can find the equal-time correlator of Φ_4:

$$\langle\Phi_4(x^a)\Phi_4(y^a)\rangle_T \simeq \frac{5}{8}T^6\left(\frac{8\pi G_b}{3}\right)^2\int\frac{d^4k}{(2\pi)^4}\frac{\exp[ik_a(x^a-y^a)]}{k^4}M\left(\frac{k}{T}\right), \tag{4.43}$$

where

$$M(\kappa) \equiv \int\frac{d^4\kappa'}{(2\pi)^4}\omega_+\omega_-\left[\frac{1}{2}+\frac{1}{\exp(\omega_+)-1}\right]\left[\frac{1}{2}+\frac{1}{\exp(\omega_-)-1}\right], \tag{4.44}$$

$$\omega_\pm \equiv \sqrt{\kappa'^a\kappa'_a + \frac{1}{4}\kappa^a\kappa_a \pm \kappa_a\kappa'^a}, \tag{4.45}$$

while we have dropped the power-law UV-divergent term ($\propto$ [cut-off]^6), *e.g.,* using dimensional regularization[2]. This UV-divergent term does not depend on temperature, and presumably can be cancelled with appropriate counter-terms in other regularization schemes.

Now, we notice that for small $k \ll \Lambda, T$, we have

$$M(\kappa) \simeq \frac{15\zeta_R(5)}{\pi^2} + \mathcal{O}(\kappa^2) \simeq 1.576 + \mathcal{O}(\kappa^2), \tag{4.46}$$

where ζ_R is the Riemann zeta function. Therefore, equation (4.43) implies that the four-dimensional Newtonian potential, due to thermal fluctuations, has a *scale-invariant* power spectrum of the amplitude of $\sim G_b T^3 \sim (T/M_5)^3$.

It is easy to understand this result on dimensional grounds. Looking at the low frequency limit $\omega \ll T$ of thermal density fluctuations (4.41), we notice that the argument inside the absolute value becomes the delta function. In other words, the densities are only correlated within a thermal wavelength T^{-1}, and only have white noise, or a flat power spectrum, on large scales[3]. Then, Poisson equation implies that the potential power spectrum scales as k^{-4}, yielding a logarithmic real-space correlation function, or equivalently, a flat dimensionless power spectrum.

So far, all we have done is to study the fluctuations of a statistically uniform 4 dimensional thermal bath. While the scale-invariance of this result is suggestive, it is not immediately clear what this might imply (if anything) for cosmological curvature perturbations on our three-brane. To answer this question, we will first assume that, at some point in its early cosmological evolution, our three-brane was in static equilibrium with its thermal four-dimensional atmosphere. Then a comparison of equations (4.37) and (4.42) implies that

$$\zeta(x^i) = -\Phi_4(x^i, x^4 = 0) \tag{4.47}$$

assuming Z_2 boundary conditions at $x^4 = 0$. Note that this boundary condition modifies the thermal spectrum (4.41) within a thermal wavelength of the three-brane; given that gravity is a long-range force, we do not expect this to significantly affect the long wave-length metric fluctuations. Therefore, using equation (4.47), we can put forth our

[2] As we have seen above, at early times, the DGP gravity on the brane decouples from the bulk gravity. Therefore, equation 2.2 (or equivalently the Z_2 boundary condition) requires $\partial\Phi_4/\partial x^4 = 0$ on the brane. In the flat brane limit (which is again appropriate for early times), this boundary condition leads to a doubling of the thermal correlation functions on the brane, akin to the method of images in electrostatics (but with images of the same charge). Here, we shall absorb this factor of 2 into the definition of bulk temperature T.

[3] Note that this is a general feature of Bose-Einstein distributions, on any space-time dimension.

prediction for the power spectrum of cosmological curvature fluctuations:

$$\begin{aligned}\frac{k^3}{2\pi^2}P_\zeta(k) &= \frac{5}{32\pi^3}\left(\frac{8\pi G_b T_b^3}{3}\right)^2\int_{-\infty}^{\infty}\frac{dx}{(1+x^2)^2}M\left(\frac{k}{a_b T_b}\sqrt{1+x^2}\right)\\ &= \left[\frac{25\zeta_R(5)}{3072\pi^4}+\mathcal{O}\left(\frac{k}{a_b T_b}\right)^2\right]\left(\frac{T_b}{M_5}\right)^6\\ &\simeq \left[8.66\times 10^{-5}+\mathcal{O}\left(\frac{k}{a_b T_b}\right)^2\right]\left(\frac{T_b}{M_5}\right)^6 \end{aligned} \tag{4.48}$$

where T_b is the temperature of the bulk atmosphere, at the moment of equilibrium, where the scale factor is a_b. Furthermore, we used the definition of five-dimensional Planck mass (4.2) to substitute for G_b. Comparing equation (4.48) with equation (4.38) gives the experimental constraint on the (effective) temperature of the atmosphere:

$$\frac{T_b}{M_5} = 0.17139 \pm 0.00077, \tag{4.49}$$

for the comoving scale of $k \sim 0.05$ Mpc^{-1}. While T_b is for the atmosphere in the bulk, based on the rate of change in spatial geometry, we may expect the "de-Sitter" temperature of the boundary to set a minimum for T_b. Therefore, we expect:

$$\frac{H}{2\pi} \lesssim T_b \simeq 0.17\ M_5, \tag{4.50}$$

The slight deviation from scale-invariance in equation (4.38), which is at the level of 4%, and is now detected with Planck at $> 5\sigma$ level, is not predicted in our simple model of thermal free five-dimensional field theory. In the next section, we will speculate on the possible origins of this deviation in our set-up, even though we postpone a full exploration for future study.

4.5 Summary and Discussion

In the context of DGP brane-world gravity, we have developed a novel holographic perspective on cosmological evolution, which can circumvent a big bang singularity in our past, and produce scale-invariant primordial curvature perturbations, consistent with modern cosmological observations. In this chapter, we first provided a pedagogical derivation for

the cosmological evolution of DGP braneworld in FRW symmetry from first principles, and then connected it to motion in the Schwarszchild bulk geometry, extending the analyses in [103] to realistic cosmologies. Focusing on the pressure singularity uncovered in [103], we showed that it is generically encountered at early times as matter density decays more slowly than a^{-4}. However, we showed that the singularity *always* happens inside a white hole horizon, and *only* happens later than Big Bang Nucleosysntheis (BBN) for a small corner of the allowed parameter space (*i.e.,* the base of black strip in figure 4.2). Therefore, it can never be created through evolution from smooth initial conditions. This yields an alternative holographic origin for the big bang, in which our universe emerges from the collapse of a five-dimensional "star" into a black hole, reminiscent of an astrophysical core-collapse supernova (figure 4.3-left). In this scenario, there is no big bang singularity in our causal past, and the only singularity is shielded by a black hole horizon. Surprisingly, we found that a thermal atmosphere in equilibrium with the brane can lead to scale-invariant curvature perturbations at the level of cosmological observations, with little fine tuning, *i.e.,* if the temperature is approximately 20% of the five-dimensional Planck mass.

We may go further and argue that other problems in standard cosmology, traditionally solved by inflation, can also be addressed in our scenario:

1. The *Horizon Problem*, which refers to the uniform temperature of causally disconnected patches, is addressed, as the "star" that collapsed into a five-dimensional black hole could have had plenty of time to reach uniform temperature across its core.

2. The *Flatness Problem*, which refers to the surprisingly small spatial curvature of our universe, is addressed by assuming a large mass/energy for the five-dimensional "star", M_*. The radius of the black hole horizon, r_h, sets the *maximum* spatial Ricci curvature (or minimum radius of curvature) for our universe, and thus can only dominate at late times. If one assumes that the initial Hubble constant is the $\sim$ five-dimensional Planck mass, which is supported by the scale of curvature perturbations above, we have $-\Omega_k \sim (M_5 r_h)^{-2} \sim M_5/M_*$, which could become sufficiently small, for massive stars.

   The curvature could of course be detectable at late times, as the Hubble constant drops, depending on the scale of dark energy. However, a detection curvature should generically accompany a detection of large scale anisotropy, as a generic black hole will have a finite angular momentum, which would distort FRW symmetry on the scale of the curvature.

3. The *Monopole Problem* refers to the absence of Grand Unified Theory (GUT) monopoles, that should generically form (and over-close the universe) after the GUT phase tran-

sition. As we have replaced the singular big bang, with the emergence of a four-dimensional universe at a finite size, the plasma temperature never reaches GUT scale, and thus the GUT phase transition will never have happened in the thermal history of the universe, preventing copious production of monopoles.

To see this, we can translate the observational constraints on the DGP cosmology (normal branch), $r_c \gtrsim 3H_0^{-1}$ [9] into an upper limit on five-dimensional Planck mass:

$$H \lesssim M_5 \lesssim \left(\frac{H_0 M_4^2}{6}\right)^{1/3} \sim 9 \text{ MeV}, \tag{4.51}$$

where we used the inequality in equation (4.50) to bound the Hubble constant. Correspondingly, the upper limit on the temperature comes from the Friedmann equation in the radiation era, for g_* species:

$$T \sim \left(\frac{M_4 H}{g_*^2}\right)^{1/4} \lesssim 3 \times 10^4 \left(\frac{g_*}{100}\right)^{-1/4} \text{ TeV} \ll T_{\text{GUT}} \sim 10^{12} \text{ TeV}. \tag{4.52}$$

Yet another attractive feature of our construction is that it lives in an asymptotically flat space-time. This potentially allows for an S-matrix description of this cosmology, through collapse of an ingoing shell, and emergence of outcoming D-brane. This might be a promising avenue, especially in light of significant recent progress in understanding scattering amplitudes in supergravity (*e.g.,* [38, 39]. Furthermore, with trivial modification, this model could also be embedded in an AdS bulk, which can potentially allow a study of the strongly-coupled dynamics of emergence through AdS/CFT correspondence. Since embedding our braneworld in a large AdS space-time (instead of Minkowski) simply amounts to adding a small constant to the right hand side of *e.g.,* equations (4.8) or (4.14), it need not significantly change any of the quantitative results that we have found here.

Let us now comment on (some) potential problems. Perhaps the most notable problem with the DGP model might be the claim [2] that superluminal propagation around non-trivial backgrounds in DGP model hinders causal evolution, and UV analyticity/completion. However this violation of causality is only a pathology for spacetimes that don't admit a consistent chronology for (super)luminal signals [33]. Such spacetimes, *e.g.,* Godel metric, even exist in General Relativity, and simply point out the absence of *global* causal evolution in those backgrounds. Therefore such geometries cannot emerge out of classical causal evolution. The second objection is more subtle, and relies on the analyticity properties of the scattering amplitudes for the DGP scalar. However, these conditions (*e.g.,* the Froissart bound) may be violated in the presence of massless bulk gravitons. Therefore, these

arguments would leave the door open for a possible UV completion via *e.g.,* string theory and/or AdS/CFT correspondence.

Another possible pathology of the DGP model is copious spontaneous production of self-accelerating branes in the bulk [103], which is estimated via Euclidean instanton methods. However one may argue that, since self-accelerating branches have catastrophic ghost instabilities, they should be excised (or exorcised) from the Hilbert space of the system. Given that one cannot classically transition from the normal branch to the self-accelerating branch, this modification would not affect the semi-classical behavior, but would prevent tunnelling into unphysical states.

Finally, let us comment on potential testability of this model. As we pointed out, the simple model of cosmological perturbations, developed in Sec. 4.4 is already ruled out by cosmological observations at more than the 5σ level, as it does not predict any deviations from scale-invariance. However, it is easy to imagine small corrections that could lead to a approximately 4% deviation from scale-invariance, especially given that bulk temperature is so close (*i.e.,* approximately 20% of) the five-dimensional Planck temperature. In the context of our model, the red tilt of the cosmological power spectrum implies that the amplitude of five-dimensional bulk graviton propagator, which enters in equation (4.43), is getting stronger in the IR, suggesting gradual unfreezing of additional polarizations of graviton. For example, this is what one would expect in cascading gravity [61], where DGP bulk is replaced by a four-brane, which is itself embedded in a 6D bulk. Similar to the ordinary DGP, the transition in flat space happens on length-scales larger than M_5^3/M_6^4, as the scalar field associated with the motion of the four-brane in the 6D bulk becomes weakly coupled, and boosts the strength of the gravitational exchange amplitude.

A related issue is that the gravitational Jeans instability of the thermal atmosphere kicks in for $k < k_J \simeq 0.2 \times T_b \, (T_b/M_5)^{3/2} \sim 10^{-2} T_b$, which may appear to limit the range of scale-invariant power spectrum to less than the current observations. However, the time-scale for the Jeans instability can be significantly longer than the Hubble time, thus limiting its maximum growth. Nevertheless, one may consider the residual Jeans instability as a potential origin for the slight red tilt (*i.e.,* $n_s < 1$) of the observed power spectrum. We defer a consistent inclusion of gravitational backreaction on the five-dimensional thermal power spectrum (which should account for the impact of Jeans instability) to a future study.

We should stress that, at this point, the development of a mechanism responsible for the observed deviation from scale-invariance is the most immediate phenomenological challenge for our scenario. The next challenge would be a study of the interactions that lead to deviations from scale-invariance, and whether they satisfy the stringent observational

bounds on primordial non-gaussianity [5]. Other interesting questions might be, given that the emergence from the five-dimensional black hole might happen at relatively low temperatures, could there be observable predictions for gravitational waves (either on cosmological scales, or for gravitational wave interferometers), or even modifications of light element abundances in Big Bang Nucleosynthesis.

Ultimately, an entire new world might emerge "Out of the White Hole", and replace Big Bang with a mere mirage of a non-existent past!

Chapter 5

Conclusion

Inspired by the holographic principle, there has been lots of effort to understand complicated physical issues and systems through holographic approaches. In the preceding chapters, we applied holographic methods to study a variety of interesting problems in gravity, condensed matter and cosmology.

In chapter 2, we studied the Randall-Sundrum II model which is constructed by taking two copies of AdS spacetime and gluing them together along a cut-off surface at some large radius and inserting a brane at this junction. Remarkably, the standard gravity arises at long distances on the brane as induced gravity. Using the Fefferman-Graham expansion around the brane and integrating out the extra radial direction, we derived the induced action on the brane while we considered three different gravity theories in the bulk: the Einstein gravity, the general $f(\mathcal{R})$ gravity and the Gauss-Bonnet gravity. As a result, we obtained the effective Newton constant G_N and the two curvature-squared couplings κ_1 and κ_2 on the brane in terms of the bulk parameters. However, since the brane is located at some finite radial direction, to make sense of the derivative expansion in our calculations, we demanded background geometry is weakly curved compared to the AdS scale.

To calculate the entanglement entropy associated with a general surface $\widetilde{\Sigma}$ on the brane, we used the holographic prescription in the context of the Randall-Sundrum II model. With Einstein gravity in the bulk, we simply followed the standard Ryu-Takayanagi prescription [204, 203], where one evaluates $A/4G$ on the bulk surfaces homologous to the boundary region and extremises. Further, we argued that the Wald entropy functional (2.28) evaluated on the bulk surface σ is the appropriate quantity we need to extremise with $f(\mathcal{R})$ gravity in the bulk. However, for the Gauss-Bonnet gravity the appropriate entropy functional is the Jacobson-Myers expression (2.49). Note that the holographic surface σ is an

extension of the surface $\widetilde{\Sigma}$ into the bulk. Therefore, in order to obtain the entanglement entropy of $\widetilde{\Sigma}$, we need to integrate over the extra holographic direction. Again, we used derivative expansion to integrate out the radial coordinate and to ensure the convergence of the expansion, we demanded not only a smooth geometry for the ambient metric but also for the entangling surface.

Carrying out all the calculations, we finally concluded that the entanglement entropy of any region surrounded by a smooth entangling surface is *finite* and the leading contribution is given precisely by the Bekenstein-Hawking area law [16, 13, 14, 115]. Hence these models confirmed a conjecture by Bianchi and Myers [19]. We also calculated the first leading corrections to the area law and found that the entanglement entropy coincides with the Wald entropy if the entangling surface is a Killing horizon but for a general surface in addition to the Wald entropy, there are terms dependent on the extrinsic curvature of the entangling surface.

So far, using the Randall-Sundrum II model with Einstein gravity or $f(\mathcal{R})$ gravity in the bulk we obtained the effective action for the boundary theory up to curvature-squared terms with one coupling, while for Gauss-Bonnet gravity in the bulk, two independent couplings appeared. However, in principle, three independent couplings could appear at this order in the boundary theory. In [97] based on a so-called squashed cone method, Solodukhin and his collaborators calculated the corresponding entropy functional with three independent parameters. Then one future direction could be to study the possibility of constructing a holographic model with three independent curvature-squared couplings and then reproducing the corresponding contributions to the entanglement entropy in the context of the Randall-Sundrum II model. Moreover, we showed that in four dimensions, the curvature-squared terms to the effective action and the corresponding contributions to the entanglement entropy contain a logarithmic dependence on the cut-off where the coefficients precisely match the standard central charges appearing in the trace anomaly. Then another interesting direction would be to explore the curvature-cubed terms in the boundary theory in higher dimensions. In particular then, one could identify logarithmic terms in six dimensions, which again must be related to trace anomaly.

In chapter 3, we studied the holographic dual of what is known as quantum Hall ferromagnetism in condensed matter theory. This phenomenon, which has been observed in graphene samples by applying strong magnetic field, is the emergence of energy gaps and Hall plateaus at integer filling fractions due to occurrence of spontaneous symmetry breaking. This effect is partially understood with certain perturbative calculations at weak coupling. The question was then whether this feature survives in a strongly coupled system as well.

To address this question, we applied a well-established string theory dual, namely the D3-D5 system. In this framework N_5 coincident D5-branes are embedded in the $AdS_5 \times S^5$ background of the D3-branes, such that they form a $(2+1)$-dimensional defect in the boundary theory. At zero charge density and in the absence of magnetic fields, the D5-brane geometry is $AdS_4 \times S^2$, which has superconformal symmetry. However, if we keep the charge density and the temperature at zero and introduce a constant external magnetic field, the D5-brane geometry changes drastically [89]. Near the boundary of $AdS_5 \times S^5$, the D5-brane is still $AdS_4 \times S^2$. However, as it enters the bulk of AdS_5, it pinches off and ends before it reaches the Poincaré horizon of AdS_5, forming what is called a Minkowski embedding. It can pinch off smoothly without creating a boundary when a cycle shrinks to zero size. This is the S^2 which shrinks and as a result, chiral symmetry is spontaneously broken.

The simple chiral symmetry breaking solutions of the D3-D5 system can be characterized as "Abelian", in that the dynamics of each D5-brane in the stack of D5-branes is treated independently and their behaviors are all identical. The phase diagram of these Abelian solutions is well known [77]. It was reproduced in the numerical results of this chapter and corresponds to the red curves in figure 3.3, 3.4, and 3.8. More specifically, the lower-left-hand wedge in figure 3.3 is the region where the "Abelian" chiral symmetry breaking solutions of the D5-brane are stable. At the red line, the chiral symmetric competitor takes over, in the sense that it has lower energy. (The same red curve re-appears in figure 3.4 and figure 3.8.)

Moreover, the D7-brane is an alternative solution of the D5-brane theory. It can be thought of as a "non-Abelian" configuration of D5-branes which is approximated by a D7-brane [158]. The stability region for the D7-brane in the temperature-density plane is similar to that of the Abelian D5-brane, but somewhat larger. It has less energy than the chiral symmetric competitor (the same competitor as for the Abelian D5-brane) to the lower left of the blue line in figure 3.3. The reader should beware that figure 3.3 does not compare the relative energies of the Abelian D5 and the D7-branes. This is done in figure 3.4.

Therefore, there are three competing solutions of the D3-D5 system: the Abelian D5-brane, the D7-brane and the chiral symmetric solution. (for $\nu > 1$ we have in addition the possibility of composite solutions.) To decide which is the preferred one at a given value of the temperature and filling fraction ν, we compared their free energies. The numerical results was shown in figure 3.4: at low temperatures, as we increase the filling fraction ν from zero, generically there are three phases. First, at low density is the Abelian D5-brane which is more stable. Then at some value of the density, as we pass the green line, there is a phase transition to the D7-brane. So beyond the green line, the D7-brane becomes the

energetically preferred solution until we approach the blue line where the chiral symmetric phase becomes more stable and chiral symmetry is restored. This part of the blue line is beyond the edge of the figures in 3.4 but can be seen in figure 3.3. while this pattern only apply to the region $0 < \nu < 1$, in section 3.4.4 we discussed the details of having composite solutions for $\nu > 1$ and the possible phase transitions were shown in figure 3.8.

There are a number of interesting directions for future work on this subject and we also include some speculations about possible new results. For example, we have not explored the blown up solutions of the D5-brane from the D5-brane point of view where it would be a non-Abelian configuration of D5-branes. There are a number of obstacles to this approach, one being that the full generalization of the Born-Infeld action is not known when the embedding coordinates of the D-brane are matrices. It would nevertheless be interesting to ask whether some of the features of the solution that we find are visible in the non-Abelian D5-brane theory. Moreover, we have done extensive numerical solutions of the embedding equations for the D5 and D7-branes. However, we have not analyzed the small fluctuations about these solutions. The spectrum of fluctuations would tell us, for example, if the solutions that we have found are stable or metastable. A search for further instabilities would be very interesting, especially considering that other D7-brane configurations are known to have instabilities to forming spatially periodic structures when the density is large enough [88, 89]. Interested reader will find further open questions around this subject in section 3.5.

Finally in chapter 4, we have developed a novel holographic perspective on cosmological evolution in the context of DGP gravity,[1] which can circumvent a big bang singularity in our past, and produce scale-invariant primordial curvature perturbations, consistent with modern cosmological observations. While most studies of DGP have been made from the viewpoint of a four-dimensional observer living on the brane, the DGP could be also examined as a theory of five-dimensional Einstein gravity coupled to the four-dimensional branes. We used the latter viewpoint by assuming five-dimensional spherical black hole metric in the bulk and studied the phenomenological viability of the brane around this five-dimensional black hole. In particular, we found a relation between bulk, brane, and black hole parameters and argued the observational constraints on them. As depicted in the plot (4.2) of the parameter space, we showed that the singularity *always* happens inside a white hole horizon, and *only* happens later than Big Bang Nucleosysntheis for a small corner of the allowed parameter space. Therefore, it can never be created through evolution from smooth initial conditions. Hence we proposed a holographic scenario: our four-dimensional brane emerges from the gravitational collapse of matter in five dimensions which avoids the

[1] This is a braneworld description of cosmology with both four-dimensional induced and five-dimensional bulk gravity named after Dvali, Gabadadze and Porati [68] who first introduced the model.

big bang singularity. In other words, in this scenario, there is no big bang singularity in our causal past, and the only singularity is shielded by a black hole horizon. Surprisingly, we found that a thermal atmosphere in equilibrium with the brane can lead to scale-invariant curvature perturbations at the level of cosmological observations, with little fine tuning. We further argued that the other problems in standard cosmology, such as the horizon problem, the flatness problem and the monopole problem, which are traditionally solved by inflation, can also be addressed in our scenario.

One interesting direction for future investigation is to consider small deformations of the bulk Schwarzschild geometry which obey the vacuum Einstein equation and explore the imprint of that on the three-brane which describes our universe. We expect these bulk deformations manifest itself as the perturbation of the holographic fluid, which is described by Brown-York stress tensor, on the brane. It is interesting to see how this fluctuation affects our story of a *holographic Big Bang* in the early universe. Another very interesting subject would be to study what the outcome of the recent BICEP2 observations means for our holographic theory of Big Bang. Recently, BICEP2 collaborators announced the discovery of "tensor" fluctuations, which could have been generated in the early universe, in the polarization of the cosmic microwave background. If this is correct, it will be our very first direct evidence for the gravitational wave, or "graviton", *i.e.,* the quantum nature of gravity. It will be also a very important clue about what happened at the very earliest moments of the Big Bang.

Permissions

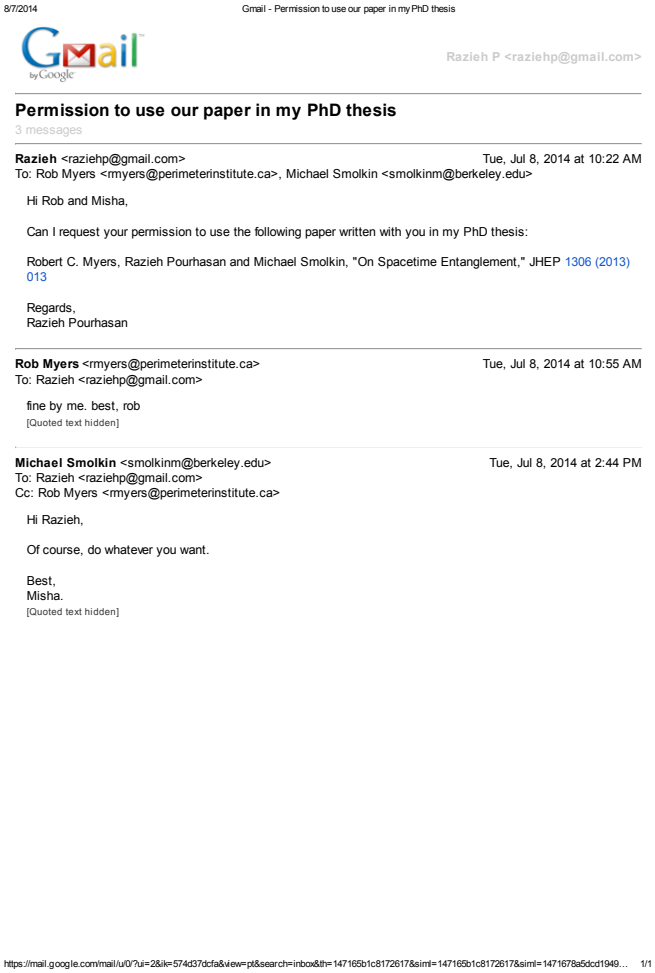

8/7/2014 Gmail - Permission to use our paper in my PhD thesis

Gmail by Google

Razieh P <raziehp@gmail.com>

Permission to use our paper in my PhD thesis

3 messages

Razieh <raziehp@gmail.com> Tue, Jul 8, 2014 at 10:22 AM
To: Rob Myers <rmyers@perimeterinstitute.ca>, Michael Smolkin <smolkinm@berkeley.edu>

Hi Rob and Misha,

Can I request your permission to use the following paper written with you in my PhD thesis:

Robert C. Myers, Razieh Pourhasan and Michael Smolkin, "On Spacetime Entanglement," JHEP 1306 (2013) 013

Regards,
Razieh Pourhasan

Rob Myers <rmyers@perimeterinstitute.ca> Tue, Jul 8, 2014 at 10:55 AM
To: Razieh <raziehp@gmail.com>

fine by me. best, rob
[Quoted text hidden]

Michael Smolkin <smolkinm@berkeley.edu> Tue, Jul 8, 2014 at 2:44 PM
To: Razieh <raziehp@gmail.com>
Cc: Rob Myers <rmyers@perimeterinstitute.ca>

Hi Razieh,

Of course, do whatever you want.

Best,
Misha.
[Quoted text hidden]

https://mail.google.com/mail/u/0/?ui=2&ik=574d37dcfa&view=pt&search=inbox&th=147165b1c8172617&siml=147165b1c8172617&siml=1471678a5dcd1949... 1/1

Gmail by Google

Razieh P <raziehp@gmail.com>

Permission request to use paper in my PhD thesis

2 messages

Razieh <raziehp@gmail.com> Mon, Jul 7, 2014 at 6:06 PM
To: "jhep-eo@jhep.sissa.it" <jhep-eo@jhep.sissa.it>

Dear Publisher,

I am writing you to request your permission to include following papers in my PhD thesis, which I co-authored (or authored) and published in JHEP:

1. Robert C. Myers, Razieh Pourhasan and Michael Smolkin, "On Spacetime Entanglement," JHEP 1306 (2013) 013

2. C. Kristjansen, R. Pourhasan, G. W. Semenoff, "A Holographic Quantum Hall Ferromagnet," JHEP 1402 (2014) 097

3. Razieh Pourhasan, "Spacetime entanglement with f(R) gravity," JHEP 1406 (2014) 004

Please note that with my thesis, I will be signing a Theses Non-Exclusive License that authorizes Library and Archives Canada to reproduce, communicate to the public on the internet, loan, distribute or sell copies of my thesis, among other things.

Sincerely
Razieh Pourhasan

JHEP Editorial Office <jhep-eo@jhep.sissa.it> Tue, Jul 8, 2014 at 8:42 AM
Reply-To: jhep-eo@jhep.sissa.it
To: Razieh <raziehp@gmail.com>
Cc: "jhep-eo@jhep.sissa.it" <jhep-eo@jhep.sissa.it>

Dear Dr. Pourhasan,

Thank you for your message.
All articles published in JHEP in 2014 are published under a CC-BY 4.0 licence (http://creativecommons.org/licenses/by/4.0/)., therefore anyone is free to re-use the content in whatever way they like provided the original authors and source (JHEP) are duly credited.

Regarding JHEP 1306 (2013) 013, on the other hand, we grant you the permission you have requested as long as also the other authors agree.

```
Best regards,
Maria Teresa Leo
JHEP Editorial Office
```

Il 08/07/2014 00:06, Razieh ha scritto:
[Quoted text hidden]

Razieh P <raziehp@gmail.com>

Permission request to use paper in my PhD thesis

1 message

Permissions <permissions@iop.org> Tue, Jul 8, 2014 at 4:45 AM
To: raziehp@gmail.com
Cc: jcap-eo@jcap.sissa.it

Dear Razieh Pourhasan,

Thank you for your request to reproduce IOP Publishing material.

The material you have requested was published under a CC BY licence (http://creativecommons.org/licenses/by/3.0/).

Therefore you may reuse the content without permission, so long as you reference it adequately and make the figure available under the same terms.

If you have any further questions or if there is any more we can do to help, please let me know.

Kind regards,

Lucy Evans

Publishing Assistant

IOP Publishing

-------- Original Message --------

Subject: Permission request to use paper in my PhD thesis
Date: Mon, 7 Jul 2014 18:57:10 -0400
From: Razieh P <raziehp@gmail.com>
To: jcap-eo@jcap.sissa.it

Dear Publisher,

I am writing you to request your permission to include following paper in my PhD thesis, which I co-authored and published in JCAP:

1. Razieh Pourhasan, Niayesh Afshordi, Robert B. Mann, "Out of the White Hole: A Holographic Origin for the Big Bang," JCAP 1404 (2014) 005

Please note that with my thesis, I will be signing a Theses Non-Exclusive License that authorizes Library and Archives Canada to reproduce, communicate to the public on the internet, loan, distribute or sell copies of my thesis, among other things.

Sincerely

Bibliography

[1] Dmitry A. Abanin, Kostya S. Novoselov, Uli Zeitler, Patrick A. Lee, A. K. Geim, and L. S. Levitov. Dissipative quantum hall effect in graphene near the dirac point. *Phys. Rev. Lett.*, 98:196806, May 2007.

[2] Allan Adams, Nima Arkani-Hamed, Sergei Dubovsky, Alberto Nicolis, and Riccardo Rattazzi. Causality, analyticity and an IR obstruction to UV completion. *JHEP*, 0610:014, 2006.

[3] P.A.R. Ade et al. Planck 2013 results. I. Overview of products and scientific results. 2013.

[4] P.A.R. Ade et al. Planck 2013 results. XVI. Cosmological parameters. 2013.

[5] P.A.R. Ade et al. Planck 2013 Results. XXIV. Constraints on primordial non-Gaussianity. 2013.

[6] Ofer Aharony, Oliver DeWolfe, Daniel Z. Freedman, and Andreas Karch. Defect conformal field theory and locally localized gravity. *JHEP*, 0307:030, 2003.

[7] Ofer Aharony, Steven S. Gubser, Juan Martin Maldacena, Hirosi Ooguri, and Yaron Oz. Large N field theories, string theory and gravity. *Phys.Rept.*, 323:183–386, 2000.

[8] Tsuneya Ando, Alan B. Fowler, and Frank Stern. Electronic properties of two-dimensional systems. *Rev.Mod.Phys.*, 54:437–672, 1982.

[9] Tahereh Azizi, M. Sadegh Movahed, and Kourosh Nozari. Observational Constraints on the Normal Branch of a Warped DGP Cosmology. *New Astron.*, 17:424–432, 2012.

[10] James M. Bardeen, B. Carter, and S.W. Hawking. The Four laws of black hole mechanics. *Commun.Math.Phys.*, 31:161–170, 1973.

[11] Y. Barlas, K. Yang, and A. H. MacDonald. Quantum hall effects in graphene-based two-dimensional electron systems. *Nanotechnology 23 052001 (2012)*, 23:052001, 2012.

[12] C. Barrabes and W. Israel. Thin shells in general relativity and cosmology: The Lightlike limit. *Phys.Rev.*, D43:1129–1142, 1991.

[13] Jacob D. Bekenstein. Black holes and entropy. *Phys.Rev.*, D7:2333–2346, 1973.

[14] Jacob D. Bekenstein. Generalized second law of thermodynamics in black hole physics. *Phys.Rev.*, D9:3292–3300, 1974.

[15] Jacob D. Bekenstein. A Universal Upper Bound on the Entropy to Energy Ratio for Bounded Systems. *Phys.Rev.*, D23:287, 1981.

[16] J.D. Bekenstein. Black holes and the second law. *Lett.Nuovo Cim.*, 4:737–740, 1972.

[17] Oren Bergman, Niko Jokela, Gilad Lifschytz, and Matthew Lippert. Quantum Hall Effect in a Holographic Model. *JHEP*, 1010:063, 2010.

[18] Oren Bergman, Niko Jokela, Gilad Lifschytz, and Matthew Lippert. Striped instability of a holographic Fermi-like liquid. *JHEP*, 1110:034, 2011.

[19] Eugenio Bianchi and Robert C. Myers. On the Architecture of Spacetime Geometry. 2012.

[20] Mike Blake, Stefano Bolognesi, David Tong, and Kenny Wong. Holographic Dual of the Lowest Landau Level. *JHEP*, 1212:039, 2012.

[21] David D. Blanco, Horacio Casini, Ling-Yan Hung, and Robert C. Myers. Relative Entropy and Holography. *JHEP*, 1308:060, 2013.

[22] Matthias Blau, K.S. Narain, and Edi Gava. On subleading contributions to the AdS/CFT trace anomaly. *JHEP*, 9909:018, 1999.

[23] Stefano Bolognesi, Joao N. Laia, David Tong, and Kenny Wong. A Gapless Hard Wall: Magnetic Catalysis in Bulk and Boundary. *JHEP*, 1207:162, 2012.

[24] Stefano Bolognesi and David Tong. Magnetic Catalysis in AdS4. *Class.Quant.Grav.*, 29:194003, 2012.

[25] Kirill I. Bolotin, Fereshte Ghahari, Michael D. Shulman, Horst L. Stormer, and Philip Kim. Observation of the fractional quantum hall effect in graphene. *Nature*, 462:196–197, 2009.

[26] Luca Bombelli, Rabinder K. Koul, Joohan Lee, and Rafael D. Sorkin. A Quantum Source of Entropy for Black Holes. *Phys.Rev.*, D34:373–383, 1986.

[27] David G. Boulware and Stanley Deser. String Generated Gravity Models. *Phys.Rev.Lett.*, 55:2656, 1985.

[28] Raphael Bousso. A Covariant entropy conjecture. *JHEP*, 9907:004, 1999.

[29] Raphael Bousso. The Holographic principle. *Rev.Mod.Phys.*, 74:825–874, 2002.

[30] Mauro Brigante, Hong Liu, Robert C. Myers, Stephen Shenker, and Sho Yaida. Viscosity Bound Violation in Higher Derivative Gravity. *Phys.Rev.*, D77:126006, 2008.

[31] John H. Brodie, Leonard Susskind, and N. Toumbas. How Bob Laughlin tamed the giant graviton from Taub - NUT space. *JHEP*, 0102:003, 2001.

[32] J. David Brown and Jr. York, James W. Quasilocal energy and conserved charges derived from the gravitational action. *Phys.Rev.*, D47:1407–1419, 1993.

[33] Jean-Philippe Bruneton. On causality and superluminal behavior in classical field theories: Applications to k-essence theories and MOND-like theories of gravity. *Phys.Rev.*, D75:085013, 2007.

[34] Alex Buchel, Jorge Escobedo, Robert C. Myers, Miguel F. Paulos, Aninda Sinha, et al. Holographic GB gravity in arbitrary dimensions. *JHEP*, 1003:111, 2010.

[35] Alex Buchel and Robert C. Myers. Causality of Holographic Hydrodynamics. *JHEP*, 0908:016, 2009.

[36] C. P. Burgess and Brian P. Dolan. Quantum hall effect in graphene: Emergent modular symmetry and the semicircle law. *Phys. Rev. B*, 76:113406, Sep 2007.

[37] C.P. Burgess and Brian P. Dolan. Particle vortex duality and the modular group: Applications to the quantum Hall effect and other 2-D systems. *Phys.Rev.*, B63:155309, 2001.

[38] Freddy Cachazo and Yvonne Geyer. A 'Twistor String' Inspired Formula For Tree-Level Scattering Amplitudes in N=8 SUGRA. 2012.

[39] Freddy Cachazo, Lionel Mason, and David Skinner. Gravity in Twistor Space and its Grassmannian Formulation. 2012.

[40] Jr. Callan, Curtis G. and Frank Wilczek. On geometric entropy. *Phys.Lett.*, B333:55–61, 1994.

[41] Xian O. Camanho and Jose D. Edelstein. Causality constraints in AdS/CFT from conformal collider physics and Gauss-Bonnet gravity. *JHEP*, 1004:007, 2010.

[42] Xian O. Camanho and Jose D. Edelstein. Causality in AdS/CFT and Lovelock theory. *JHEP*, 1006:099, 2010.

[43] B. Carter. Axisymmetric Black Hole Has Only Two Degrees of Freedom. *Phys.Rev.Lett.*, 26:331–333, 1971.

[44] H. Casini. Geometric entropy, area, and strong subadditivity. *Class.Quant.Grav.*, 21:2351–2378, 2004.

[45] H. Casini. Relative entropy and the Bekenstein bound. *Class.Quant.Grav.*, 25:205021, 2008.

[46] H. Casini and M. Huerta. A Finite entanglement entropy and the c-theorem. *Phys.Lett.*, B600:142–150, 2004.

[47] H. Casini and M. Huerta. A c-theorem for the entanglement entropy. *J.Phys.*, A40:7031–7036, 2007.

[48] H. Casini and Marina Huerta. On the RG running of the entanglement entropy of a circle. *Phys.Rev.*, D85:125016, 2012.

[49] Horacio Casini, Marina Huerta, and Robert C. Myers. Towards a derivation of holographic entanglement entropy. *JHEP*, 1105:036, 2011.

[50] William E. Caswell. Asymptotic behavior of non-abelian gauge theories to two-loop order. *Phys. Rev. Lett.*, 33:244–246, Jul 1974.

[51] Christos Charmousis, Ruth Gregory, Nemanja Kaloper, and Antonio Padilla. DGP Specteroscopy. *JHEP*, 0610:066, 2006.

[52] Joseph G. Checkelsky, Lu Li, and N. P. Ong. Zero-energy state in graphene in a high magnetic field. *Phys. Rev. Lett.*, 100:206801, May 2008.

[53] Joseph G. Checkelsky, Lu Li, and N. P. Ong. Divergent resistance at the dirac point in graphene: Evidence for a transition in a high magnetic field. *Phys. Rev. B*, 79:115434, Mar 2009.

[54] Sidney R. Coleman and Brian Russell Hill. No More Corrections to the Topological Mass Term in QED in Three-Dimensions. *Phys.Lett.*, B159:184, 1985.

[55] Hael Collins and Bob Holdom. Brane cosmologies without orbifolds. *Phys.Rev.*, D62:105009, 2000.

[56] Joshua H. Cooperman and Markus A. Luty. Renormalization of Entanglement Entropy and the Gravitational Effective Action. 2013.

[57] Jan de Boer, Manuela Kulaxizi, and Andrei Parnachev. AdS(7)/CFT(6), Gauss-Bonnet Gravity, and Viscosity Bound. *JHEP*, 1003:087, 2010.

[58] Jan de Boer, Manuela Kulaxizi, and Andrei Parnachev. Holographic Lovelock Gravities and Black Holes. *JHEP*, 1006:008, 2010.

[59] Jan de Boer, Manuela Kulaxizi, and Andrei Parnachev. Holographic Entanglement Entropy in Lovelock Gravities. *JHEP*, 1107:109, 2011.

[60] Sebastian de Haro, Sergey N. Solodukhin, and Kostas Skenderis. Holographic reconstruction of space-time and renormalization in the AdS/CFT correspondence. *Commun.Math.Phys.*, 217:595–622, 2001.

[61] Claudia de Rham, Gia Dvali, Stefan Hofmann, Justin Khoury, Oriol Pujolas, et al. Cascading gravity: Extending the Dvali-Gabadadze-Porrati model to higher dimension. *Phys.Rev.Lett.*, 100:251603, 2008.

[62] Cedric Deffayet. Cosmology on a brane in Minkowski bulk. *Phys.Lett.*, B502:199–208, 2001.

[63] Oliver DeWolfe, Daniel Z. Freedman, and Hirosi Ooguri. Holography and defect conformal field theories. *Phys.Rev.*, D66:025009, 2002.

[64] Xi Dong. Holographic Entanglement Entropy for General Higher Derivative Gravity. *JHEP*, 1401:044, 2014.

[65] Xu Du, I. Skachko, F. Duerr, A. Luican, and E. Y. Andrei. Fractional quantum hall effect and insulating phase of dirac electrons in graphene. *Nature*, 462:192–195, 2009.

[66] Gia Dvali and Sergey N. Solodukhin. Black Hole Entropy and Gravity Cutoff. 2008.

[67] G.R. Dvali and Gregory Gabadadze. Gravity on a brane in infinite volume extra space. *Phys.Rev.*, D63:065007, 2001.

[68] G.R. Dvali, Gregory Gabadadze, and Massimo Porrati. 4-D gravity on a brane in 5-D Minkowski space. *Phys.Lett.*, B485:208–214, 2000.

[69] Ethan Dyer and Kurt Hinterbichler. Boundary Terms, Variational Principles and Higher Derivative Modified Gravity. *Phys.Rev.*, D79:024028, 2009.

[70] Roberto Emparan. Black hole entropy as entanglement entropy: A Holographic derivation. *JHEP*, 0606:012, 2006.

[71] Roberto Emparan, Gary T. Horowitz, and Robert C. Myers. Exact description of black holes on branes. *JHEP*, 0001:007, 2000.

[72] Roberto Emparan, Clifford V. Johnson, and Robert C. Myers. Surface terms as counterterms in the AdS/CFT correspondence. *Phys.Rev.*, D60:104001, 1999.

[73] Roberto Emparan and Harvey S. Reall. Black holes in higher dimensions. *Living Reviews in Relativity*, 11(6), 2008.

[74] Johanna Erdmenger, Veselin G. Filev, and Dimitrios Zoakos. Magnetic Catalysis with Massive Dynamical Flavours. *JHEP*, 1208:004, 2012.

[75] Johanna Erdmenger, Zachary Guralnik, and Ingo Kirsch. Four-dimensional superconformal theories with interacting boundaries or defects. *Phys.Rev.*, D66:025020, 2002.

[76] Nick Evans, Astrid Gebauer, Keun-Young Kim, and Maria Magou. Holographic Description of the Phase Diagram of a Chiral Symmetry Breaking Gauge Theory. *JHEP*, 1003:132, 2010.

[77] Nick Evans, Astrid Gebauer, Keun-Young Kim, and Maria Magou. Phase diagram of the D3/D5 system in a magnetic field and a BKT transition. *Phys.Lett.*, B698:91–95, 2011.

[78] Nick Evans, Kristan Jensen, and Keun-Young Kim. Non Mean-Field Quantum Critical Points from Holography. *Phys.Rev.*, D82:105012, 2010.

[79] Nick Evans and Ed Threlfall. Chemical Potential in the Gravity Dual of a 2+1 Dimensional System. *Phys.Rev.*, D79:066008, 2009.

[80] Z. F. Ezawa and K. Hasebe. Interlayer exchange interactions, su(4) soft waves, and skyrmions in bilayer quantum hall ferromagnets. *Phys. Rev. B*, 65:075311, Jan 2002.

[81] Z.F. Ezawa. Quantum Hall effects: Field theoretical approach and related topics. *World Scientific*, 2000.

[82] Wenjuan Fang, Sheng Wang, Wayne Hu, Zoltan Haiman, Lam Hui, et al. Challenges to the DGP Model from Horizon-Scale Growth and Geometry. *Phys.Rev.*, D78:103509, 2008.

[83] Charles Fefferman and C. Robin Graham. The ambient metric. 2007.

[84] H. A. Fertig. Energy spectrum of a layered system in a strong magnetic field. *Phys. Rev. B*, 40:1087–1095, Jul 1989.

[85] Veselin G. Filev. Hot Defect Superconformal Field Theory in an External Magnetic Field. *JHEP*, 0911:123, 2009.

[86] Veselin G. Filev and Matthias Ihl. Flavoured Large N Gauge Theory on a Compact Space with an External Magnetic Field. *JHEP*, 1301:130, 2013.

[87] Veselin G. Filev, Matthias Ihl, and Dimitrios Zoakos. A Novel (2+1)-Dimensional Model of Chiral Symmetry Breaking. *JHEP*, 1312:072, 2013.

[88] Veselin G. Filev, Clifford V. Johnson, R.C. Rashkov, and K.S. Viswanathan. Flavoured large N gauge theory in an external magnetic field. *JHEP*, 0710:019, 2007.

[89] Veselin G. Filev, Clifford V. Johnson, and Jonathan P. Shock. Universal Holographic Chiral Dynamics in an External Magnetic Field. *JHEP*, 0908:013, 2009.

[90] Eanna E. Flanagan, Donald Marolf, and Robert M. Wald. Proof of classical versions of the Bousso entropy bound and of the generalized second law. *Phys.Rev.*, D62:084035, 2000.

[91] Valeri P. Frolov, D.V. Fursaev, and A.I. Zelnikov. Statistical origin of black hole entropy in induced gravity. *Nucl.Phys.*, B486:339–352, 1997.

[92] Mitsutoshi Fujita, Wei Li, Shinsei Ryu, and Tadashi Takayanagi. Fractional Quantum Hall Effect via Holography: Chern-Simons, Edge States, and Hierarchy. *JHEP*, 0906:066, 2009.

[93] Dmitri V. Fursaev. Entanglement entropy in critical phenomena and analogue models of quantum gravity. *Phys.Rev.*, D73:124025, 2006.

[94] Dmitri V. Fursaev. Proof of the holographic formula for entanglement entropy. *JHEP*, 0609:018, 2006.

[95] Dmitri V. Fursaev. Entanglement entropy in quantum gravity and the Plateau grob-lem. *Phys.Rev.*, D77:124002, 2008.

[96] Dmitri V. Fursaev. 'Thermodynamics' of Minimal Surfaces and Entropic Origin of Gravity. *Phys.Rev.*, D82:064013, 2010.

[97] Dmitri V. Fursaev, Alexander Patrushev, and Sergey N. Solodukhin. Distributional Geometry of Squashed Cones. 2013.

[98] D.V. Fursaev. Black hole thermodynamics, induced gravity and gravity in brane worlds. pages 462–470, 2000.

[99] A. K. Geim and K. S. Novoselov. The rise of graphene. *Nat. Mater.*, 6:183, 2007.

[100] G. W. Gibbons and S. W. Hawking. Cosmological event horizons, thermodynamics, and particle creation. *Phys. Rev. D*, 15:2738–2751, May 1977.

[101] M. O. Goerbig. Electronic properties of graphene in a strong magnetic field. *Rev. Mod. Phys.*, 83:1193–1243, Nov 2011.

[102] M. O. Goerbig and N. Regnault. Analysis of a su(4) generalization of halperins wave function as an approach towards a su(4) fractional quantum hall effect in graphene sheets. *Phys. Rev. B*, 75:241405, Jun 2007.

[103] Ruth Gregory, Nemanja Kaloper, Robert C. Myers, and Antonio Padilla. A New perspective on DGP gravity. *JHEP*, 0710:069, 2007.

[104] Gianluca Grignani, Namshik Kim, and Gordon W. Semenoff. D3-D5 Holography with Flux. *Phys.Lett.*, B715:225–229, 2012.

[105] Gianluca Grignani, Namshik Kim, and Gordon W. Semenoff. D7-anti-D7 bilayer: holographic dynamical symmetry breaking. *Phys.Lett.*, B722:360–363, 2013.

[106] David J. Gross and Frank Wilczek. Ultraviolet behavior of non-abelian gauge theories. *Phys. Rev. Lett.*, 30:1343–1346, Jun 1973.

[107] Steven S. Gubser. AdS/CFT and gravity. *Phys.Rev.*, D63:084017, 2001.

[108] Steven S. Gubser. AdS/CFT and gravity. *Phys.Rev.*, D63:084017, 2001.

[109] V. P. Gusynin, V. A. Miransky, and I. A. Shovkovy. Catalysis of dynamical flavor symmetry breaking by a magnetic field in 2 + 1 dimensions. *Phys. Rev. Lett.*, 76:1005–1005, Feb 1996.

[110] V.P. Gusynin, V.A. Miransky, and I.A. Shovkovy. Dynamical flavor symmetry breaking by a magnetic field in (2+1)-dimensions. *Phys.Rev.*, D52:4718–4735, 1995.

[111] V.P. Gusynin and S.G. Sharapov. Unconventional integer quantum Hall effect in graphene. *Phys.Rev.Lett.*, 95:146801, 2005.

[112] S. W. Hawking. Gravitational radiation from colliding black holes. *Phys. Rev. Lett.*, 26:1344–1346, May 1971.

[113] Stephen Hawking, Juan Martin Maldacena, and Andrew Strominger. de Sitter entropy, quantum entanglement and AdS/CFT. *JHEP*, 0105:001, 2001.

[114] Stephen Hawking, Juan Martin Maldacena, and Andrew Strominger. de Sitter entropy, quantum entanglement and AdS/CFT. *JHEP*, 0105:001, 2001.

[115] S.W. Hawking. Black holes in general relativity. *Commun.Math.Phys.*, 25:152–166, 1972.

[116] S.W. Hawking. Black hole explosions. *Nature*, 248:30–31, 1974.

[117] S.W. Hawking. Particle Creation by Black Holes. *Commun.Math.Phys.*, 43:199–220, 1975.

[118] Matthew Headrick. Entanglement Renyi entropies in holographic theories. *Phys.Rev.*, D82:126010, 2010.

[119] Matthew Headrick. Entanglement Renyi entropies in holographic theories. *Phys.Rev.*, D82:126010, 2010.

[120] Simeon Hellerman and Leonard Susskind. Realizing the quantum Hall system in string theory. 2001.

[121] Tomoyoshi Hirata and Tadashi Takayanagi. AdS/CFT and strong subadditivity of entanglement entropy. *JHEP*, 0702:042, 2007.

[122] Diego M. Hofman. Higher Derivative Gravity, Causality and Positivity of Energy in a UV complete QFT. *Nucl.Phys.*, B823:174–194, 2009.

[123] Ryszard Horodecki, Pawel Horodecki, Michal Horodecki, and Karol Horodecki. Quantum entanglement. *Rev.Mod.Phys.*, 81:865–942, 2009.

[124] Ling-Yan Hung, Robert C. Myers, and Michael Smolkin. On Holographic Entanglement Entropy and Higher Curvature Gravity. *JHEP*, 1104:025, 2011.

[125] Ling-Yan Hung, Robert C. Myers, and Michael Smolkin. On Holographic Entanglement Entropy and Higher Curvature Gravity. *JHEP*, 1104:025, 2011.

[126] Ling-Yan Hung, Robert C. Myers, and Michael Smolkin. Some Calculable Contributions to Holographic Entanglement Entropy. *JHEP*, 1108:039, 2011.

[127] C. Imbimbo, A. Schwimmer, S. Theisen, and S. Yankielowicz. Diffeomorphisms and holographic anomalies. *Class.Quant.Grav.*, 17:1129–1138, 2000.

[128] W. Israel. Singular hypersurfaces and thin shells in general relativity. *Nuovo Cim.*, B44S10:1, 1966.

[129] Werner Israel. Event horizons in static vacuum space-times. *Phys. Rev.*, 164:1776–1779, Dec 1967.

[130] Werner Israel. Event horizons in static electrovac space-times. *Commun.Math.Phys.*, 8:245–260, 1968.

[131] Yukinori Iwashita, Tsutomu Kobayashi, Tetsuya Shiromizu, and Hirotaka Yoshino. Holographic entanglement entropy of de Sitter braneworld. *Phys.Rev.*, D74:064027, 2006.

[132] Vivek Iyer and Robert M. Wald. Some properties of Noether charge and a proposal for dynamical black hole entropy. *Phys.Rev.*, D50:846–864, 1994.

[133] Ted Jacobson. Black hole entropy and induced gravity. 1994.

[134] Ted Jacobson. Thermodynamics of spacetime: The einstein equation of state. *Phys. Rev. Lett.*, 75:1260–1263, Aug 1995.

[135] Ted Jacobson. Gravitation and vacuum entanglement entropy. *Int.J.Mod.Phys.*, D21:1242006, 2012.

[136] Ted Jacobson, Gungwon Kang, and Robert C. Myers. On black hole entropy. *Phys.Rev.*, D49:6587–6598, 1994.

[137] Ted Jacobson and Robert C. Myers. Black hole entropy and higher curvature interactions. *Phys.Rev.Lett.*, 70:3684–3687, 1993.

[138] Daniel L. Jafferis, Igor R. Klebanov, Silviu S. Pufu, and Benjamin R. Safdi. Towards the F-Theorem: N=2 Field Theories on the Three-Sphere. *JHEP*, 1106:102, 2011.

[139] Dileep P. Jatkar and Aninda Sinha. New Massive Gravity and AdS_4 counterterms. *Phys.Rev.Lett.*, 106:171601, 2011.

[140] Kristan Jensen, Andreas Karch, Dam T. Son, and Ethan G. Thompson. Holographic Berezinskii-Kosterlitz-Thouless Transitions. *Phys.Rev.Lett.*, 105:041601, 2010.

[141] Clifford V. Johnson. D-brane primer. pages 129–350, 2000.

[142] Niko Jokela, Matti Jarvinen, and Matthew Lippert. A holographic quantum Hall model at integer filling. *JHEP*, 1105:101, 2011.

[143] Niko Jokela, Matti Jarvinen, and Matthew Lippert. Fluctuations of a holographic quantum Hall fluid. *JHEP*, 1201:072, 2012.

[144] Niko Jokela, Gilad Lifschytz, and Matthew Lippert. Magneto-roton excitation in a holographic quantum Hall fluid. *JHEP*, 1102:104, 2011.

[145] Niko Jokela, Gilad Lifschytz, and Matthew Lippert. Magnetic effects in a holographic Fermi-like liquid. *JHEP*, 1205:105, 2012.

[146] Niko Jokela, Gilad Lifschytz, and Matthew Lippert. Holographic anyonic superfluidity. *JHEP*, 1310:014, 2013.

[147] T. Jungwirth and A. H. MacDonald. Pseudospin anisotropy classification of quantum hall ferromagnets. *Phys. Rev. B*, 63:035305, Dec 2000.

[148] Nemanja Kaloper. Gravitational shock waves and their scattering in brane-induced gravity. *Phys.Rev.*, D71:086003, 2005.

[149] Andreas Karch and Lisa Randall. Localized gravity in string theory. *Phys.Rev.Lett.*, 87:061601, 2001.

[150] Andreas Karch and Lisa Randall. Locally localized gravity. *JHEP*, 0105:008, 2001.

[151] Andreas Karch and Lisa Randall. Open and closed string interpretation of SUSY CFT's on branes with boundaries. *JHEP*, 0106:063, 2001.

[152] A. Kehagias. Exponential and power law hierarchies from supergravity. *Phys.Lett.*, B469:123–128, 1999.

[153] D. V. Khveshchenko. Magnetic-field-induced insulating behavior in highly oriented pyrolitic graphite. *Phys. Rev. Lett.*, 87:206401, Oct 2001.

[154] D. V. Khveshchenko. Composite dirac fermions in graphene. *Phys. Rev. B*, 75:153405, Apr 2007.

[155] Igor R. Klebanov, Silviu S. Pufu, and Benjamin R. Safdi. F-Theorem without Supersymmetry. *JHEP*, 1110:038, 2011.

[156] K.G. Klimenko. Three-dimensional Gross-Neveu model in an external magnetic field. *Theor.Math.Phys.*, 89:1161–1168, 1992.

[157] C. Kristjansen, R. Pourhasan, and G.W. Semenoff. A Holographic Quantum Hall Ferromagnet. *JHEP*, 1402:097, 2014.

[158] Charlotte Kristjansen and Gordon W. Semenoff. Giant D5 Brane Holographic Hall State. *JHEP*, 1306:048, 2013.

[159] R. Laflamme. Entropy of a Rindler Wedge. *Phys.Lett.*, B196:449–450, 1987.

[160] R.B. Laughlin. Quantized Hall conductivity in two-dimensions. *Phys.Rev.*, B23:5632–5733, 1981.

[161] Robert G. Leigh, Anastasios C. Petkou, and P. Marios Petropoulos. Holographic Fluids with Vorticity and Analogue Gravity. *JHEP*, 1211:121, 2012.

[162] Michael Levin and Xiao-Gang Wen. Detecting Topological Order in a Ground State Wave Function. *Phys.Rev.Lett.*, 96:110405, 2006.

[163] Aitor Lewkowycz and Juan Maldacena. Generalized gravitational entropy. *JHEP*, 1308:090, 2013.

[164] E.H. Lieb and M.B. Ruskai. Proof of the strong subadditivity of quantum-mechanical entropy. *J.Math.Phys.*, 14:1938–1941, 1973.

[165] Hong Liu and Mark Mezei. A Refinement of entanglement entropy and the number of degrees of freedom. *JHEP*, 1304:162, 2013.

[166] David Lovelock. Divergence-free tensorial concomitants. *Aequationes Math.*, 4:127, 1970.

[167] David Lovelock. The einstein tensor and its generalizations. *Journal of Mathematical Physics*, 12(3), 1971.

[168] Markus A. Luty, Massimo Porrati, and Riccardo Rattazzi. Strong interactions and stability in the DGP model. *JHEP*, 0309:029, 2003.

[169] Joseph D. Lykken, Jacob Sonnenschein, and Nathan Weiss. The Theory of anyonic superconductivity: A Review. *Int.J.Mod.Phys.*, A6:5155–5214, 1991.

[170] Kei-ichi Maeda, Shuntaro Mizuno, and Takashi Torii. Effective gravitational equations on brane world with induced gravity. *Phys.Rev.*, D68:024033, 2003.

[171] Juan Martin Maldacena. The Large N limit of superconformal field theories and supergravity. *Adv.Theor.Math.Phys.*, 2:231–252, 1998.

[172] Juan Martin Maldacena. TASI 2003 lectures on AdS / CFT. pages 155–203, 2003.

[173] Donald Marolf and Rafael Sorkin. Perfect mirrors and the selfaccelerating box paradox. *Phys.Rev.*, D66:104004, 2002.

[174] Donald Marolf and Rafael D. Sorkin. On the status of highly entropic objects. *Phys.Rev.*, D69:024014, 2004.

[175] K. Moon, H. Mori, Kun Yang, S. M. Girvin, A. H. MacDonald, L. Zheng, D. Yoshioka, and Shou-Cheng Zhang. Spontaneous interlayer coherence in double-layer quantum hall systems: Charged vortices and kosterlitz-thouless phase transitions. *Phys. Rev. B*, 51:5138–5170, Feb 1995.

[176] A. F. Morpurgo. Condensed-matter physics: Dirac electrons broken to pieces. *Nature*, pages 170–171, 2009.

[177] S. Q. Murphy, J. P. Eisenstein, G. S. Boebinger, L. N. Pfeiffer, and K. W. West. Many-body integer quantum hall effect: Evidence for new phase transitions. *Phys. Rev. Lett.*, 72:728–731, Jan 1994.

[178] R.C. Myers and S.E. Vazquez. Quark Soup al dente: Applied Superstring Theory. *Class.Quant.Grav.*, 25:114008, 2008.

[179] Robert C. Myers. Higher-derivative gravity, surface terms, and string theory. *Phys. Rev. D*, 36:392–396, Jul 1987.

[180] Robert C. Myers, Miguel F. Paulos, and Aninda Sinha. Holographic studies of quasi-topological gravity. *JHEP*, 1008:035, 2010.

[181] Robert C. Myers and M.J. Perry. Black Holes in Higher Dimensional Space-Times. *Annals Phys.*, 172:304, 1986.

[182] Robert C. Myers, Razieh Pourhasan, and Michael Smolkin. On Spacetime Entanglement. *JHEP*, 1306:013, 2013.

[183] Robert C. Myers and Brandon Robinson. Black Holes in Quasi-topological Gravity. *JHEP*, 1008:067, 2010.

[184] Robert C. Myers and Ajay Singh. Comments on Holographic Entanglement Entropy and RG Flows. *JHEP*, 1204:122, 2012.

[185] Robert C. Myers and Aninda Sinha. Seeing a c-theorem with holography. *Phys.Rev.*, D82:046006, 2010.

[186] Robert C. Myers and Aninda Sinha. Holographic c-theorems in arbitrary dimensions. *JHEP*, 1101:125, 2011.

[187] Alberto Nicolis and Riccardo Rattazzi. Classical and quantum consistency of the DGP model. *JHEP*, 0406:059, 2004.

[188] Qian Niu, D.J. Thouless, and Yong-Shi Wu. Quantized Hall Conductance As A Topological Invariant. *Phys. Rev. 3372*, B31:3372, 1985.

[189] Shin'ichi Nojiri and Sergei D. Odintsov. On the conformal anomaly from higher derivative gravity in AdS/CFT correspondence. *Int.J.Mod.Phys.*, A15:413–428, 2000.

[190] Kentaro Nomura and Allan H. MacDonald. Quantum hall ferromagnetism in graphene. *Phys. Rev. Lett.*, 96:256602, Jun 2006.

[191] K.S. Novoselov, A.K. Geim, S.V. Morozov, D. Jiang, M.I. Katsnelson, et al. Two-dimensional gas of massless Dirac fermions in graphene. *Nature*, 438:197, 2005.

[192] Rodrigo Olea. Mass, angular momentum and thermodynamics in four-dimensional Kerr-AdS black holes. *JHEP*, 0506:023, 2005.

[193] Hirosi Ooguri and Zheng Yin. TASI lectures on perturbative string theories. pages 5–81, 1996.

[194] N. M. R. Peres, F. Guinea, and A. H. Castro Neto. Electronic properties of disordered two-dimensional carbon. *Phys. Rev. B*, 73:125411, Mar 2006.

[195] L. Pilo, R. Rattazzi, and A. Zaffaroni. The Fate of the radion in models with metastable graviton. *JHEP*, 0007:056, 2000.

[196] Martin B. Plenio and Shashank Virmani. An Introduction to entanglement measures. *Quant.Inf.Comput.*, 7:1–51, 2007.

[197] Joseph Polchinski. Dirichlet Branes and Ramond-Ramond charges. *Phys.Rev.Lett.*, 75:4724–4727, 1995.

[198] H. David Politzer. Reliable perturbative results for strong interactions? *Phys. Rev. Lett.*, 30:1346–1349, Jun 1973.

[199] Razieh Pourhasan. Spacetime Entanglement with f(R) Gravity. 2014.

[200] Razieh Pourhasan, Niayesh Afshordi, and Robert B. Mann. Out of the White Hole: A Holographic Origin for the Big Bang. *JCAP*, 1404:005, 2014.

[201] Lisa Randall and Raman Sundrum. A Large mass hierarchy from a small extra dimension. *Phys.Rev.Lett.*, 83:3370–3373, 1999.

[202] Lisa Randall and Raman Sundrum. An Alternative to compactification. *Phys.Rev.Lett.*, 83:4690–4693, 1999.

[203] Shinsei Ryu and Tadashi Takayanagi. Aspects of Holographic Entanglement Entropy. *JHEP*, 0608:045, 2006.

[204] Shinsei Ryu and Tadashi Takayanagi. Holographic derivation of entanglement entropy from AdS/CFT. *Phys.Rev.Lett.*, 96:181602, 2006.

[205] A. D. Sakharov. Vacuum Quantum Fluctuations in Curved Space and the Theory of Gravitation. *Soviet Physics Doklady*, 12:1040, 1968.

[206] Ivo Savonije and Erik P. Verlinde. CFT and entropy on the brane. *Phys.Lett.*, B507:305–311, 2001.

[207] A. Schwimmer and S. Theisen. Entanglement Entropy, Trace Anomalies and Holography. *Nucl.Phys.*, B801:1–24, 2008.

[208] Gordon W. Semenoff. Condensed-matter simulation of a three-dimensional anomaly. *Phys. Rev. Lett.*, 53:2449–2452, Dec 1984.

[209] Gordon W. Semenoff, Pasquale Sodano, and Yong-Shi Wu. Renormalization of the statistics parameter in three-dimensional electrodynamics. *Phys. Rev. Lett.*, 62:715–718, Feb 1989.

[210] Gordon W. Semenoff and Fei Zhou. Magnetic Catalysis and Quantum Hall Ferromagnetism in Weakly Coupled Graphene. *JHEP*, 1107:037, 2011.

[211] G.W. Semenoff, I.A. Shovkovy, and L.C.R. Wijewardhana. Phase transition induced by a magnetic field. *Mod.Phys.Lett.*, A13:1143–1154, 1998.

[212] G.W. Semenoff, I.A. Shovkovy, and L.C.R. Wijewardhana. Universality and the magnetic catalysis of chiral symmetry breaking. *Phys.Rev.*, D60:105024, 1999.

[213] Kallol Sen, Aninda Sinha, and Nemani V. Suryanarayana. Counterterms, critical gravity and holography. *Phys.Rev.*, D85:124017, 2012.

[214] Naokazu Shibata and Kentaro Nomura. Coupled charge and valley excitations in graphene quantum hall ferromagnets. *Phys. Rev. B*, 77:235426, Jun 2008.

[215] Igor A. Shovkovy. Magnetic Catalysis: A Review. *Lect.Notes Phys.*, 871:13–49, 2013.

[216] David A. Siegel, Cheol-Hwan Park, Choongyu Hwang, Jack Deslippe, Alexei V. Fedorov, Steven G. Louie, and Alessandra Lanzara. Many-body interactions in quasi-freestanding graphene. *Proceedings of the National Academy of Sciences*, 108(28):11365–11369, 2011.

[217] Kostas Skenderis. Lecture notes on holographic renormalization. *Class.Quant.Grav.*, 19:5849–5876, 2002.

[218] Sergey N. Solodukhin. Entanglement entropy of black holes and AdS/CFT correspondence. *Phys.Rev.Lett.*, 97:201601, 2006.

[219] Sergey N. Solodukhin. Entanglement entropy, conformal invariance and extrinsic geometry. *Phys.Lett.*, B665:305–309, 2008.

[220] Thomas P. Sotiriou and Valerio Faraoni. f(R) Theories Of Gravity. *Rev.Mod.Phys.*, 82:451–497, 2010.

[221] Mark Srednicki. Entropy and area. *Phys.Rev.Lett.*, 71:666–669, 1993.

[222] Leonard Susskind. String theory and the principles of black hole complementarity. *Phys.Rev.Lett.*, 71:2367–2368, 1993.

[223] Leonard Susskind. The World as a hologram. *J.Math.Phys.*, 36:6377–6396, 1995.

[224] Leonard Susskind and John Uglum. Black hole entropy in canonical quantum gravity and superstring theory. *Phys.Rev.*, D50:2700–2711, 1994.

[225] Gerard 't Hooft. A Planar Diagram Theory for Strong Interactions. *Nucl.Phys.*, B72:461, 1974.

[226] Gerard 't Hooft. Determinism and dissipation in quantum gravity. pages 397–413, 1999.

[227] Gerard 't Hooft. Quantum gravity as a dissipative deterministic system. *Class.Quant.Grav.*, 16:3263–3279, 1999.

[228] Gerard 't Hooft. How does God play dice? (Pre)determinism at the Planck scale. 2001.

[229] Gerard 't Hooft. Quantum mechanics and determinism. 2001.

[230] Gerard 't Hooft. Determinism in free bosons. *Int.J.Theor.Phys.*, 42:355–361, 2003.

[231] D. J. Thouless, M. Kohmoto, M. P. Nightingale, and M. den Nijs. Quantized hall conductance in a two-dimensional periodic potential. *Phys. Rev. Lett.*, 49:405–408, Aug 1982.

[232] Csaba Tőke, Paul E. Lammert, Vincent H. Crespi, and Jainendra K. Jain. Fractional quantum hall effect in graphene. *Phys. Rev. B*, 74:235417, Dec 2006.

[233] William G. Unruh and Robert M. Wald. Acceleration radiation and the generalized second law of thermodynamics. *Phys. Rev. D*, 25:942–958, Feb 1982.

[234] William G. Unruh and Robert M. Wald. Entropy bounds, acceleration radiation, and the generalized second law. *Phys. Rev. D*, 27:2271–2276, May 1983.

[235] A.I. Vainshtein. To the problem of nonvanishing gravitation mass. *Phys.Lett.*, B39:393–394, 1972.

[236] V. Vedral. The role of relative entropy in quantum information theory. *Rev.Mod.Phys.*, 74:197–234, 2002.

[237] Erik P. Verlinde and Herman L. Verlinde. RG flow, gravity and the cosmological constant. *JHEP*, 0005:034, 2000.

[238] Herman L. Verlinde. Holography and compactification. *Nucl.Phys.*, B580:264–274, 2000.

[239] Robert M. Wald. Black hole entropy is the Noether charge. *Phys.Rev.*, D48:3427–3431, 1993.

[240] Brian Whitt. Fourth Order Gravity as General Relativity Plus Matter. *Phys.Lett.*, B145:176, 1984.

[241] Edward Witten. SL(2,Z) action on three-dimensional conformal field theories with Abelian symmetry. 2003.

[242] Alexandre Yale. Simple counterterms for asymptotically AdS spacetimes in Lovelock gravity. *Phys.Rev.*, D84:104036, 2011.

[243] Kun Yang, S. Das Sarma, and A. H. MacDonald. Collective modes and skyrmion excitations in graphene quantum hall ferromagnets. *Phys. Rev. B*, 74:075423, Aug 2006.

[244] A. F. Young, C. R. Dean, L. Wang, H. Ren, P. Cadden-Zimansky, K. Watanabe, T. Taniguchi, J. Hone, K. L. Shepard, and P. Kim. Spin and valley quantum hall ferromagnetism in graphene. *Nature Physics*, 8:550–556, 2012.

[245] A.B. Zamolodchikov. Irreversibility of the Flux of the Renormalization Group in a 2D Field Theory. *JETP Lett.*, 43:730–732, 1986.

[246] Y. Zhang, Z. Jiang, J. P. Small, M. S. Purewal, Y.-W. Tan, M. Fazlollahi, J. D. Chudow, J. A. Jaszczak, H. L. Stormer, and P. Kim. Landau-level splitting in graphene in high magnetic fields. *Phys. Rev. Lett.*, 96:136806, Apr 2006.

[247] Yuanbo Zhang, Yan-Wen Tan, Horst L. Stormer, and Philip Kim. Experimental observation of the quantum Hall effect and and Berry's phase in graphene. *Nature*, 438:201–204, 2005.